Prediction of Risks of Cardiac Mortality and Secondary Cancers after Thoracic Radiotherapy in Adolescents and Young Adults

Allison Toltz

Medical Physics Unit
McGill University, Montreal
August 2012

A thesis submitted to the McGill University in partial fulfillment of the requirements of the degree of Master of Science in Medical Physics.

Abstract

Intensity modulated proton therapy (IMPT) is believed to improve the therapeutic ratio by reducing the dose to normal tissue as compared to three dimensional conformal (photon) radiotherapy (3D-CRT). This hypothesis is investigated in this work by predicting the risks of late radiation-induced effects for young patients receiving radiotherapy for Hodgkin's and non-Hodgkin's lymphoma (HL and NHL) or breast cancer (BC) using radiobiological modeling. The late effects considered were cardiac mortality and secondary cancer in the lungs and breasts (for female patients).

Patient data was acquired for twenty-eight patients who were under thirty years of age and were treated with radiotherapy for HL, NHL, or BC in Quebec in 2010. The original computed tomography simulation images were used to re-plan the patients with IMPT using Eclipse treatment planning software (version 10, Varian Medical Systems, Palo Alto, CA). The dose-volume data of the original photon plans and the new proton plans were analyzed using the relative seriality model to assess the risks of late effects. The relative seriality model was utilized to predict excess risk of cardiac mortality. The Schneider[1] modified linear quadratic model was used to predict the excess absolute risk for induction of lung cancer and breast cancer. Parameters for each model were derived from retrospective studies in the literature.

Dosimetric plan comparison revealed IMPT reduced dose to the organs at risk of interest as compared to 3D-CRT. Overall the excess risk of cardiac mortality and the excess absolute risks for lung and breast cancers were reduced for IMPT as compared to 3D-CRT.

1. Schneider U. Mechanistic model of radiation-induced cancer after fractionated radiotherapy using the linear-quadratic formula. Medical Physics 2009;36:1138.

Résumé

La radiothérapie par modulation d'intensité de protons (IMPT) améliore le ratio thérapeutique en réduisant la dose délivrée aux tissus sains, par rapport à la radiothérapie conformationelle trois dimensions par photons (3D-CRT). L'objectif de cet étude est de confirmer cette hypothèse dans ces deux modalités de traitement par une comparaison de de risque prédictible d'effets secondaires à long terme dû aux rayonnements ionisants pour des jeunes patients traités par radiothérapie pour des lymphomes Hodgkiniens et non-Hodgkiniens (HL et NHL) ou pour un cancer du sein (BC) à l'aide des modèles radiobiologiques. Les effets secondaire à long terme étudiés sont la mortalité cardiaque et les cancers secondaires du poumon ou du sein (pour les patientes).

Les données de vingt-huit patients de moins de trente ans ayant été traités par radiothérapie pour HL, NHL, ou BC au Québec en 2010 ont été collectées. Les images original de tomodensitomètres[i] ont été utilisées pour re-plannifier les patients avec l'IMPT à l'aide du logiciel de planification de traitement Eclipse (version 10, Varian Medical Systems, Palo Alto, CA). Les données des histogrammes dose-volume du plan original en photon ainsi que la replanification en proton ont été analysées pour évaluer les risques d'effet secondaires à long terme. Le modèle de sérialité relative[1,ii] a été utilisé pour prédire le risque excessif de mortalité cardiaque. Le model linéaire quadratique modifié de Schneider[2] a été utilisé afin de prédire l'excès absolu de risque[iii] de cancer du poumon et du sein. Les paramètres de chaque modèles ont été dérivés d'études rétrospectives tirées de la littérature.

La comparaison dosimétrique des plans a démontré que l'IMPT réduit la dose délivrée aux organes à risque par rapport à la 3D-CRT. En général, le risque excessif de mortalité cardiaque et l'excès absolu de risque de cancer du poumon et du sein sont réduits avec l'IMPT par rapport à la 3D-CRT.

[i] Connu sur le nom “computed tomography.”
[ii] Connu sur le nom “relative seriality model.”
[iii] Connu sur le nom “excess absolute risk.”

1. Källman P, A. Ågren, A. Brahme. Tumour and normal tissue responses to fractionated non-uniform dose delivery. International Journal of Radiation Biology 1992;62:249-62.
2. Schneider U. Mechanistic model of radiation-induced cancer after fractionated radiotherapy using the linear-quadratic formula. Medical Physics 2009;36:1138.

Acknowledgements

I would like to acknowledge and thank my supervisors William Parker and Dr. Jan P. Seuntjens for their support throughout the entire undertaking of the thesis project and their guidance, availability for discussion, and encouragement.

I would also like to thank the other members of the collaborative proton project research group, in particular Naomi Shin for her advice and collaboration, Dr. Carolyn Freeman and Dr. David Roberge for their medical expertise, input on the direction for the project, and comments on the expression of the results, and Dr. Cecile Laude for her involvement in the data collection and contouring supervision and assistance with translation of the abstract.

This work was funded by a grant from the Fonds de recherche Santé Québec (FRSQ). Assistance and troubleshooting in the use of Eclipse treatment planning software was provided by Paul Meskell of Varian Medical Systems for the purposes of installation of proton beam data and dose calculation algorithms.

I would also like to thank the staff of the Medical Physics Unit at the Montreal General Hospital for their patience and instruction in the use of the treatment planning software and clinical treatment planning techniques. I would also like to thank my fellow graduate students in medical physics and biomedical engineering for their support, and my colleague Jessica Perez for her assistance with translation of the abstract.

Table of Contents

List of Figures

Chapter 3

Chapter 4

List of Tables

Chapter 1

Introduction

1 Introduction

The term radiotherapy is used to describe the process of using ionizing radiation for the treatment of disease. Radiotherapy is a critical element of the therapeutic regimen for cancer, which afflicts approximately one in two men and one in three women over the course of a lifetime among Canadians and Americans. Cancer is the leading cause of death in Canadians and second leading cause of death in Americans (being surpassed only by heart disease)[1,2]. Adolescents and young adults represent 2% of all new cases of cancer diagnosed per year, and for this group the most common cancers are testicular

cancer in young men and thyroid cancer in young women. For both sexes, the second-most common cancer is Hodgkin's lymphoma. The high incidence of this disease is particular to this age group. Treatment for adolescents and young adults diagnosed with cancer has evolved since the advents of radiotherapy and chemotherapy, and today therapy usually involves some combination of these two treatment options. For young patients with a favorable prognosis, the long-term consequences of their cancer treatments are of concern. Long-term follow up studies of young cancer patients have shown premature death due to therapy-induced effects. These data have been combined with atomic bomb survivor data to develop biological models for radiation-induced normal tissue toxicity. These models can then be used to evaluate the potential toxicity of cancer treatments. Radiation dose-volume-specific models can be used to predict the risks of late effects for a given radiotherapy treatment plan. This work makes use of these types of models to compare the risks of differing radiotherapy modalities for adolescent and young adult cancer patients.

1.1 Cancers in Adolescents and Young Adults

The consequences of developing cancer in the ages of adolescence and young adulthood can be quite severe as both the disease and its treatment can affect quality of life and physical, psychological, and social well-being. The developing tissues of children and adolescents are thought to be more sensitive to some carcinogenic effects, particularly exposure to ionizing radiation, and this is believed to contribute to the expression and diagnosis of cancer in adolescents and young adults. As a result, the types of cancers

diagnosed in this age group differ from those observed in children and also from those observed in the elderly.

A differentiation between cancers of epithelial tissues, which line cavities and organ surfaces in the body, and non-epithelial tissues is relevant for the study of cancers in this age group. Non-epithelial cancers are more common during childhood, and these include leukemias and embryonal tumors. Epithelial cancers are more common adult cancers and are known as carcinomas. The cancers in adolescents and young adults are representative of a transition from the non-epithelial types to epithelial types. In Canada between 2002 and 2006, testicular cancer (non-epithelial) represented 27% of cancers in male adolescents and young adults followed by Hodgkin's lymphoma (non-epithelial) at 14%, and over the same time period, thyroid cancer (epithelial) represented 23% of cancers in female adolescents and young adults followed by Hodgkin's lymphoma at 12%[3].

Survival for these diseases is among the highest for the cancers common to this age group. Thyroid cancer has a five year survival of 99%, followed by testicular cancer at 96% and Hodgkin's lymphoma at 95%. This favorable prognosis results in concern with regard to late treatment-related effects. This work focuses on patients receiving thoracic radiotherapy for Hodgkin's lymphoma or breast cancer.

1.1.1 Hodgkin's Lymphoma

There are approximately 9000 new cases of Hodgkin's lymphoma per year in the U.S.A[2] and 900 new cases per year in Canada[1], and there is a predominance of 1.2 to 1 for male patients in both countries. The age-incidence peaks at age 25, declines and plateaus

through middle age, and then increases again with older age[4]. The disease typically presents with swelling of the lymph nodes in the body above the diaphragm, particularly in the lower neck and supraclavicular nodes[4]. Less than 10% of patients initially present with subdiaphragmatic involvement, and mediastinal cases are typically anterior to the ascending aorta.

After diagnosis, the extent of the disease is established through surgical biopsy, physical examination, blood tests, chest radiograph, and fluorodeoxyglucose positron emission tomography (FDG PET) scan. The primary goal of therapy for Hodgkin's lymphoma at any staging is curative[5]. In the past Hodgkin's lymphoma was treated with extended-field irradiation of 40 Gy or more, but treatment now commonly comprises a short course of chemotherapy followed by involved-field radiation therapy at lower doses. This is the result of clinical trials which have demonstrated that the ABVD regimen (Adriamycin bleomycin vinblastine dacarbazine) is the most effective and least toxic chemotherapy regimen, that combined modality therapy is superior to wide-field radiation therapy alone, and that there is no advantage to wide-field radiation therapy over involved-field radiation therapy when combined with chemotherapy.

Treatment-related complications can affect quality of life as well as survival. One of the most common non-lethal side effects of treatment for Hodgkin's lymphoma, hypothyroidism occurs in nearly 50% of patients irradiated in the neck[4]; and some chemotherapy regimens are known to cause infertility. Hodgkin's lymphoma patients are at an increased risk of death from cardiovascular disease and second cancers for more than 25 years after treatment. Hodgkin's lymphoma survivors are at a higher risk of

secondary malignancy and cardiovascular events than recurrent Hodgkin's lymphoma beyond 20 years after treatment (Figure 1-1). Leukemia, breast cancer, and lung cancer in particular are the secondary cancers in this patient population with risks related to both chemotherapy and radiotherapy.

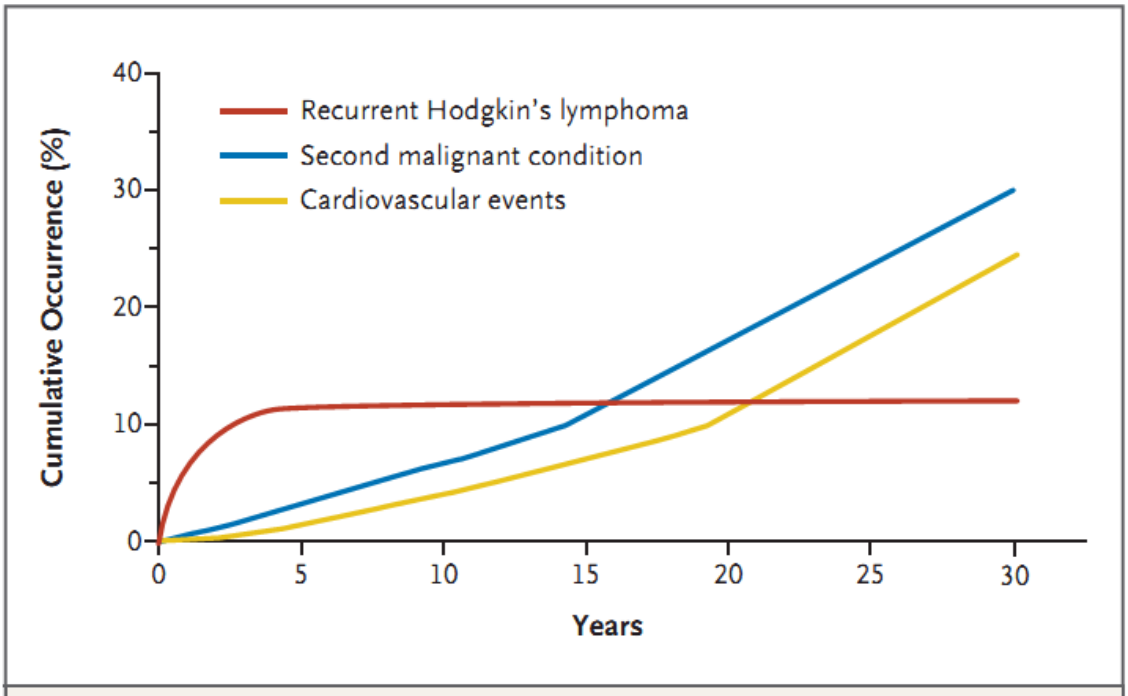

Figure 1. Approximate Cumulative Risk of Recurrent Hodgkin's Lymphoma, Second Malignant Conditions, and Cardiovascular Events among Patients Receiving Both Radiotherapy and Chemotherapy for Early-Stage Hodgkin's Lymphoma.

Figure 1-1: Competing serious outcomes for Hodgkin's lymphoma patients.[5]

1.1.2 Breast Cancer

Breast cancer is the most commonly diagnosed cancer for women, but in adolescent and young adult women breast cancer comprises only 7% of all new cancer cases per year. Breast cancer in men is rare, and less than 1% of all breast cancer cases occur in men in

Canada and the U.S.[6,2]. The five year survival for breast cancer in adolescent and young adult women is 73% [3]. The mortality rate for breast cancer in women has decreased by 25% since the mid-1980s, and this is largely attributed to effectiveness of mammographic screening and adjuvant systemic therapy[6]. However, widespread screening in asymptomatic women is typically reserved for those between the ages of 50 and 69. The poorer survival in young patients as compared to average survival for breast cancer is likely due to reduced screening, more aggressive disease, and delayed diagnosis in this age group. Breast masses are not uncommon in adolescent and young women but most are benign; malignancy accounted for between 0% and 9.5% of breast masses in a review of published series of breast masses in adolescents[7].

1.2 Secondary Effects of Radiotherapy

Exposure to ionizing radiation in the therapeutic setting can lead to acute and late side effects. Acute effects are those which occur during or immediately after radiotherapy treatment, and late effects are those which exhibit a latency period of months or years after treatment before expression. Early response to radiation damage is considered deterministic only, not occurring below a threshold dose and always occurring above the threshold dose with severity proportional to the dose. The symptoms of acute response to radiation in the thorax include esophagitis, dysphagia, heartburn, pneumonitis, and pericarditis[8]. The expression of late radiation-induced damage can be either deterministic, as in most late normal tissue responses, or stochastic, occurring with a probability increasing linearly with dose but with severity independent of dose, as in the case of carcinogenesis. Late response to thoracic radiation involves cardiovascular and

pulmonary toxicity as well as induction of secondary malignancy. The risks of the most serious late radiation-induced toxicities in thoracic radiotherapy are investigated in this work.

1.2.1 Cardiotoxicity

Evidence of radiation-induced cardiotoxicity is apparent through large-scale retrospective studies of Hodgkin's lymphoma and childhood cancer patients. In a study by Oeffinger et al. [9] of chronic health conditions of cancer survivors who were under twenty-one years of age (at the time of diagnosis between 1970 and 1986), survivors were 10 to 15 times more likely than their matched siblings to suffer from grade 3 (severe) or grade 4 (life-threatening or disabling) cardiac conditions. Aleman et al. [10] conducted a cause-specific mortality study in a cohort of Hodgkin's lymphoma patients treated between 1965 and 1987 with a median follow up of 17.8 years. Out of a total of 1261 patients, 534 (42%) had died, and among those deaths, 291 were due to Hodgkin's lymphoma, 116 were due to secondary malignancy, and 50 were due to heart disease. The excess cardiovascular mortality was highest among patients treated with radiotherapy only. In another study by Lee et al.[11] of 210 Hodgkin's lymphoma patients treated with curative radiotherapy at the University of Minnesota (between 1970 and 1986), after a median follow up of 15.6 years, 64 patients (30%) had died, and among those deaths 11 were due to Hodgkin's lymphoma, 25 were due to secondary malignancy, and 16 were due to cardiovascular failure.

Radiation induced heart disease is expressed through three different clinical manifestations: pericarditis, myocardial damage, and cardiovascular disease[12]. The latency and dose-response for each of these conditions differ. Pericarditis is considered an acute effect which may occur when more than 30% of the heart receives a dose of more than 50 Gy, and its mean latency is one year. Myocardial damage has been diagnosed at lower mean doses to the heart with a mean latency of more than 5 years. Cardiovascular disease is progressive with time but has a mean latency of 10 years, and this effect has been observed for mean heart doses as low as 5 Gy.

The mechanisms responsible for radiation-induced heart disease after radiotherapy are presently being investigated through experimental study of rats and mice. From previous studies in experimental animals, radiation exposure has been observed to cause both micro-vascular and macro-vascular disease[12]. The former is characterized by a decrease in capillary density resulting in chronic ischemic heart disease, and the latter is characterized by the increased rate of development of age-related atherosclerosis in the coronary arteries.

Other factors influence the risk of radiotherapy-associated heart disease aside from radiation dose and volume irradiated. Patient baseline cardiac risk due to age, gender, family history, smoking, etc. and cardiotoxic chemotherapy are confounding factors. In particular, anthracycline-containing chemotherapy regimens, which are used routinely for treatment of breast cancer and Hodgkin's lymphoma, are known to increase the risks of cardiomyopathy and congestive heart failure[13]. Additionally, one in four deaths among

Americans was attributable to heart disease in the general population in a cause of death for 2008 study[14].

In this work the risk of radiation-induced cardiotoxicity resulting in death was modeled. The clinical manifestations of lethal cardiotoxicity were specified as congestive heart failure resulting from ischemic heart disease, myocardial infarction, or coronary artery disease.

1.2.2 Secondary Malignancy

The development of a secondary malignancy, a cancer whose histology is distinctly different from a previously diagnosed cancer, is common among childhood survivors of cancer. In particular Hodgkin's lymphoma patients are frequently associated with the development of secondary malignancies[15]. This is attributed to both the therapy for the primary disease and also genetic predisposition. The enhanced radio-sensitivity of children is thought to be related to both the increased susceptibility to mutagenetic effects and also the high rate of cell proliferation during childhood development[16].

The risk of developing a second cancer among childhood survivors of cancer is estimated to be three to six times greater than that of the general population[17]. And although secondary malignancy is a comparatively rare complication (in a study by Oeffinger et al.[9], 2.34% of childhood cancer survivors developed a secondary malignancy whereas 34% were diagnosed with non-life-threatening chronic health conditions), it is associated with mortality[17].

There are two main types of secondary cancers following primary childhood cancer: leukemias and solid tumors. Certain secondary cancers have been observed to be more common after particular primary cancers. For Hodgkin's lymphoma patients the most common secondary cancers are breast cancer, thyroid cancer, and lung cancer. Of the female Hodgkin's lymphoma patients younger than thirty years of age and treated with radiotherapy, 30% to 40% develop breast cancer within 25 years after treatment[5]. In a German study of Hodgkin's lymphoma patients treated between 1981 and 1998, breast cancer was the most common secondary cancer for those treated between the ages of 16 and 34 (accounting for 30.8% of secondary cancers diagnosed), and lung cancer accounted for 13.3% of secondary cancers among those treated between the ages of 25 and 34[18]. Because Hodgkin's lymphoma is one of the most common first cancers associated with the development of second cancers, it is hypothesized that both the primary diagnosis and the specific therapy for treatment of Hodgkin's lymphoma contribute to the development of secondary cancer[17].

Radiation-associated breast cancer has a typical latency of 15 to 20 years from primary diagnosis in Hodgkin's lymphoma patients. The risk has been observed to be highest among patients diagnosed at a young age and also increasing with radiation dose. The breast tumors typically develop within or at the edge of the radiation fields[17].

Only induction of specific secondary malignancies is investigated in this work, but it is worth noting that non-lethal consequences of cancer therapy, such as endocrine and metabolic complications, are the most common late effects observed in survivors of childhood cancer.

1.3 Modeling Risks of Late Effects of Radiotherapy

The Emami et al.[19] paper published in 1991 compiled a comprehensive overview from literature and medical expert experience regarding normal tissue tolerance to therapeutic irradiation. The paper tabulated TD 5/5 and TD 50/5, doses at which probability of complication within five years of treatment was 5% and 50% respectively for whole and partial organ volumes. Burman et al.[20] published a paper fitting the Emami data to a Lyman[21] model where the normal tissue complication probability (NTCP) of a uniformly irradiated organ was modeled as an analytic function. The concept was taken further by Kutcher et al. [22] who proposed a method for reducing a non-uniform dose distribution into a partial volume receiving the maximum dose, termed dose-volume histogram (DVH) reduction. The model came to be known as the Lyman-Kutcher-Burman (LKB) model and is still the most widely used NTCP model[23].

Many retrospective clinical studies relating dose-volume data to outcomes using mathematical models have been published since the Emami paper. The Quantitative Analyses of Normal Tissue Effects in the Clinic (QUANTEC) papers[23] were published as an update to the Emami papers and to provide guidance on the use of toxicity risks. Biological models require validation, but they can provide useful planning constraints to be observed in the radiotherapy treatment process.

The models used in this work take into account the complete three-dimensional dose distribution throughout the organs of interest. Because organs at risk in radiotherapy patients are typically irradiated with a non-uniform dose distribution, modeling toxicity

requires a method for describing a heterogeneous dose distribution through a corresponding homogeneous partial-volume dose distribution. The parameters for a given model have been determined through retrospective fitting for observed toxicity in an irradiated population including atomic bomb survivors and long-term follow-up of radiotherapy patients.

The biological models for normal tissue toxicity serve as a useful tool for exploring possible advantages of differing radiotherapy techniques. Dosimetric comparison using parameters such as mean or maximum dose to critical organs or volumes receiving a specified dose are current clinical methods used for evaluating treatment plans. Predictive risk modeling provides another definitive method of comparison for risks of late normal tissue toxicity for radiotherapy techniques.

1.4 Thesis Objectives

1.4.1 Purpose

This study is funded by a grant from the Fonds de la Recherche en Santé du Québec (FRSQ). The project aims to develop a methodology for the evaluation of potential advantages of proton therapy among child, adolescent, and young adult cancer patients[24]. The purpose of this work, in the context of the grant, is to evaluate the risks of specific late effects of radiotherapy in adolescent and young adult patients with Hodgkin's and non-Hodgkin's lymphoma and breast cancer. The late effects investigated are cardiac mortality, induction of secondary lung cancer, and induction of secondary breast cancer. The original radiotherapy treatment plans are evaluated, and new radiotherapy plans

utilizing modulated scanning proton therapy are generated and the associated risks predicted.

1.4.2 Hypothesis

It is hypothesized that the proton therapy plans will exhibit a reduction in the risks of the specified effects when compared to the original radiotherapy plans. This is attributed to the greater normal structure sparing, particularly distal to the target, achieved with modulated scanning proton beams.

1.4.3 Thesis Outline

This thesis is organized into six chapters. Following the introduction the second chapter discusses the modern radiotherapy techniques that are being compared and also the models used to predict risks of late effects. The third chapter details the patient population, the methods used for generating proton therapy treatment plans, and the application of the models. The fourth chapter presents the results of the treatment plans and modeled risks for both radiotherapy techniques, and the fifth chapter provides discussion of these results and acknowledges some limitations. The final chapter draws conclusions from this study and proposes recommendations for future work. Derivations of the biological models used in this work are detailed in Appendices A and B, and individual patient treatment plan and risk modeling results are listed in Appendix C.

1.5 References

1. Canadian Cancer Statistics 2011. Toronto: Canadian Cancer Society, Statistics Canada, Provincial/Territorial Cancer Registries, Public Health Agency of Canada; 2011.

2. Cancer Facts & Figures 2012. Atlanta: American Cancer Society; 2012.

3. Canadian Cancer Statistics Special Topic: Cancer in Adolescents and Young Adults (15-29 Years). Toronto: Canadian Cancer Society; 2009.

4. Horning SJ. Hodgkin's Lymphoma. In: Abeloff, ed. Abeloff's Clinical Oncology. 4th ed. Philadelphia: Churchill Livingstone Elsevier; 2008.

5. Armitage JO. Early-Stage Hodgkin's Lymphoma. The New England Journal of Medicine 2010;363:653-62.

6. Canadian Cancer Statistics Special Topic: Breast Cancer. Toronto: Canadian Cancer Society; 2007.

7. Simmons PS, Jayasinghe YL, Wold LE, Melton LJ, 3rd. Breast carcinoma in young women. Obstet Gynecol 2011;118:529-36.

8. Delaney T, Kooy, H., ed. Proton and Charged Particle Radiotherapy. Philadelphia: Lippincott Williams & Wilkins; 2008.

9. Oeffinger K, Mertens, A., Sklar, C., Kawashima, T. et al. Chronic Health Conditions in Adult Survivors of Childhood Cancer. New England Journal of Medicine 2006;355:1572-82.

10. Aleman BM, van den Belt-Dusebout AW, Klokman WJ, Van't Veer MB, Bartelink H, van Leeuwen FE. Long-term cause-specific mortality of patients treated for Hodgkin's disease. J Clin Oncol 2003;21:3431-9.

11. Lee CKK, D. Aeppli, M. E. Nierengarten. The Need for Long-Term Surveillance for Patients Treated with Curative Radiotherapy for Hodgkin's Disease: University of Minnesota Experience. International Journal of Radiation Oncology Biology Physics 2000;48:169-79.

12. Andratschke N, Maurer J, Molls M, Trott KR. Late radiation-induced heart disease after radiotherapy. Clinical importance, radiobiological mechanisms and strategies of prevention. Radiother Oncol 2011;100:160-6.

13. Gagliardi G, Constine LS, Moiseenko V, et al. Radiation dose-volume effects in the heart. International journal of radiation oncology, biology, physics 2010;76:S77-85.

14. Heron M. Deaths: Leading Causes for 2008: U.S. Department of Health and Human Services, Centers for Disease Control and Prevention, National Center for Health Statistics, National Vital Statistics System; 2012.

15. Schneider U, Lomax A, Pemler P, et al. The impact of IMRT and proton radiotherapy on secondary cancer incidence. Strahlentherapie und Onkologie : Organ der Deutschen Rontgengesellschaft [et al] 2006;182:647-52.

16. Schneider U, Lomax A, Timmermann B. Second cancers in children treated with modern radiotherapy techniques. Radiotherapy and oncology : journal of the European Society for Therapeutic Radiology and Oncology 2008;89:135-40.

17. Bhatia S, Sklar C. Second cancers in survivors of childhood cancer. Nature reviews Cancer 2002;2:124-32.

18. Behringer K, Josting A, Schiller P, et al. Solid tumors in patients treated for Hodgkin's disease: a report from the German Hodgkin Lymphoma Study Group. Ann Oncol 2004;15:1079-85.

19. Emami B, Lyman, J., et al. Tolerance of Normal Tissue to Therapeutic Irradiation. International Journal of Radiation Oncology Biology Physics 1991;21:109-22.

20. Burman C, Kutcher, G.J., Emami, B., and Goitein, M. Fitting of Normal Tissue Tolerance Data to an Analytic Function. International Journal of Radiation Oncology Biology Physics 1991;21:123-35.

21. Lyman J. Complicaqtion Probability as Assessed from Dose-Volume Histograms. Radiat Res 1985;Supplement 8:S-13 - S-9.

22. Kutcher GJ, Burman, C. et al. Histogram Reduction Method for Calculating Complication Probabiliities for Three-Dimensional Treatment Planning Evaluations. International Journal of Radiation Oncology Biology Physics 1991;21:137-46.

23. Bentzen SM, Constine LS, Deasy JO, et al. Quantitative Analyses of Normal Tissue Effects in the Clinic (QUANTEC): an introduction to the scientific issues. Int J Radiat Oncol Biol Phys 2010;76:S3-9.

24. Roberge D. FRSQ-MSSS REcherches Sur le Cancer. In. Centre Universitaire de Santé McGill, Hôpital Général de Montréal: Fonds de la recherche en santé Québec; 2009.

Chapter 2

Theory

2 Theory

Historical advances in radiotherapy have improved outcomes for many with malignant disease. Revolutionary diagnostic radiology techniques, including the development of computed tomography (CT), magnetic resonance imaging (MRI), and fluorodeoxyglucose positron emission tomography (FDG-PET), allow for more precise localization of disease. Radiotherapy and computerized simulation evolved to implement this information and moved from wide-field irradiation to more conformal treatment plans. For some diseases including Hodgkin's lymphoma, radiotherapy doses have been lowered over the last several decades to reduce the adverse late effects as a reflection of the success of chemotherapy regimens as part of treatment. Careful long-term observation of radiotherapy patients and the late effects they experience provides ongoing cause for further improvements in radiotherapy. This information can also be used to predict the risks of late effects through biological modeling.

2.1 Radiotherapy and Treatment Planning

The modern approach to treatment planning involves the use of treatment planning software, which allows for the visualization of the patient anatomy in three dimensions and also calculates the dose distribution volumetrically. The user is responsible for ensuring target coverage and meeting normal tissue constraints through the selection of beam arrangement, energies, and the use of accessories. The final plan is arrived upon after a process of trial and error where the dose distribution will be calculated for an initial plan, and the plan will then be modified if target coverage or normal tissue sparing

are inadequate. The dose distribution will then be recalculated, and the process will be repeated until the plan satisfied the physician's specified criteria. For treatment plans involving the use of intensity modulated radiotherapy (IMRT), which requires inverse planning using an optimization algorithm, the iterative process converging on a final plan is automated.

2.1.1 Photon Beam Therapy

Guidelines for photon beam therapy are detailed in ICRU Report No. 62[1], which provides standardized definitions of target volumes, margins, organs at risk, and recommendations for dose conformity and homogeneity. The ideal irradiation technique would deliver the full prescription dose homogenously to the target volume and no dose to surrounding normal tissues. External beam therapy does not approach this ideal, so criteria have been developed that place restrictions on the allowable dose heterogeneity within the target. Photon therapy techniques have evolved in an effort to improve dose conformity to the target while minimizing dose to surrounding healthy tissue. The planning target volume (PTV) is based on the gross tumor volume (GTV) with a margin for microscopic disease (CTV) and additional margins to account for setup/positioning uncertainties, internal organ motion, and machine tolerances.

2.1.1.1 Three-Dimensional Conformal Radiotherapy

Three-dimensional conformal radiotherapy (3D-CRT) refers to external beam photon therapy which conforms to the prescribed dose to the target while keeping dose to specified organs at risk below dose constraints[2]. The target localization is three-

dimensional and achieved through anatomical and functional imaging. Figure 2-1 illustrates the dose distribution achievable using this technique.

Dose delivery may involve use of multileaf collimators (MLCs), shielding blocks, or wedges to shape irregular fields, shield critical organs, or compensate for missing tissue. The positions and use of these accessories are defined by the user selection.

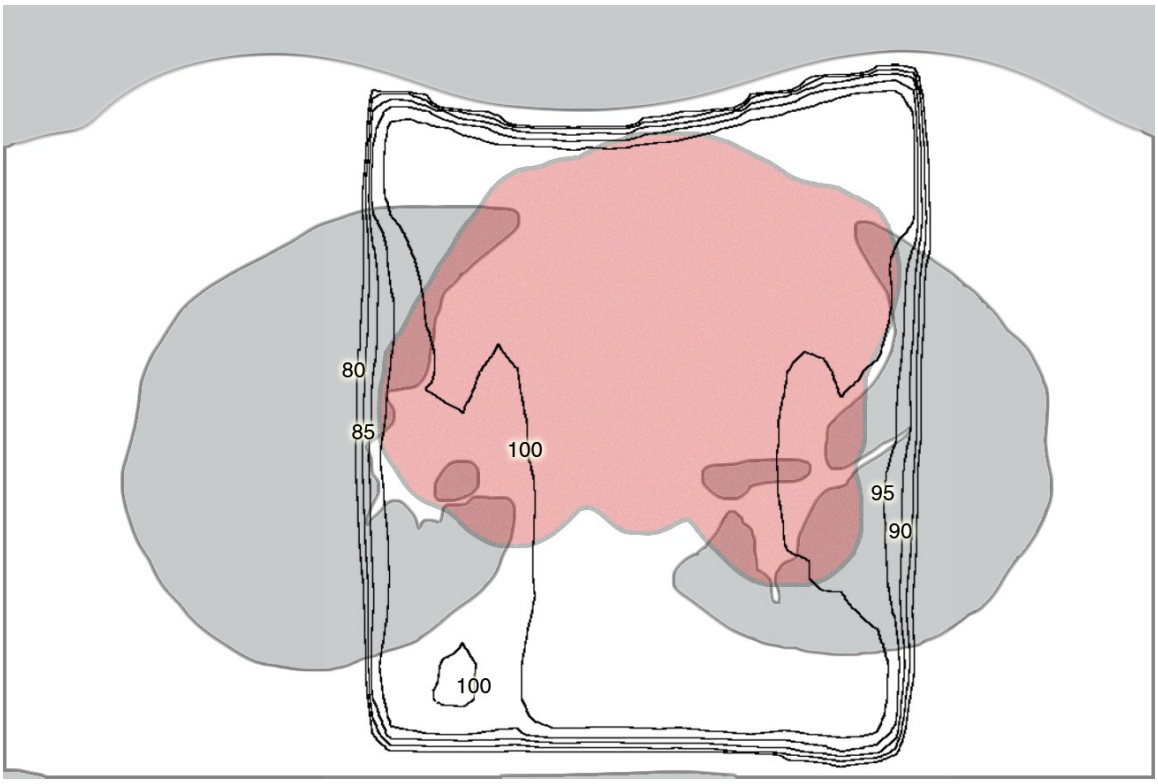

Figure 2-1: Isodose distribution drawing for two opposing anterior/posterior posterior/anterior 6 MeV photon beams, a technique common to three-dimensional conformal radiotherapy for Hodgkin's lymphoma. Target contour in red.

2.1.1.2 Intensity Modulated Radiotherapy

Intensity modulated radiotherapy (IMRT) is an advanced form of conformal radiotherapy which involves either static or dynamic MLCs to shape the field and modulate the beam

intensity. The resulting treatment plan delivers a homogeneous dose to the target and a low dose 'bath' to the surrounding normal tissues.

IMRT relies on inverse treatment planning for determining the required intensity modulated beam paths through a three-dimensional dataset of patient anatomy. The beam arrangement and energies, target objectives, and healthy tissue constraints are input by the user, and an optimization algorithm calculates the optimal intensity of each beamlet to conform to the input objectives.

2.1.2 Proton Beam Therapy

Guidelines for proton beam therapy are detailed in ICRU Report No. 78[3], which provides beam delivery and property descriptions, dosimetry techniques, treatment planning guidelines, and discussion of other important considerations. The physical properties of proton radiation therapy offer an improvement in dose conformity over 3D-CRT. This is achieved without increasing the normal tissue irradiated at a low dose as in IMRT. High energy proton beams have a finite range, and most of the dose is deposited at the end of this range forming what is known as a Bragg Peak. After the Bragg Peak, the dose deposition falls off steeply, and there is almost no exit dose. Thus proton beams offer distal dose conformity while sparing surrounding structures. This concept is illustrated in Figure 2-2.

The radiobiological characteristics of proton beams have not conclusively demonstrated significant clinical advantages over the use of x-rays, notwithstanding the relative biological effectiveness (RBE) which is 10% greater than for photons. Long term study

of patients treated with proton therapy is expected to clarify the degree of normal tissue sparing and subsequent reduction of late effects over 3D-CRT or IMRT. Treatment planning for proton beams is dependent on the delivery technique, as with photon beams. Currently photon therapy target definitions and planning margins are used for proton therapy, but it is noted in ICRU Report No. 78[3] that planning uncertainties exist for proton therapy that are not taken into account with this methodology. These additional uncertainties are in regard to the effect of heterogeneities and the algorithms used to estimate dose. Several institutions have implemented new methodology for proton therapy treatment planning, but no recognized formalism or protocol yet exists to address this issue.

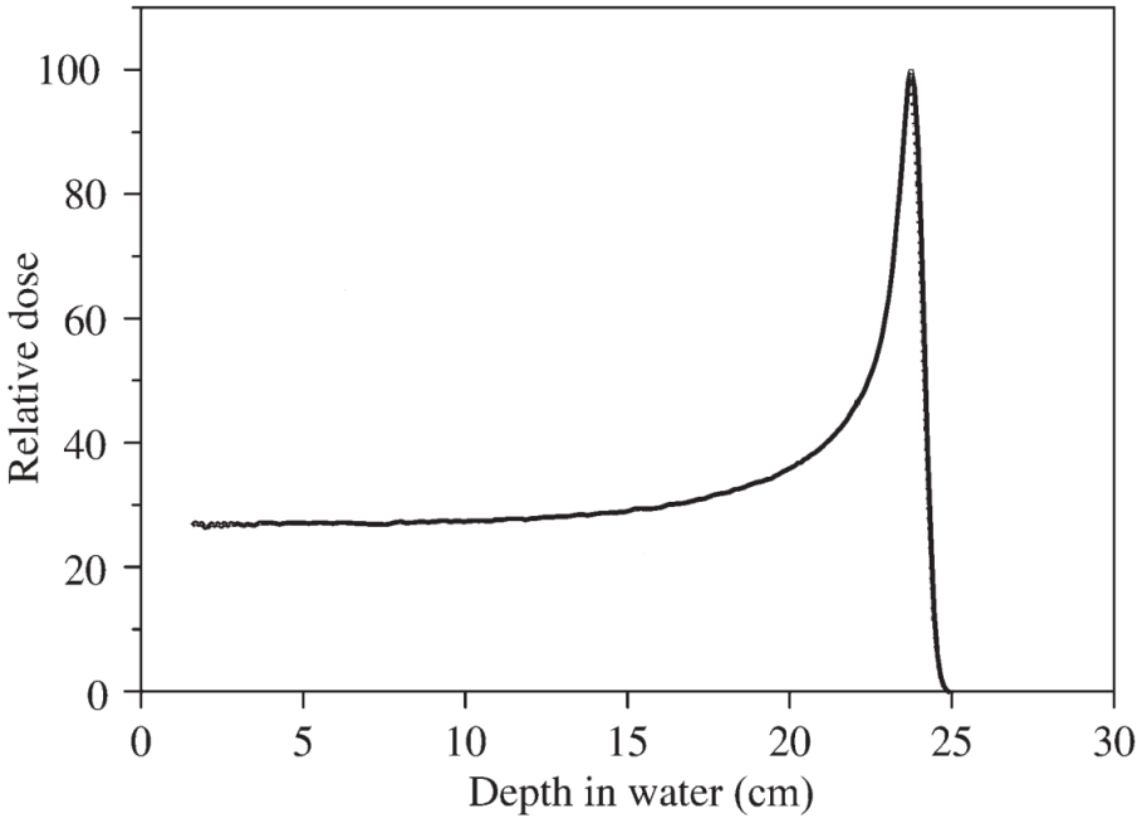

Figure 2-2: Depth dose profile in water of 200 MeV monoenergetic proton beam[3].

There are several components to proton beam therapy that play a significant role in the physical characteristics of the treatment beam. The proton beam accelerator produces a monoenergetic beam, but energy modulation may (in the case of a cyclotron) or may not (in the case of a synchrotron) require an external energy-selection system. The beam delivery technique is the next major component and may be classified as either passive or active. The passive delivery requires patient-specific collimators and field shaping devices, while the active delivery requires a sophisticated magnetic beam steering system. A more detailed discussion of the delivery systems follows.

2.1.2.1 Passive Scattering Delivery

In passive scattering delivery, the primary proton beam is scattered and degraded in a set of absorbers to create a beam whose diameter, energy range, and maximum energy deliver a uniform dose to the target at all depths. The superposition of weighted proton beams of different energies results in a Spread Out Bragg Peak (SOBP); this concept is illustrated in Figure 2-3.

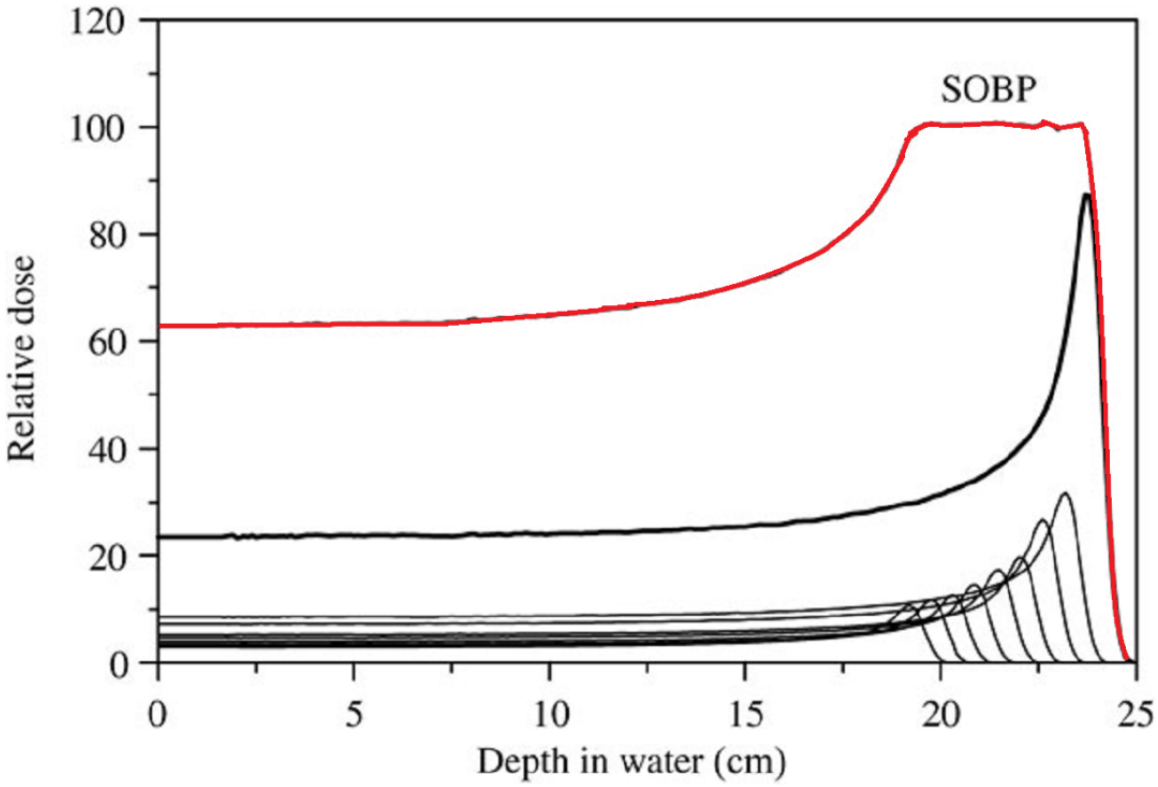

Figure 2-3: Depth dose profile in water for superposition of weighted proton beams of differing energies resulting in a spread-out Bragg peak (SOBP)[3].

The energy modulation is produced using a rotating cylinder of varying thickness or a series of plates in the path of the pencil beam. This device is called the range shifter. The lateral spread of the proton beam is achieved using one or more scattering foils, and the field is shaped using apertures to confine the beam to the projected target cross-section. A diagram of the passive scattering beam delivery system is illustrated in Figure 2-4. The single field dose distribution is then made to conform to the distal surface of the target volume using a compensator.

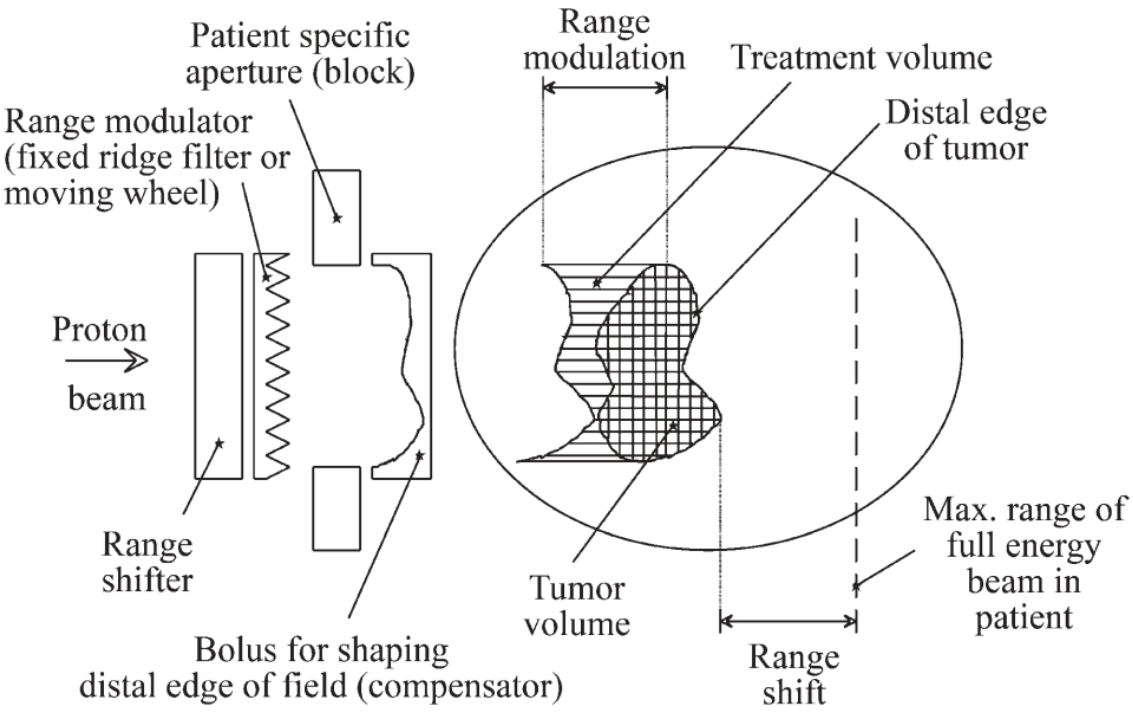

Figure 2-4: Diagram of beam delivery system devices used for beam shaping in passive scattering proton beam[3].

The advantage of the passive scattering technique is that the entire target volume is irradiated simultaneously, and this results in a lower sensitivity to the time structure and motion during delivery. Passive scattering delivery exhibits an important limitation in that the distal edge dose distribution is imposed on the proximal edge of the target volume, and this exposes normal tissue volumes in the proximal region to high dose.

Another disadvantage of this technique is that the double scattering system introduces a larger penumbra due to the large effective source size. Furthermore, the neutron contamination of the proton beam is increased for each traversal through material in the path of the beam, and so the scattering foils, range modulator, apertures, and compensator

are all sources of neutron contamination. An ideal passive scattering beam delivery system could limit the number of patient-specific devices by implementing multileaf collimators for the beam shaping, and when a synchrotron is used as the proton accelerator, a range modulator would not be necessary.

2.1.2.2 Modulated Scanning Delivery

The dynamic beam delivery system magnetically scans the proton beam across the target cross-section while changing the energy of the beam. The proton pencil beam deposits dose in spots whose location, size, and intensity are predetermined using inverse treatment planning. This concept is illustrated in Figure 2-5.

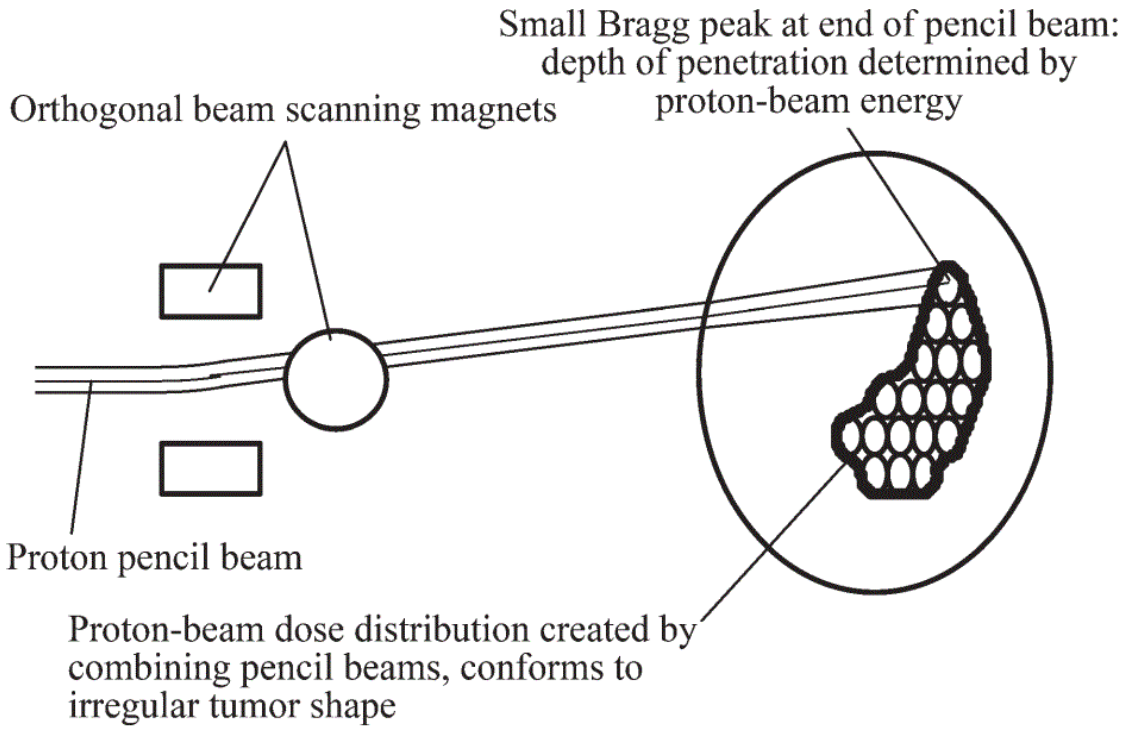

Figure 2-5: Diagram of beam delivery for variable-energy, spot scanned proton pencil beam[3].

Variation in intensity as a function of the beam position is achieved by computer-controlled scanning speed or intensity modulation. This delivery technique overcomes the disadvantages introduced in a passive scattering delivery technique because field shaping devices are not required. The dose conforms to the target in both the distal and proximal directions, and the only beam manipulation material placed in the path of the beam is the range modulator. A diagram of the modulated scanning beam delivery system is illustrated in Figure 2-6. Even the range modulation device is rendered unnecessary with the use of an energy-selection compatible proton accelerator. Thus the neutron contamination of the beam delivery system is effectively negated when compared to the passive scattering system.

The most significant advantage of modulated scanning delivery is the ability to implement intensity-modulated proton therapy (IMPT) to allow target conformity in both distal and proximal surfaces while improving normal tissue sparing. Figure 2-7 illustrates the dose distribution achievable using this technique.

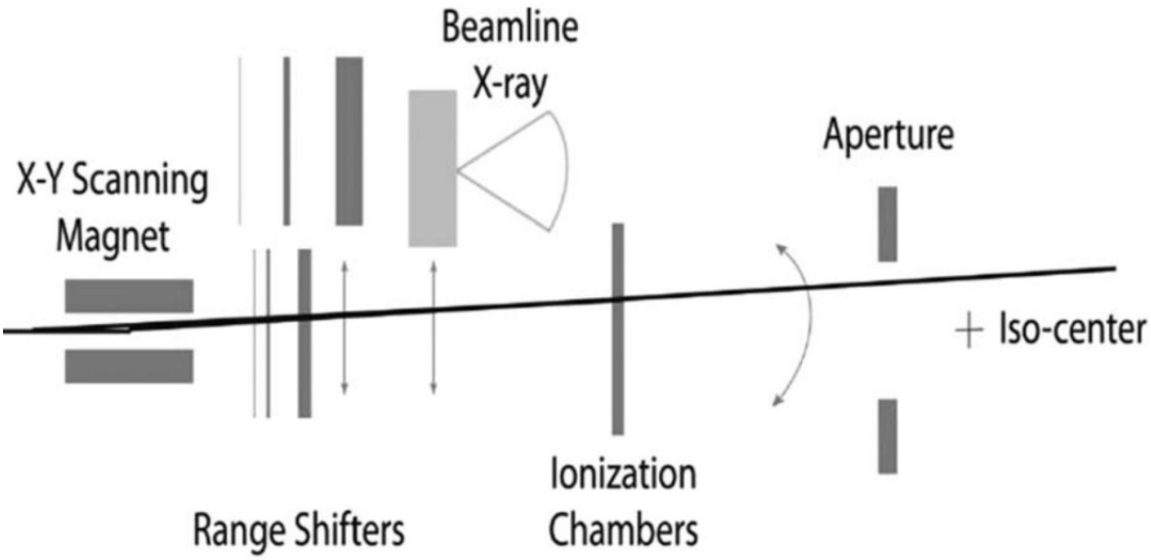

Figure 2-6: Diagram of beam delivery system devices for spot-scanned proton beam[3].

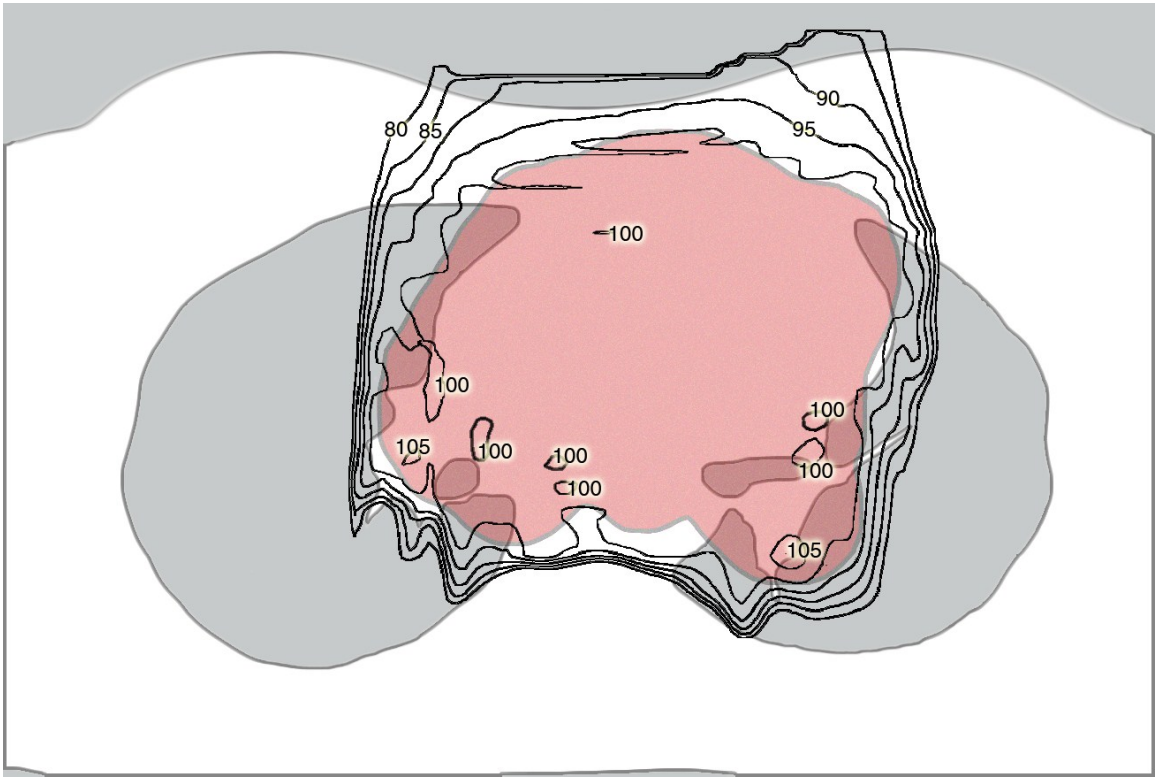

Figure 2-7: Isodose distribution drawing for intensity modulated proton therapy for Hodgkin's lymphoma. Target contour in red.

The important limitations of the modulated scanning delivery are its sensitivity to time and motion. The possible motion of the patient or internal organ motion during delivery can be compensated through repainting where the delivery of scanning pencil beams is repeated multiple times. The time required for energy modulation, the size of the target volume, and the method of scanning (whether discrete or continuous) affect the sensitivity of this technique.

The IMPT delivery technique is explored in this work for the purposes of modality comparison between photon therapy and proton therapy.

2.2 Biological Modeling

The evaluation and comparison of treatment plans can be achieved by examining dose-volume information. However, this is not necessarily a direct method of examining treatment efficacy or toxicity. Biological modeling using follow-up information from radiotherapy patients offers a method of interpreting the dose-volume data of a treatment plan to predict outcomes[4, 5]. The incidence of late-effects in a radiotherapy population has been implemented into mathematical models for the prediction of the most serious radiation-induced injuries. The use of CT data for treatment planning is a key element in the application of a model to a given data set. With this information, a patient-specific risk of a given effect can be predicted given a dose-volume distribution of a treatment plan.

2.2.1 Modeling Excess Risk of Cardiac Mortality

Modeling of radiation-induced heart disease has been addressed by few due to a number of difficulties. The definition of the cranial extent of the heart, the inclusion of the pericardium, and the definition of subvolumes such as myocardium have not been standardized[6]. Long-term follow-up from 3D-conformal radiotherapy for breast cancer and Hodgkin's lymphoma patients is relatively scarce and, furthermore, it lacks 3D dose-volume data for accurate modeling. The physical models for radiation-induced heart disease thus rely on dose-reconstruction, accomplished based on data in the recorded radiotherapy charts and the simulator films, to establish the dose distribution in the heart[7]. The selection of endpoint has not proven consistent among cardiotoxicity modeling studies. The Gagliardi group[8] modeled cardiac mortality using data from two randomized trials among breast cancer patients for adjuvant therapy after surgery. The first (Oslo) study noted death due to myocardial infarction. In the second (Stockholm) study, death from ischemic heart disease was scored. The Eriksson group[7] modeled risk of death due to ischemic heart disease among a cohort of Hodgkin's lymphoma patients treated in Stockholm. Both the LKB (Lyman-Kutcher-Berman) and the relative seriality models have been used to predict risk of cardiotoxicity, but the LKB has been shown to predict risk of pericarditis well, while the relative seriality model has been used to predict long-term cardiac mortality[6].

2.2.1.1 Correction for Fractionation Schedule

The model used for predicting risk of cardiac mortality assumes a fractionation schedule of 2 Gy per fraction. For patients whose fractionation schedule deviated from this, the dose given in standard fractionation D_s (d_s = 2 Gy) was calculated for a dose D and a dose per fraction d assuming α/β = 3 Gy by Eq. 2.1.

$$D_s = \frac{D \times \left(1 + \frac{d}{\alpha/\beta}\right)}{\left(1 + \frac{d_s}{\alpha/\beta}\right)} \qquad [2.1]$$

D_s, d_s total dose and dose per fraction for standard fractionation
D, d total dose and dose per fraction for nonstandard fractionation
α/β dose at which linear cell kill is equivalent to quadratic cell kill (in this work for late responding normal tissue)

2.2.1.2 Relative Seriality Model

The relative seriality model was used to predict the excess risk of cardiac mortality for each patient. This model incorporates the volume dependence of the radiation response of an organ. The derivation of the relative seriality model is detailed in Appendix A.

The probability $P(D)$ for a given effect for a subvolume of the organ receiving dose D is given by the Poisson statistical model for cell kill (Eq 2.2) where D_{50} is the 50% response dose and γ is the maximum value of the normalized dose-response gradient[9].

$$P(D) = 2^{-e^{e\gamma\left(1-\frac{D}{D_{50}}\right)}} \qquad [2.2]$$

P(D) probability for a given effect for a subvolume receiving dose D

D_{50} dose for 50% probability of response

γ maximum value of the normalized dose-response gradient

The probability of an organ's response is then determined based on the structure of the subunits within the organ where the organization of subunits may be classified as either serial or parallel. This concept is illustrated in Figure 2-8.

The parameter for seriality *s* is introduced as a measure of the relative seriality of the tissue Eq. 2.3[9].

$$s = \frac{m}{n \cdot m} = \frac{1}{n} \qquad [2.3]$$

s seriality term

m number of serial subunits

n number of parallel subunits

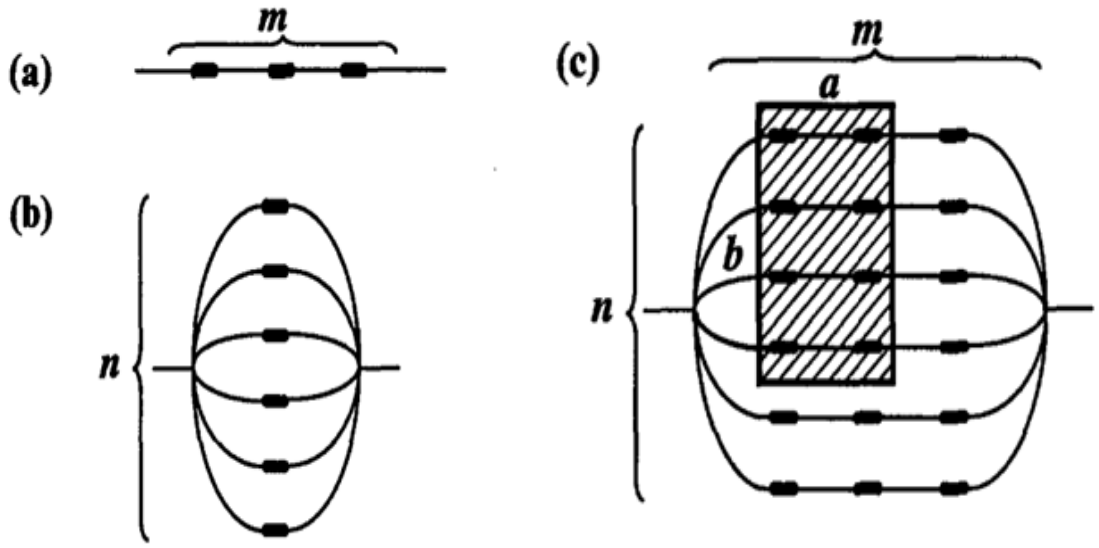

Figure 2-8: Diagram of tissue sub-volume organization. (a) *m* serial subunits, (b) *n* parallel subunits, (c) serial-parallel structure where area $a \cdot b$ is irradiated[9].

The probability of the response for the whole organ P as a function of the dose to a subvolume D_i is given by Eq. 2.4.

$$\boldsymbol{P = \left[1 - \prod_{i=1}^{M} [1 - [P(D_i)]^s]^{\Delta v}\right]^{\frac{1}{s}}} \qquad \textbf{[2.4]}$$

P probability of response of organ

$P(D)$ probability of the response of the organ for subvolume irradiated to dose D_i

s seriality term

Δv fractional volume of subvolume relative to whole organ volume

i individual subvolume

M total number of subvolumes

2.2.1.3 Parameters in the Relative Seriality Model

The values for the parameters D_{50}, γ, and *s* were drawn from fitting studies in the literature. The Gagliardi group used the χ^2 method to fit the clinical data from the Oslo and Stockholm breast cancer studies to the relative seriality model. The Eriksson group used the maximum likelihood method to fit the clinical data from the Stockholm Hodgkin's lymphoma study, and they also combined this data set with the Oslo and Stockholm breast cancer studies to form a third set of parameters. The probability of cardiac mortality at 15 years post-irradiation for a single plan was evaluated for each set of parameters and then the average was taken in this work. The values for the three sets of parameters are given in Table 2-1.

Table 2-1: Parameter values for modeling risk of cardiac mortality with the relative seriality model.

Parameter	*Gagliardi*[8] *BC*	*Eriksson*[7] *HL*	*Eriksson*[7] *BC + HL*
D_{50}, dose at which 50% probability of complication (Gy)	52.3	70.3	63.0
γ, maximum relative slope of the dose-response curve for cardiac mortality	1.28	0.96	0.94
s, relative seriality factor	1	1	1

2.2.2 Modeling Secondary Cancer

The modeling of radiation-induced secondary malignancy attempts to link the observed incidence of cancers at very low doses (as in the cases of atomic bomb survivors and

nuclear energy workers) to the medium and higher doses of radiotherapy patients. The relationship between dose and cancer-induction is linear in the low-dose region (up to 2 Gy), but at doses above 2 Gy, the dose-response relationship for cancer induction is no longer linear due to the increasing importance of the sterilization of already mutated cells[10]. The organ equivalent dose (OED) concept for radiation-induced cancer was introduced by Schneider and others[10] to evaluate the risk of cancer induction for an organ irradiated in a heterogeneous dose distribution. The OED is the dose which, if uniformly applied to an organ, corresponds to the same secondary cancer risk as the heterogeneous dose distribution.

Induction of cancer due to radiation is a stochastic effect, and the risk represents the population-based probability for the induction of cancer. The concept is more tangible when expressed as number of excess cases observed for a given population when everyone in that population is exposed to the same radiation dose. The risk for an individual person in that population is then the ratio of the number of excess cases per number of (exposed) individuals in the population. The resulting excess absolute risk for secondary cancer is therefore expressed as the number of cases per 10,000 persons (per year at a specified number of years post-irradiation).

2.2.2.1 Schneider Model

The Schneider model for risk of secondary malignancy combines the linear-quadratic model of cell kill with the linear-no-threshold model for cancer-induction at low doses[5]. The set of differential equations describes the number of cells surviving one dose fraction

N(D) for the cell kill parameter α' (known ratio for late responding tissues α/β = 3 Gy and dose per fraction *d*), the repair and repopulation rate *R(D),* and the mutational process resulting in carcinogenesis $M_c(D)$ Eq. 2.5-2.7[5].

$$\frac{dN(D)}{dD} = -\alpha' \cdot N(D) \quad [2.5.a]$$

$$\alpha' = \alpha + \beta d \quad [2.5.b]$$

$$\frac{dR(D)}{dD} = -\alpha' \cdot R(D) + \xi[N_0 - N(D) - R(D)] \quad [2.6]$$

$$\frac{dM_c(D)}{dD} = -\alpha' \cdot M_c(D) + \mu[N(D) + R(D)] \quad [2.7]$$

N(D) number of cells surviving one fraction of dose *D*

R(D) number of cells repaired and repopulated cells after one fraction of dose *D*

$M_c(D)$ number of mutated cells (resulting in carcinogenesis) after one fraction of dose *D*

μ mutation parameter (particular to organ tissue of interest)

ξ repopulation parameter (particular to organ tissue of interest)

α/β dose at which linear cell kill is equal to quadratic cell kill (in this work for normal tissue)

d dose per fraction

The differential equations are first-order nonhomogeneous linear differential equations for which solutions can be found using the set of initial conditions (Eq. 2.8.a-b) describing the number of original normal cells N_0 and initial numbers of repopulating cells and mutated cells[5].

$$N(0) = N_0 \quad [2.8.a]$$

$$R(0) = M_c(0) = 0 \quad [2.8.b]$$

The solutions for these differential equations are given as Eq. 2.9-11. The derivation is detailed in Appendix B.

$$N(D) = N_0 \cdot e^{-\alpha' \cdot D} \quad [2.9]$$

$$R(D) = \frac{N_0}{(\alpha' + \xi)}\left[\xi - \alpha' \cdot e^{-\alpha' D} - \xi \cdot e^{-\alpha' D} + \alpha' \cdot e^{-(\alpha' + \xi)D}\right] \quad [2.10]$$

$$M_c(D) = \mu N_0 \cdot \frac{e^{-\alpha' \cdot D}}{\alpha' \cdot R_f}\left[1 - 2R_f + {R_f}^2 e^{\alpha' \cdot D} - (1 - R_f)^2 \cdot e^{-\frac{\alpha' \cdot R_f}{1 - R_f} \cdot D}\right] \quad [2.11]$$

N_0 number of original cells

ξ repopulation parameter

R_f repopulation fraction

μ mutation parameter

α repairable damage component

$\alpha' = \alpha + \beta d$

α/β = 3 Gy

d dose per fraction

These solutions describe the number of original cells *N(D)*, the number of repaired and repopulated cells *R(D)*, and the number of mutated cells resulting in carcinogenesis $M_c(D)$ after one fraction of dose *D*. The Excess Absolute Risk of carcinoma in an organ EAR_{organ} is then the volume weighted sum of the number of mutated cells per the original number of cells over all subvolumes in the organ as shown in Eq. 2.12[5].

$$EAR_{organ} = \frac{M_c(D)}{N_0} = \frac{1}{V_{organ}} \sum_i V_i \cdot M_c(D_i) \qquad [2.12]$$

V_{organ} volume of the organ

V_i volume of subvolume

D_i dose to subvolume

$M_c(D)$ number of mutated cells resulting in carcinogenesis after one dose fraction D

N_0 number of original cells

The excess absolute risk for cancer induction in an organ is expressed as the number of excess cases per 10,000 persons per year.

2.2.2.2 Parameters for the Schneider Model

The values for the parameters R_f, α, and μ were drawn from fitting studies in the literature. The Schneider group[11] used the least squares method to fit the clinical data from the Travis et al.[12] study of breast cancer incidence among women treated for Hodgkin's disease. The Schneider group[13] again used the least squares method to fit the clinical data from the Travis et al. study[14] of lung cancer incidence in patients treated for Hodgkin's disease. These sets of parameters were used to model the risk for induction of secondary cancers in the lungs and breasts in this work, and their values are given in Table 2-2.

Table 2-2: Parameter values for modeling secondary cancer induction in the lungs and breasts using the Schneider model.

Parameter	*Schneider Breast Cancer*[11]	*Schneider Lung Cancer*[13]
R_f, repopulation and repair fraction	0.62	0.84
α, represents the repairable damage component from the linear quadratic model (Gy^{-1})	0.067	0.061
μ, slope of cancer induction from linear-no-threshold model *(cases per 10,000 persons per year per Gy)*	4.8	2.7

The organ-specific repopulation and repair capability R_f was fitted to a value between 0 and 1 where $R_f = 0$ indicates tissue which is unable to repopulate/repair whereas $R_f = 1$ corresponds to complete repopulation/repair. The parameter α was fitted assuming the ratio $\alpha/\beta = 3$ Gy[11]. The value for the parameter μ was taken from Preston et al. [15] and modified by the Schneider group to account for the age distribution of the Travis study cohort to which the model parameters were fitted. Thus the $\mu_{Preston}$ is the excess absolute risk for organ-specific cancer induction from the Preston et al. study expressed in units of excess cases per 10,000 persons per year per Gy. The coefficients c_1 and c_2 are organ-specific and shown in Table 2-3, and the average age at irradiation e and attained age a were modified from 30 and 70 years to 22 and 40 years respectively. The values for the parameter μ were calculated by the Schneider groups using Eq. 2.13, and the values used in this work are shown in Table 2-3.

$$\mu = \mu_{Preston} e^{\{c_1 e + c_2 \log(a)\}} \qquad [2.13]$$

Table 2-3: Parameter values used to evaluate the slope of the cancer induction risk μ.

Parameter	*Breast Cancer Induction*	*Lung Cancer Induction*
c_1	*-0.037*	*-0.02317*
c_2	*1.7*	*3.486*
$\mu_{Preston}$ *(cases per 10,000 persons per year per Gy)*	*9.2*	*7.5*
μ *(cases per 10,000 persons per year per Gy)*	*4.8*	*2.7*

2.3 References

1. ICRU Report 62: Prescribing, Recording, and Reporting Photon Beam Therapy (Supplement ot ICRU Report 50). Bethesda, Md.: International Commission on Radiation Units and Measurements; 1999.

2. Radiation Oncology Physics: A Handbook for Teachers and Students. Vienna: International Atomic Energy Agency; 2005.

3. ICRU Report 78: Prescribing, Recording and Reporting Proton-Beam Therapy. Oxford: Oxford University Press; 2007.

4. Gagliardi G, Constine LS, Moiseenko V, et al. Radiation dose-volume effects in the heart. International journal of radiation oncology, biology, physics 2010;76:S77-85.

5. Schneider U. Mechanistic model of radiation-induced cancer after fractionated radiotherapy using the linear-quadratic formula. Medical Physics 2009;36:1138.

6. Kong FM, Pan C, Eisbruch A, Ten Haken RK. Physical models and simpler dosimetric descriptors of radiation late toxicity. Semin Radiat Oncol 2007;17:108-20.

7. Eriksson F, G. Gagliardi, A. Liedberg, I. Lax, C. Lee, S. Levitt, B. Lind, L.E. Rutqvist. Long term cardiac mortality following radiation therapy for Hodgkin's disease: analysis with the relative seriality model. Radiotherapy and Oncology 2000;55:153-62.

8. Gagliardi G, I. Lax, A. Ottolenghi, L.E. Rutqvist. Long-term cardiac mortality after radiotherapy of breast cancer-application of the relative seriality model. The British Journal of Radiology 1996;69:839-46.

9. Källman P, A. Ågren, A. Brahme. Tumour and normal tissue responses to fractionated non-uniform dose delivery. International Journal of Radiation Biology 1992;62:249-62.

10. Schneider U, Zwahlen D, Ross D, Kaser-Hotz B. Estimation of radiation-induced cancer from three-dimensional dose distributions: Concept of organ equivalent dose. International journal of radiation oncology, biology, physics 2005;61:1510-5.

11. Schneider U, Sumila M, Robotka J, Gruber G, Mack A, Besserer J. Dose-response relationship for breast cancer induction at radiotherapy dose. Radiat Oncol 2011;6:67.

12. Travis LB, D. Hill, G. Dores, M. Gospodarowicz, F. van Leeuwen, E. Holowaty, M. Andersson, et al. Breast Cancer Rollowing Radiotherapy and Chemotherapy Among Young Women with Hodgkin Disease. Journal of the American Medical Association 2003;290:465-75.

13. Schneider U, Stipper A, Besserer J. Dose-response relationship for lung cancer induction at radiotherapy dose. Z Med Phys 2010;20:206-14.

14. Travis LB, M. Gospodarowicz, R. Curtis, E.A. Clarke, M. Andersson, B. Glimelius, et al. Lung Cancer Following Chemotherapy and Radiotherapy for Hodgkin's Disease. Journal of the National Cancer Institute 2002;94:182-92.

15. Preston DL, Ron E, Tokuoka S, et al. Solid cancer incidence in atomic bomb survivors: 1958-1998. Radiat Res 2007;168:1-64.

Chapter 3

Methods

3.1 Patient Cohort

Patients under investigation in this study fulfilled the following requirements:

- Patient received radiotherapy at one of the participating hospitals in the province of Quebec (Table 3-1); all radiotherapy centers in the province participated in this study
- Patient was under the thirty years of age on the date of first treatment
- Patient was treated for malignant disease with curative intent
- Patient received radiotherapy in the thorax

The chemotherapy regimens and their abbreviations are denoted in Table 3-2. Patient population characteristics are noted in Table 3-3.

Table 3-1: Participating institutions in the province of Quebec.

Name	*City*	*Abbreviation*
Hôpital Maisonneuve-Rosemont	Montreal	HMR
Montreal General Hospital	Montreal	MGH
Centre de Santé et Services Sociaux de Rimouski-Neigette	Rimouski	Rimouski
Centre de Santé et Services Sociaux de Chicoutimi	Chicoutimi	Chicoutimi
Centre Hospitalier Universitaire de Québec	Quebec City	CHUQ
Centre Hospitalier Régional de Trios-Rivières	Trios-Rivières	Trios-Rivières
Centre Hospitalier Universitaire Sherbrooke	Sherbrooke	Sherbrooke
Hôpital Général Juif	Montreal	HGJ
L'Hôpital Notre-Dame Centre	Montreal	CHUM
Centre de Santé et de Services Sociaux de Gatineau	Gatineau	Gatineau

Table 3-2: Chemotherapy regimens and abbreviations.

Chemotherapy regimen abbreviation	*Chemotherapy drugs*	
ABVD	doxorubicin bleomycin	vinblastine dacarbazine
ABVE-PC	doxorubicin bleomycin vincristine	etoposide prednisone cyclophosphamide
CHOP	cyclophosphamide doxorubicin	vincristine prednisolone
BEAM	carmustine etopisode	cytarabine melphalan
ICE	ifosfamide carboplatin etoposide	
CT	cyclophosphamide docetaxel	
none		no chemotherapy
unknown	chemotherapy administered, regimen unknown	

Table 3-3: Patient population characteristics. (Abbreviations for diagnosis: Hodgkin's lymphoma (HL), non-Hodgkin's lymphoma (NHL), breast cancer (BC).)

Patient Number	*Sex*	*Age*	*Diagnosis*	*Staging*	*Chemotherapy*	*Radiation Dose (Gy)*	*Hospital of Treatment*
Lymphoma Cohort							
1	f	28	HL	IIA	none	20	HGJ
2	m	17	HL	IIIA	ABVE-PC	21	CHUM
3	f	15	HL	IVA	ABVE-PC	21	CHUQ
4	m	12	HL	IVA	ABVE	21	CHUM
5	m	21	HL	IIBX	ABVD	21	CHUM
6	f	14	HL	IVA	ABVE-PC	21	CHUM
7	f	29	HL	IIA	ABVD	21	CHUM
8	m	17	HL	IIA	ABVE-PC	21	CHUM
9	m	27	HL	IIA	ABVD	21	CHUM
10	m	23	HL	IV-EBX	ABVD	21	CHUM
11	m	21	HL	IIB	none	26.5	MGH
12	m	19	HL	IB	ABVD	30	HMR
13	f	28	HL	IIIB	ABVD, ICE, BEAM	30	HGJ
14	m	26	NHL	IIA	CHOP	30	CHUQ
15	f	18	HL	IIB	ABVD	30	Trois-Rivieres
16	m	23	HL	IIA	unknown	30	HMR
17	m	19	HL	IIA	ABVD	30.6	Chicoutimi
18	m	26	HL	IIB	ABVD	30.6	Rimouski
19	f	29	HL	IIA	ABVD	30.6	CHUM
20	f	25	NHL	IIB	CHOP	30.6	CHUM
21	f	20	HL	IIAX	ABVD	30.6	CHUM
22	f	26	HL	IIA	ABVD	30.6	CHUM
23	m	27	HL	IA	ABVD	36	Trois-Rivieres
24	f	27	HL	IIB	BEAM	36	Gatineau
Breast Cancer Cohort							
1	f	23	BC	IIB	none	50	MGH
2	f	28	BC	III	none	50	Sherbrooke
3	f	29	BC	IA	CT	42.4	HGJ
4	f	28	BC	III	unknown	50	CHUM

3.2 Target and Organs at Risk Delineation

The planning target volume (PTV) as specified by the treating physician was not modified for this study, and thus the new proton plans were references to the original PTV for the purposes of plan comparison. Where a PTV was not contoured (for one HL patient and all four BC patients), a single physician from our institution contoured an estimate of the PTV based on the dose distribution in the treated volume of the photon plans.

The organs at risk (OAR) for this work were specified as the heart, the lungs, and the breasts; the latter solely for female patients. Prior to planning, these organs were contoured for each patient's CT set using Eclipse treatment planning software (version 10, Varian Medical Systems, Palo Alto, CA, USA). Upon examination after the data collection, the structures contoured and their boundaries were found to be inconsistent among patients. A methodology was developed for the purpose of imposing consistency and accuracy in the definition of OARs. All contouring was done by the author whereupon approval by a single physician was sought.

3.2.1 Heart

The Feng heart atlas[1] was used as a benchmark for the delineation of the heart volume. This atlas was developed specifically for the study of cardiac exposure to radiation during radiotherapy. The superior limit of the heart was taken as "just inferior to the left pulmonary artery," and the inferior limit was reached at the slice in which "the heart

blends with the diaphragm." The superior vena cava was included in the heart volume, and the descending aorta was excluded.

3.2.2 Lungs

The lung volume was initially defined using the auto-segmentation lung wizard in Eclipse. The volume was then modified to exclude the carina and to form smooth, non-overlapping boundaries with the heart.

3.2.3 Breasts

The White et al.[2] breast cancer atlas was used as a benchmark for the delineation of the breast volumes. This atlas was developed to provide consensus definitions for radiotherapy for breast cancer. The cranial and caudal boundaries include reference to clinical palpation, but as definition through palpation was not possible in this work, the author outlined an initial estimate of the breast volume which was later approved or modified by a single physician. In accordance with the breast cancer atlas, the anterior limit was taken as the skin, and the posterior limit excluded the chestwall muscles, ribs, and the pectoralis muscles. The lateral boundary was taken as the mid-axillary line, and the medial boundary as the sternal-rib junction.

3.3 Treatment Planning

3.3.1 Photon Treatment Plan Characteristics

Dose distributions resulting from original 3D-CRT plans were imported into the treatment planning system "as is," in terms of absolute dose, for this work. The plan characteristics were similar among all patients for each disease site and are described below.

All Hodgkin's lymphoma and non-Hodgkin's lymphoma patients were treated with the same beam configuration technique: parallel opposed anterior-posterior/posterior-anterior (AP/PA). A pair of photon beams at gantry angles of 0 degrees and 180 degrees were used, and a multileaf collimator was used to define the field so as to conform to the anterior-posterior projection of the target volume. The dose distribution resulting from this technique is shown in Figure 3-1. The energies of photon beams used in the patient cohort varied, but all plans used beams of one or more of the following energies: 6 MV, 10 MV, 18 MV, and 23 MV.

The breast cancer patients were treated with a single anterior-posterior beam for nodal irradiation in addition to their chest wall and tumor bed treatments (tangential opposed wedged beams and oblique electron boost). The dose distributions resulting from the photon techniques are shown in Figure 3-2.

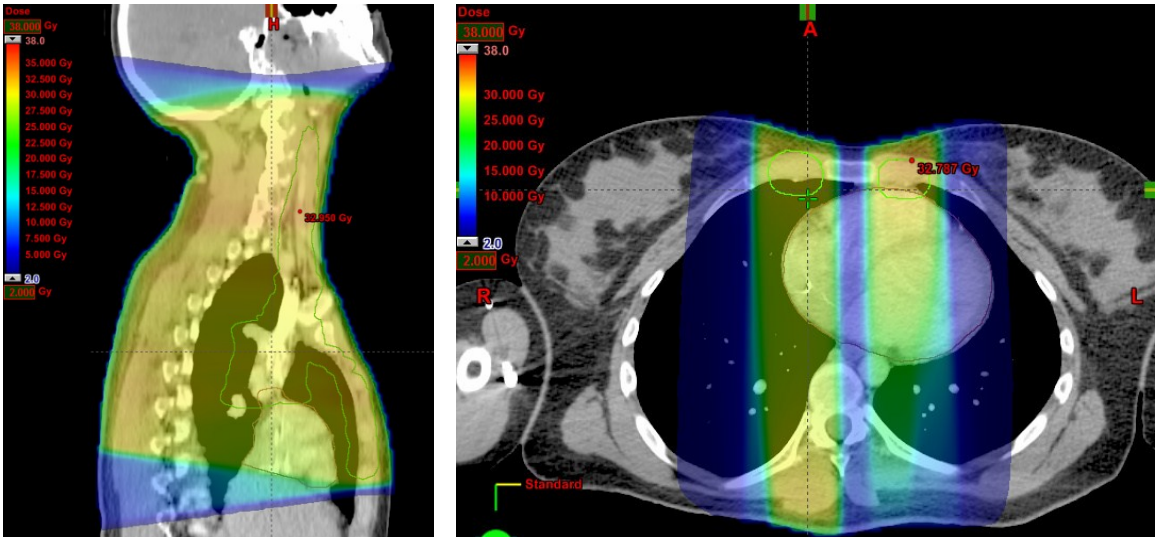

Figure 3-1: 3D-CRT treatment plan for HL patient; sagittal (left) and axial (right) dose distribution for same patient in this study. Dose colorwash lower limit 2 Gy, upper limit 38 Gy, PTV contour in green.

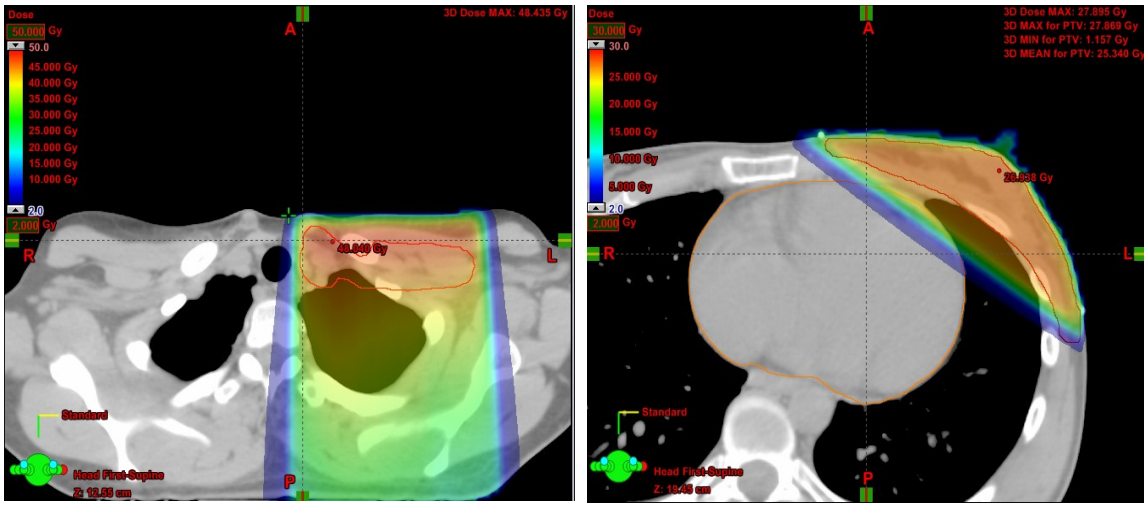

Figure 3-2: 3D-CRT treatment plan for BC: Left single AP field for nodal irradiation; Right tangential opposed wedged beams for remaining breast irradiation. Note: two different patients are shown in this figure.

3.3.2 Proton Treatment Planning

Proton treatment planning was performed using Eclipse treatment planning software (version 10.0, Varian Medical Systems, Palo Alto, California). The modulated scanning proton beam mode was selected, and the proton convolution superposition algorithm (version 8.08.9, Varian Medical Systems) was used for dose calculation. The proton optimization algorithm is based on a dose deposition coefficients matrix where the spots are located on a rectangular grid of points. The dose at each point for a given distribution of spot weights is calculated, and then the optimizer is run to find the weight distribution that minimizes the difference between actual dose and prescribed dose at each point [3]. The optimizer requires user input for beam number and angles as well as target and OAR definitions and constraints.

The general guidelines in Table 3-4 were observed in the treatment planning process; these were drawn from the chapter on treatment planning in ICRU Report 78: Prescribing, Reporting, and Recording Proton-Beam Therapy[4].

Table 3-4: Treatment planning guidelines inferred from ICRU Report 78.

Avoid	*Consider*
Complex heterogeneity	Lack of skin sparing
Surface irregularity	Lateral and distal/proximal margins may differ
Aiming directly at sensitive structures	

3.3.3 Proton Planning Stratagems

The goal for target coverage was defined as covering 100% of the PTV with 90% of the prescribed dose (ie $V_{90\%} = 100\%$). This was based on what was dosimetrically achievable in accordance with our planning experience and the proton dose optimizer available to us. For planning purposes only, a margin of 2 mm was added to the PTV to ensure the target. Structures modifying the OARs to exclude PTV were created to avoid conflicts in the optimization process where there was overlap between the PTV and the OARs. An avoidance ring was created from extracting the wall of the PTV + 2mm and adding an outer margin of 3 cm. The beam number and arrangement were modified when inadequate target coverage was observed (ie $V_{90\%} < 90\%$). The spot weights selected by the optimizer would sometimes result in hotspots where the local dose value was greater than 120% of the prescription dose. The choice of beamlet weights was not supported for the scanning delivery technique[3] in Eclipse (version 8.9). The hotspots were therefore resolved by creating small avoidance structures around the hot spots and applying an upper constraint in the optimizer.

3.3.4 Application of the Models

The dose-volume data for each patient's photon and proton plans were exported from Eclipse (version 10, Varian Medical Systems, Palo Alto, California) in DICOM-RT format and converted into MATLAB (R2008a, The Mathworks Inc., Natick, Massachusetts) matrix format using the Computational Environment for Radiation

Research (CERR) platform (version 4.0 Beta 4, Washington University in St. Louis, Missouri) for this analysis.

A maximum probability for cardiac mortality was computed for each patient using Eq. 2.2 where the dose to the organ *D* was set to the prescription dose to the target. The model for cardiac mortality assumes a 2 Gy / fraction schedule; therefore all patients who received a fractionation scheme differing from 2 Gy/fraction were corrected for a biologically equivalent dose[5] using Eq. 2.1. Excess risk of cardiac mortality at fifteen years post-irradiation was computed for each patient using Eq. 2.4 for each set of parameters (Table 2-1); again the dose in each voxel was corrected for a fractionation scheme differing from 2 Gy/fraction schedule using Eq. 2.1.

Excess absolute risk of lung and breast cancer at thirty years post-irradiation was computed for each patient assuming an α/β ratio of 3 Gy which is the accepted α/β for late effects[6]. A maximum excess absolute risk of induction of lung and breast cancer was computed for each patient (risk of breast cancer for female patients only) using Eq. 2.12 where $M_c(D)$ was computed for dose *D* set to the prescription dose to the target. These values were taken as representative of 'maximum excess risks' against which the values for probability of cardiac mortality and secondary cancer resulting from the heterogeneous dose distributions of the IMPT and 3D-CRT plans were compared.

3.4 References

1. Feng M, Moran JM, Koelling T, et al. Development and validation of a heart atlas to study cardiac exposure to radiation following treatment for breast cancer. International Journal of Radiation Oncology Biology Physics 2011;79:10-8.

2. White J, A. Tai, D. Arthur, T. Buchholz, et al. Breast Cancer Atlas for Radiation Therapy Planning: Consensus Definitions.

3. Proton Algorithm Reference Guide. In: Varian Medical Systems; 2009.

4. ICRU Report 78: Prescribing, Recording and Reporting Proton-Beam Therapy. Oxford: Oxford University Press; 2007.

5. Fowler J. Brief Summary of Radiobiological Principles in Fractionated Radiotherapy. Seminars in Oncology 1992;2:16-21.

6. Andratschke N, Maurer J, Molls M, Trott KR. Late radiation-induced heart disease after radiotherapy. Clinical importance, radiobiological mechanisms and strategies of prevention. Radiother Oncol 2011;100:160-6.

Chapter 4

Results

4.1 Treatment planning results

4.1.1 Hodgkin's Lymphoma Case

Planning results for a single Hodgkin's lymphoma patient in the lymphoma cohort are presented below. The planning target volume is shown in Figure 4-1. The heart and body contours are also shown in this image for perspective. The photon and proton plan dose distributions are shown in Figure 4-2. The dose volume histograms in Figure 4-4 show the cumulative dose-volumes for the planning target volume and the heart, the lungs, and the breasts. Dosimetric indices for heart, lungs, and breasts are shown for each modality with a percent reduction in Table 4-1.

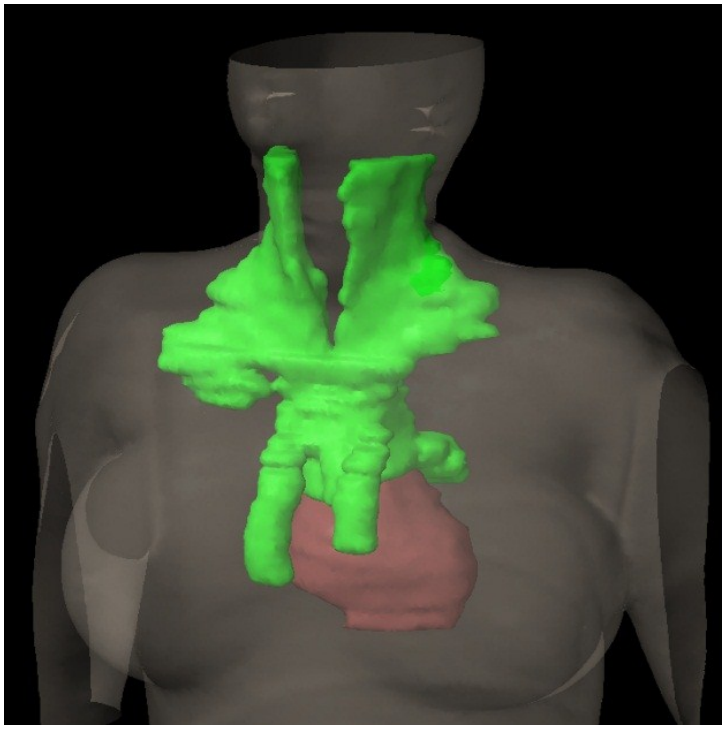

Figure 4-1: Body contour (grey), PTV (green), and heart (red) for Hodgkin's lymphoma case.

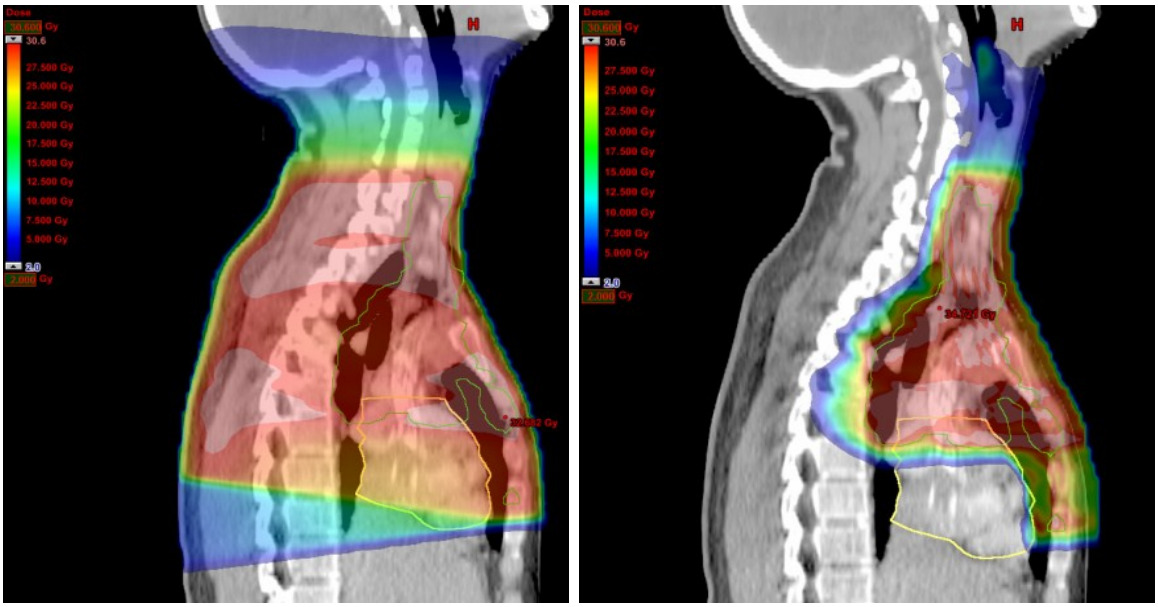

Figure 4-2: Hodgkin's lymphoma case dose distribution comparison (left) 3D-CRT plan (right) IMPT plan. PTV (green), heart (yellow). Dose color wash upper limit 30.6 Gy, lower limit 2 Gy.

Table 4-1: Dosimetric indices for Hodgkin's lymphoma case.

Dosimetric Index for *Organ at Risk*	*Treatment Modality* 3D-CRT	IMPT	% Reduction
Heart			
mean dose (Gy)	15.9	5.3	67
$V_{2\ Gy}$ (%)	83.8	26.0	69
$V_{5\ Gy}$ (%)	65.7	22.2	66
V_{Rx} (%)	8.2	5.0	39
Lungs			
mean dose (Gy)	15.1	8.2	46
$V_{20\ Gy}$ (%)	41.9	21.8	48
$V_{5\ Gy}$ (%)	59.1	37.1	37
Breasts			
mean dose (Gy)	1.7	0.6	65
$V_{2\ Gy}$ (%)	10.5	3.4	32
$V_{5\ Gy}$ (%)	5.3	2.9	45

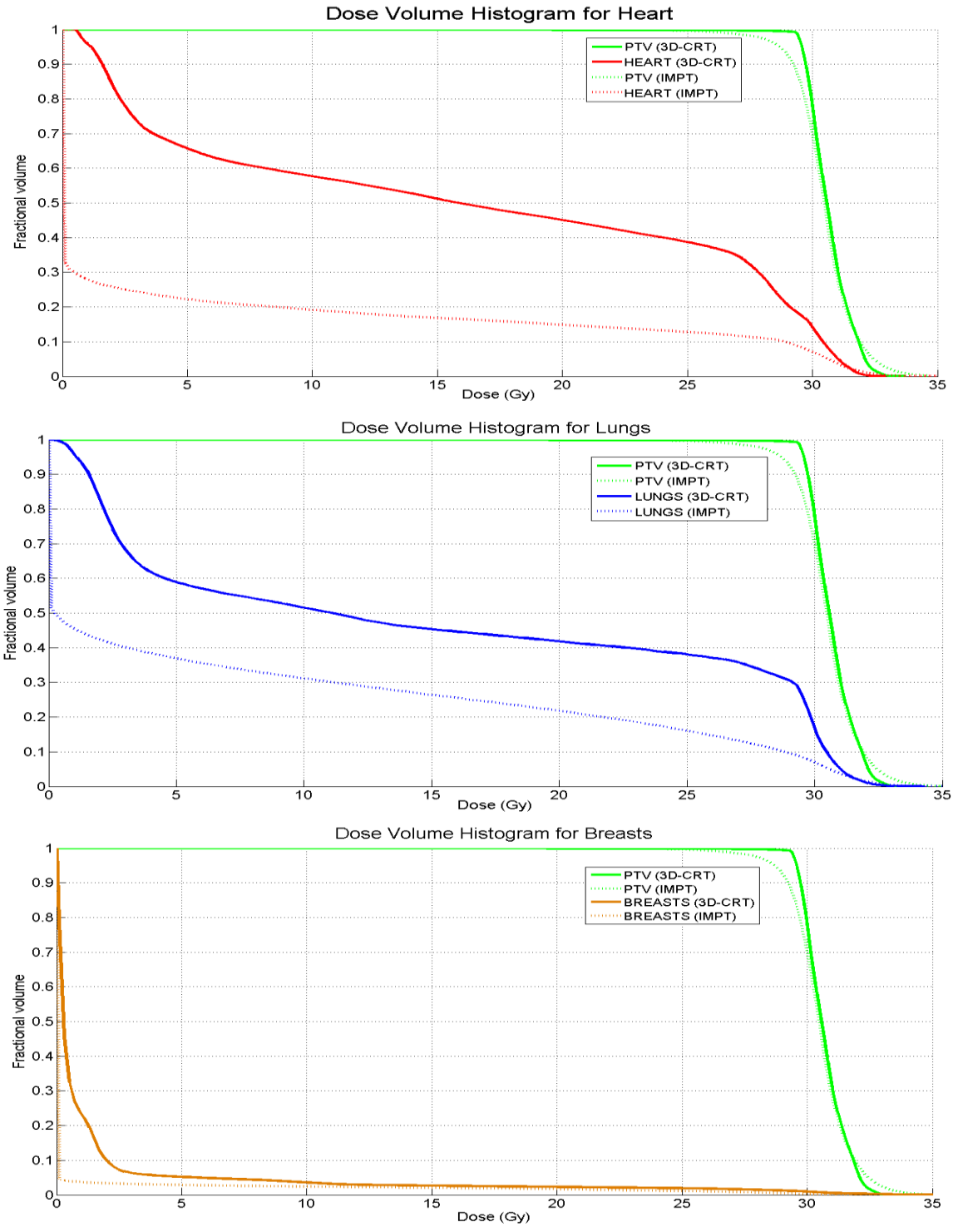

Figure 4-3: Dose volume histograms for Hodgkin's lymphoma case. (Top) PTV and Heart, (Middle) PTV and lungs, (Bottom) PTV and breasts. [Note: The IMPT planning aim for PTV $V_{90\%}$ = 100% could not be achieved for this patient.]

4.1.2 Lymphoma Cohort

4.1.2.1 Dose to Heart

The mean, range, and standard deviations of selected dosimetric indices for the heart for the lymphoma cohort are shown in Table 4-2. The relative volume of heart receiving 2 Gy in the 3D-CRT plan versus the IMPT plan is shown for all patients in the lymphoma cohort in Figure 4-4. The $V_{2\ Gy}$ is lower for all IMPT plans than for the corresponding 3D-CRT plans; the line in Figure 4-4 indicates the point at which the $V_{2\ Gy}$ for IMPT is equal to the $V_{2\ Gy}$ for 3D-CRT. The points farthest from this line are the patients for whom the largest absolute reduction in $V_{2\ Gy}$ was observed. The flared point indicates the Hodgkin's lymphoma case selection presented in 4.1.1. The maximum relative volume of heart receiving the low dose of 2 Gy among the lymphoma cohort was 95% for 3D-CRT plans and 67% for IMPT. On average, the IMPT plans reduced the relative volume of heart receiving 2 Gy by 41%.

Table 4-2: Dosimetric indices for heart for lymphoma cohort. Individual patient results in Appendix C: Table C-1.

Dosimetric Index *Heart*	*Statistic*	*3D-CRT*	*IMPT*
$V_{2\ Gy}$ (%)	mean	49.7	30.7
	range	0 - 94.5	0 - 63.0
	sd	26.8	18.7
$V_{5\ Gy}$ (%)	mean	40.4	27.4
	range	0 - 82.7	0 - 63.0
	sd	23.4	17.6
V_{Rx} (%)	mean	8.0	7.1
	range	0 - 31.0	0 - 40.5
	sd	7.3	8.8

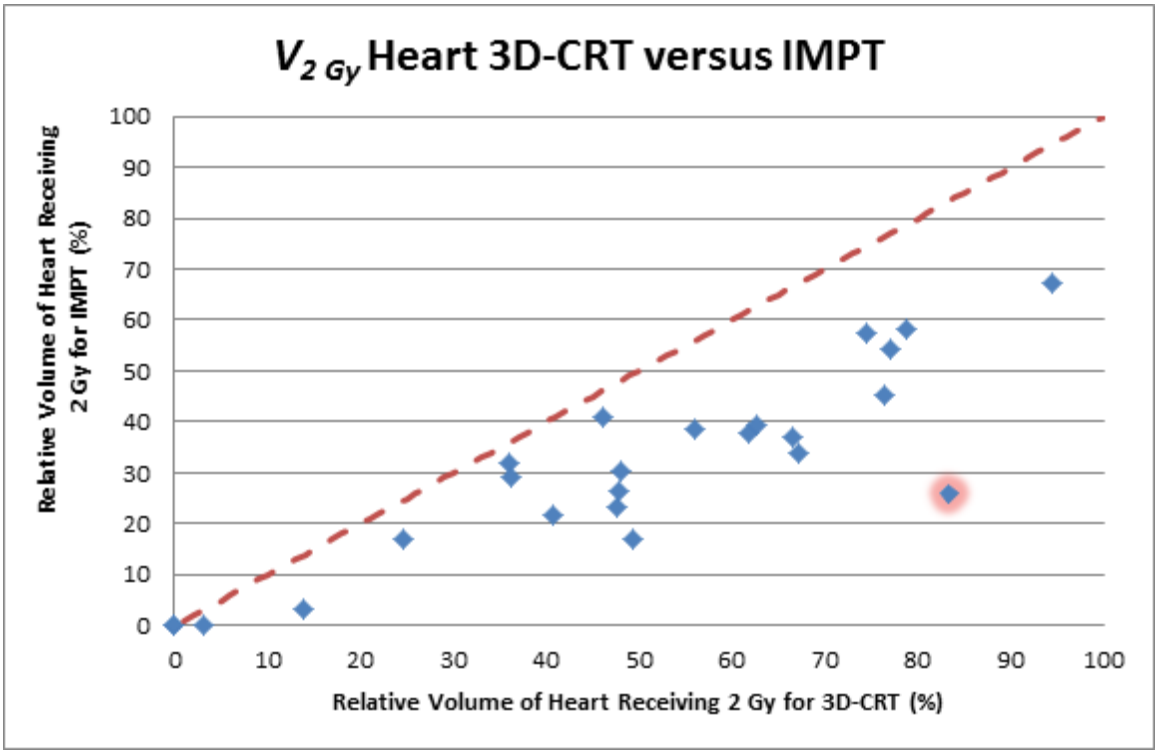

Figure 4-4: Relative volume of heart receiving dose of 2 Gy or greater for lymphoma patient cohort for IMPT versus 3D-CRT. Dashed line indicates equal $V_{2\ Gy}$ (heart) between the two modalities. Flared point represents the Hodgkin's lymphoma case selection presented in 4.1.1.

4.1.2.2 Dose to Lungs

The mean, range, and standard deviations of selected dosimetric indices for the lungs for the lymphoma cohort are shown in Table 4-3. The relative volume of lungs receiving 20 Gy in the 3D-CRT plan versus the IMPT plan is shown for all patients in the lymphoma cohort in Figure 4-5. The $V_{20\ Gy}$ is lower for all IMPT plans than for the corresponding 3D-CRT plans; the line in Figure 4-5 indicates the point at which the $V_{20\ Gy}$ for IMPT is equal to the $V_{20\ Gy}$ for 3D-CRT. The points farthest from this line are the patients for whom the largest absolute reduction in $V_{20\ Gy}$ was observed. The maximum relative volume of lungs receiving an intermediate dose of 20 Gy among the lymphoma cohort

was 42% for 3D-CRT plans and 22% for IMPT. On average, the IMPT plans reduced the relative volume of lungs receiving 20 Gy by 54%.

Table 4-3: Dosimetric results for lungs for lymphoma cohort. Individual patient results in Appendix C: Table C-3.

Dosimetric Index *Lungs*	*Statistic*	*3D-CRT*	*IMPT*
Mean Lung Dose (Gy)	mean	8.6	4.7
	range	3.1 - 15.1	1.1 - 8.15
	sd	3.0	1.8
$V_{20\ Gy}$ (%)	mean	23.0	10.3
	range	2.5 - 41.9	0.5 - 21.8
	sd	2.8	5.8
V_{Rx} (%)	mean	6.0	2.8
	range	0.5 - 17.6	0.3 - 6.2
	sd	4.4	1.6

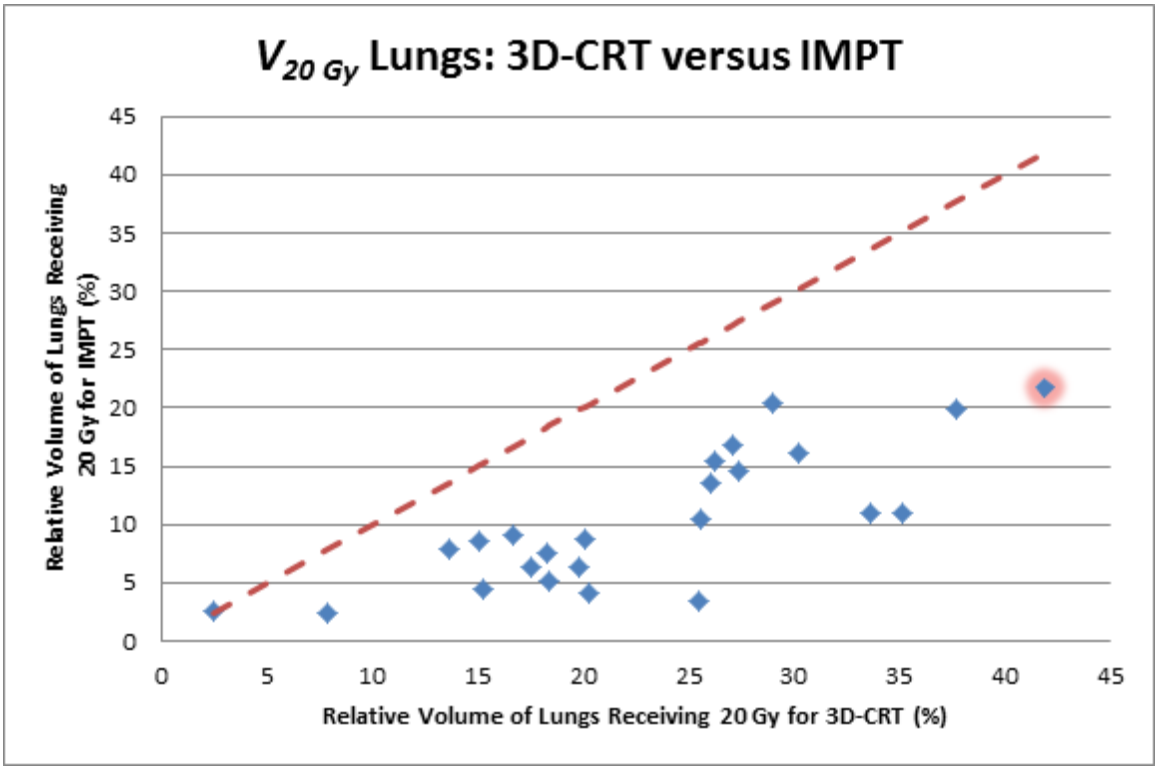

Figure 4-5: Relative volume of lungs receiving dose of 20 Gy or greater for lymphoma patient cohort for IMPT versus 3D-CRT. Dashed line indicates equal $V_{20\ Gy}$ (lungs) between the two modalities. Flared point represents the $V_{20\ Gy}$ for the Hodgkin's lymphoma case selection presented in 4.1.1.

4.1.2.3 Dose to Breasts

The mean, range, and standard deviations of selected dosimetric indices for the breasts for the female lymphoma patients are shown in Table 4-4. The relative volume of breasts receiving 2 Gy in the 3D-CRT plan versus the IMPT plan is shown for all patients in the lymphoma cohort in Figure 4-6. The $V_{2\ Gy}$ is lower for all IMPT plans than for the corresponding 3D-CRT plans; the line in Figure 4-6 indicates the point at which the $V_{2\ Gy}$ for IMPT is equal to the $V_{2\ Gy}$ for 3D-CRT. The points farthest from this line are the patients for whom the largest absolute reduction in $V_{2\ Gy}$ was observed. The maximum relative volume of breasts receiving a dose of 2 Gy among female patients in the

lymphoma cohort was 33% for 3D-CRT plans and 15% for IMPT. On average, the IMPT plans reduced the relative volume of breasts receiving 2 Gy by 56%.

Table 4-4: Dosimetric results for breasts for female patients in lymphoma cohort. Individual patient results in Appendix C: Table C-5.

Dosimetric Index *Breasts*	*Statistic*	*3D-CRT*	*IMPT*
$V_{2\,Gy}$ (%)	mean	13.6	6.1
	range	1.7 - 32.8	0.1 - 14.5
	sd	10.0	4.6
$V_{5\,Gy}$ (%)	mean	10.6	5.1
	range	1.1 - 33.9	0.0 - 12.1
	sd	9.8	4.0
V_{Rx} (%)	mean	2.1	0.0
	range	0.0 - 5.8	0.0 - 0.1
	sd	2.2	0.0

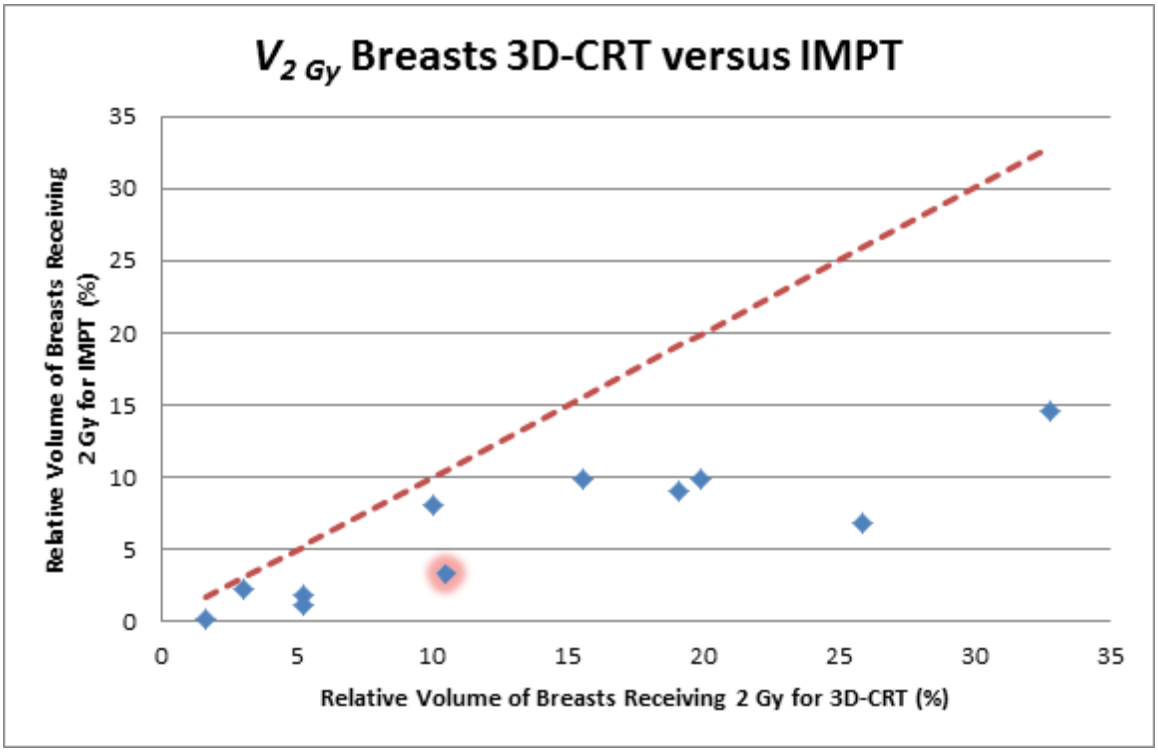

Figure 4-6: Relative volume of breasts receiving dose of 2 Gy or greater for female lymphoma patients for IMPT versus 3D-CRT. Dashed line indicates equal $V_{2\ Gy}$ (breasts) between the two modalities. Flared point represents the Hodgkin's lymphoma case selection presented in 4.1.1.

4.1.3 Breast Cancer Case

Planning results for a single breast cancer patient in the breast cancer cohort are presented below. The planning target volume is shown in Figure 4-7. The lung and body contours are also shown in this image for perspective. Dosimetric indices are shown in Table 4-5. The photon and proton plan dose distributions are shown in Figure 4-8. The dose volume histograms in Figure 4-9 show the cumulative dose-volumes for the planning target volume and the heart and lungs.

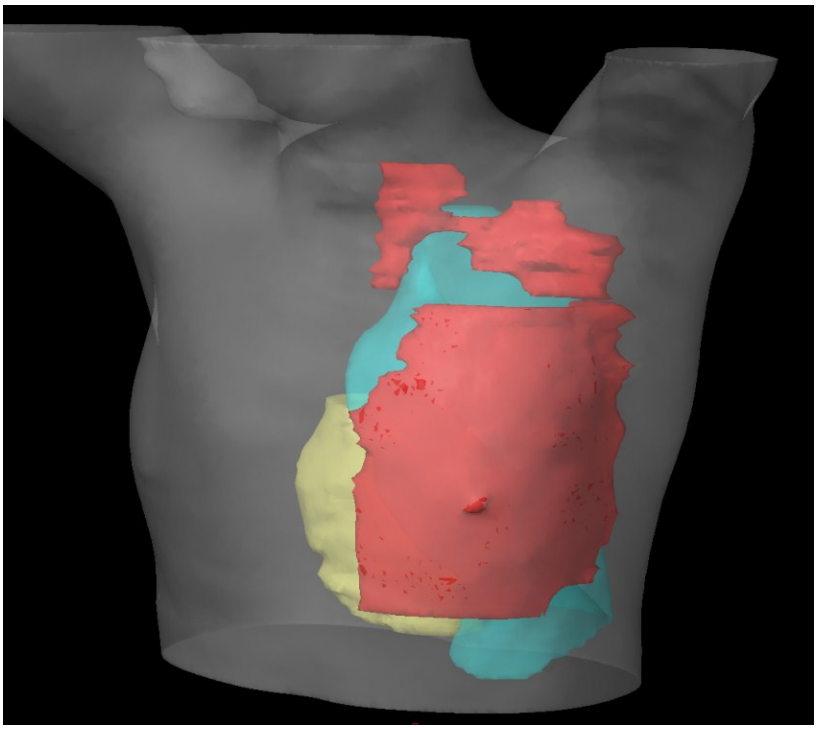

Figure 4-7: Body contour (grey), PTV (red), heart (yellow), and ipsilateral lung (blue) for breast cancer case.

Table 4-5: Dosimetric indices for breast cancer case.

Dosimetric Index for *Organ at Risk*	*Treatment Modality*		% Reduction
	3D-CRT	IMPT	
Heart			
mean dose (Gy)	4.1	0.7	83
$V_{2\ Gy}$ (%)	23.4	4.8	79
$V_{5\ Gy}$ (%)	10.6	3.5	67
V_{Rx} (%)	0.0	0.0	0
Lungs			
mean dose (Gy)	12.5	6.8	46
$V_{20\ Gy}$ (%)	26.7	14.7	45
$V_{5\ Gy}$ (%)	32.6	27.9	14

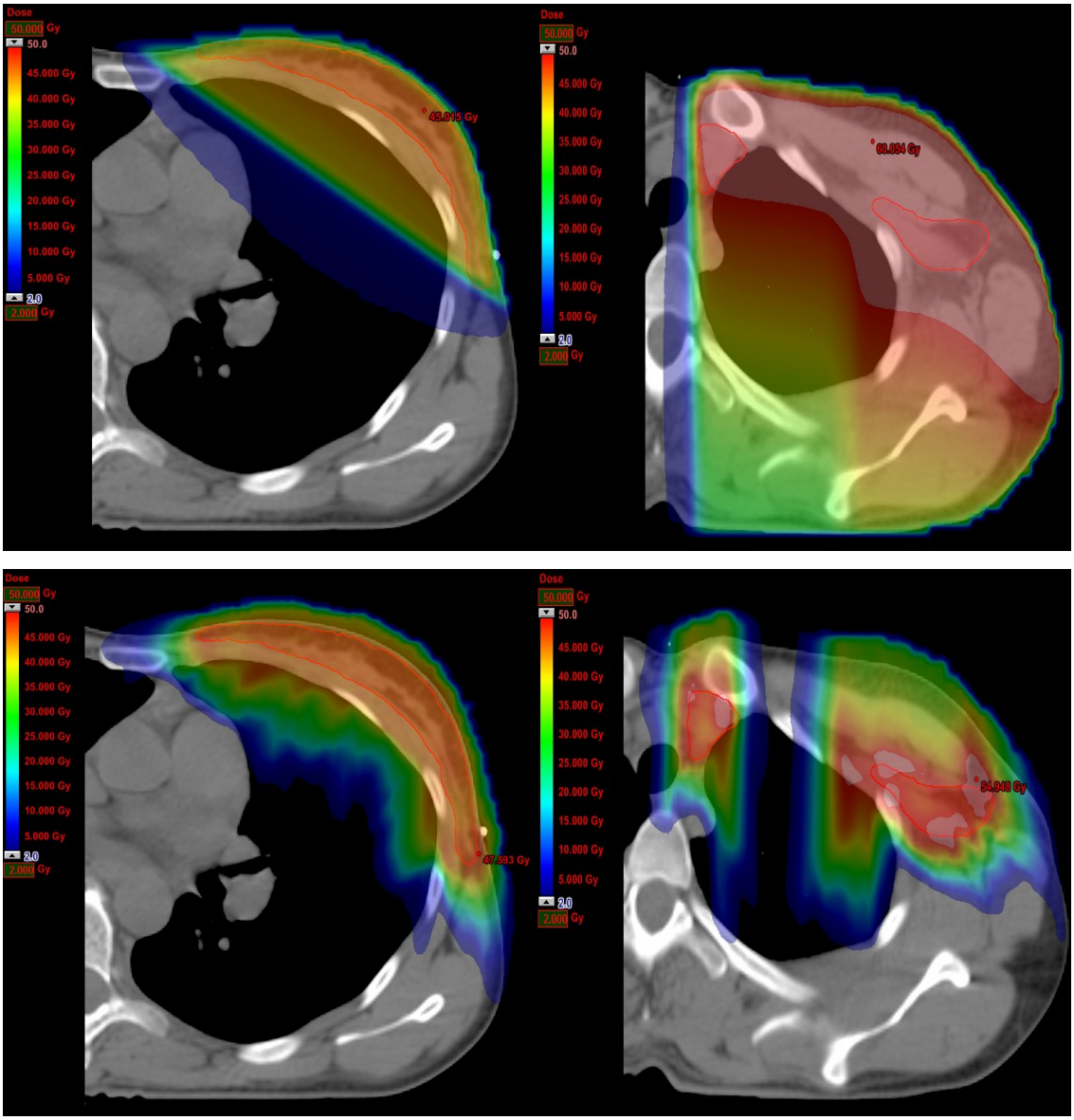

Figure 4-8: Breast cancer case dose distribution comparison between (top) 3D-CRT plan and (bottom) IMPT plan. Left: Remaining breast target volume (red). Right: Nodal target volume (red). Dose color wash upper limit 50 Gy, lower limit 2 Gy.

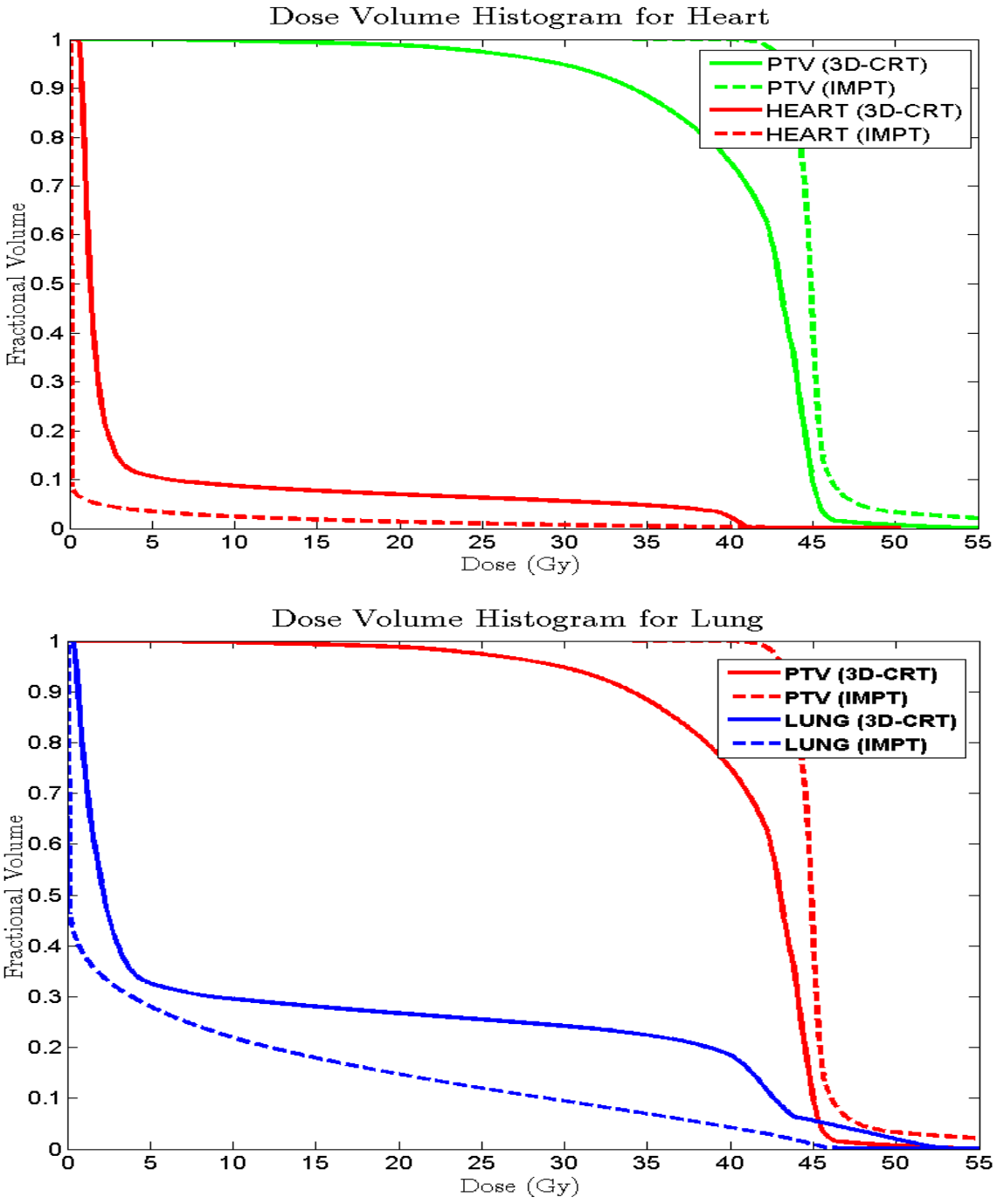

Figure 4-9: Dose volume histograms for breast cancer case. (Top) PTV and heart, (Bottom) PTV and ipsilateral lung. [Note: the discrepancy between 3D-CRT and IMPT plans in the PTV coverage for this patient is the result of the creation of a CTV and PTV for the purposes of proton planning because the orignal 3D-CRT plans were created without the dilineation of a target volume.]

4.1.4 Breast Cancer Cohort Results

4.1.4.1 Dose to Heart

The mean, range, and standard deviations of selected dosimetric indices for the heart for the breast cancer cohort are shown in Table 4-6. The relative volume of heart receiving 2 Gy in the 3D-CRT plan versus the IMPT plan is shown for all patients in the breast cancer cohort in Figure 4-10. The $V_{2\ Gy}$ is lower for three of the four IMPT plans than for the corresponding 3D-CRT plans; the line in Figure 4-10 indicates the point at which the $V_{2\ Gy}$ for IMPT is equal to the $V_{2\ Gy}$ for 3D-CRT. The points farthest from this line are the patients for whom the largest absolute reduction in $V_{2\ Gy}$ was observed. The flared point indicates the breast cancer case selection presented in 4.1.3. The maximum relative volume of heart receiving a low dose of 2 Gy among the breast cancer cohort was 42% for 3D-CRT plans and 5% for IMPT. For one patient, the volume of heart receiving 2 Gy was increased from 0% for 3D-CRT to 1.5% for IMPT. Excluding this case, on average the IMPT plans reduced the relative volume of heart receiving 2 Gy by 72%.

Table 4-6: Dosimetric indices for heart for breast cancer cohort. Individual patient results in Appendix C: Table C-2.

Dosimetric Index *Heart*	*Statistic*	*3D-CRT*	*IMPT*
$V_{2\ Gy}$ (%)	mean	18.1	2.9
	range	0 – 41.6	0.7 – 4.8
	sd	18.4	2.1
$V_{5\ Gy}$ (%)	mean	4.1	1.7
	range	0 – 10.6	0.3-3.5
	sd	5.1	1.6
V_{Rx} (%)	mean	0.5	0.0
	range	0 – 1.9	-
	sd	7.3	0

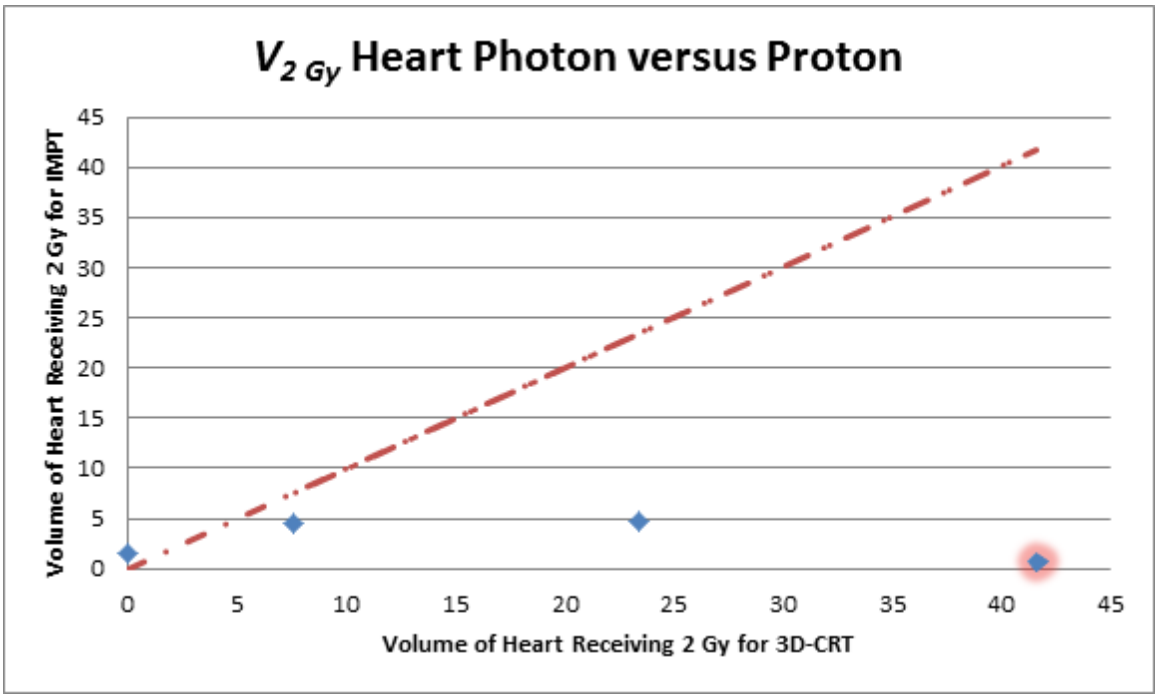

Figure 4-10: Relative volume of heart receiving dose of 2 Gy or greater for breast cancer patient cohort for IMPT versus 3D-CRT. Dashed line indicates equal $V_{2\ Gy}$ (heart) between the two modalities. Flared point represents the breast cancer case selection presented in 4.1.3.

4.1.4.2 Dose to Ipsilateral Lung

The mean, range, and standard deviations of selected dosimetric indices for the ipsilateral lung for the breast cancer cohort are shown in Table 4-7. The relative volume of ipsilateral lung receiving 20 Gy in the 3D-CRT plan versus the IMPT plan is shown for all patients in the breast cancer cohort in Figure 4-11. The $V_{20\ Gy}$ is lower for only one of the IMPT plans than for the corresponding 3D-CRT plans; the line in Figure 4-11 indicates the point at which the $V_{20\ Gy}$ for IMPT is equal to the $V_{20\ Gy}$ for 3D-CRT. The maximum relative volume of ipsilateral lung receiving an intermediate dose of 20 Gy among the breast cancer cohort was 27% for 3D-CRT plans and 27% for IMPT. No

average behavior was observed for the $V_{20\ Gy}$ when comparing the IMPT plans and the 3D-CRT plans.

Table 4-7: Dosimetric results for lungs for breast cancer cohort. Individual patient results in Appendix C: Table C-4.

Dosimetric Index *Ipsilateral Lung*	*Statistic*	*3D-CRT*	*IMPT*
Mean Lung Dose (Gy)	mean	9.0	7.5
	range	3.9-14.6	3.7-11.9
	sd	5.4	3.4
$V_{20\ Gy}$ (%)	mean	17.3	16.5
	range	7.4-26.7	8.1-26.5
	sd	10.8	7.6
V_{Rx} (%)	mean	0.6	0.4
	range	0.0-1.9	0.0-0.8
	sd	0.9	0.3

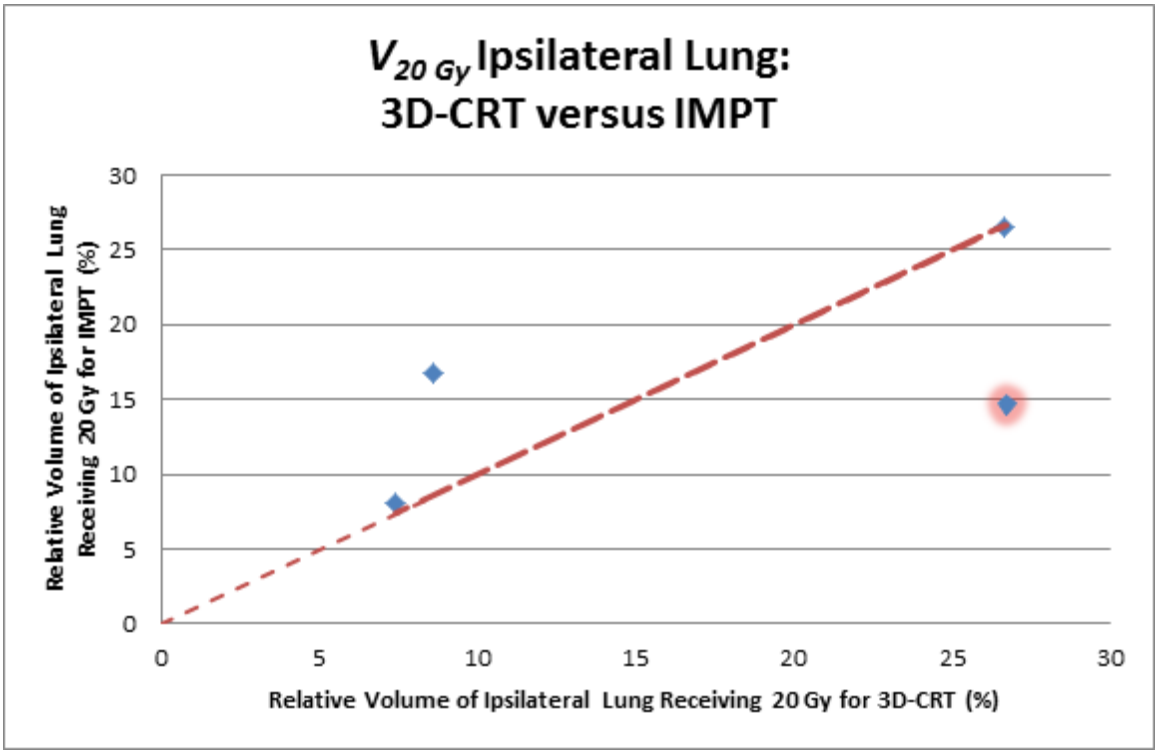

Figure 4-11: Relative volume of ipsilateral lung receiving dose of 20 Gy or greater for breast cancer patient cohort. Dashed line indicates equal $V_{20\ Gy}$ (lung) between the two modalities. Flared point represents the breast cancer case selection presented in 4.1.3.

4.2 Risk Modeling Results

4.2.1 Hodgkin's Lymphoma Case

Risk modeling results for the same Hodgkin's lymphoma case as presented in 4.1.1 are presented in this section. The excess risk of cardiac mortality was averaged over the three sets of parameters, and the average excess risk as well as the range over the three sets of parameters is shown in Table 4-8 for each treatment modality. The excess absolute risks for lung and breast cancer for the Hodgkin's lymphoma case are shown in Table 4-8. The percent reduction for each risk from 3D-CRT to IMPT is also shown in Table 4-8.

Table 4-8: Risk modeling results for Hodgkin's lymphoma case. Excess risk of cardiac mortality is evaluated at 15 years post irradiation, and excess absolute risks for lung and breast cancers are evaluated at 30 years post irradiation. Averaged excess risk of cardiac mortality over three parameter sets, and range expresses range of results over three parameter sets.

	Excess Risk of Cardiac Mortality (%)		*Excess Absolute Risk for Lung Cancer*	*Excess Absolute Risk for Breast Cancer*
Treatment Modality	Average	Range	*(cases per 10,000 persons)*	
3D-CRT	1.8	1.3-2.6	28.7	8.3
IMPT	0.7	0.5-0.9	16.2	1.7
% Reduction	63	27-81	56	80

4.2.2 Lymphoma Cohort

4.2.2.1 Excess Risk of Cardiac Mortality at Fifteen Years Post-Irradiation

The mean, range, and standard deviation of the results for excess risk for cardiac mortality for each set of parameters among the lymphoma cohort are shown in Table 4-9. The excess risk for cardiac mortality averaged over the three sets of parameters is shown for all patients in the lymphoma cohort in Figure 4-12. The maximum for the mean (over the three parameter sets) excess risk of cardiac mortality among the lymphoma cohort was 6.9% for 3D-CRT plans and 2.2% for IMPT. The mean excess risk for cardiac mortality was reduced from 0.9% for 3D-CRT to 0.5% for IMPT.

Table 4-9: Excess risk of cardiac mortality at 15 years post irradiation results for lymphoma cohort. Individual patient results in Appendix C: Table C-6.

Parameter Set	*Statistic*	*3D-CRT*	*IMPT*
Gagliardi BC	mean	0.6	0.3
	range	0 – 6.0	0 - 1.3
	sd	1.3	0.4
Eriksson HL + BC	mean	1.3	0.8
	range	0.02 - 6.9	0.0 - 2.2
	sd	1.5	0.7
Eriksson HL	mean	0.8	0.4
	range	0.01 - 4.4	0.0 - 1.3
	sd	0.9	0.4
Over all parameter sets	mean	0.9	0.5
	range	0 - 6.9	0.0 - 2.2
	sd	1.3	0.5

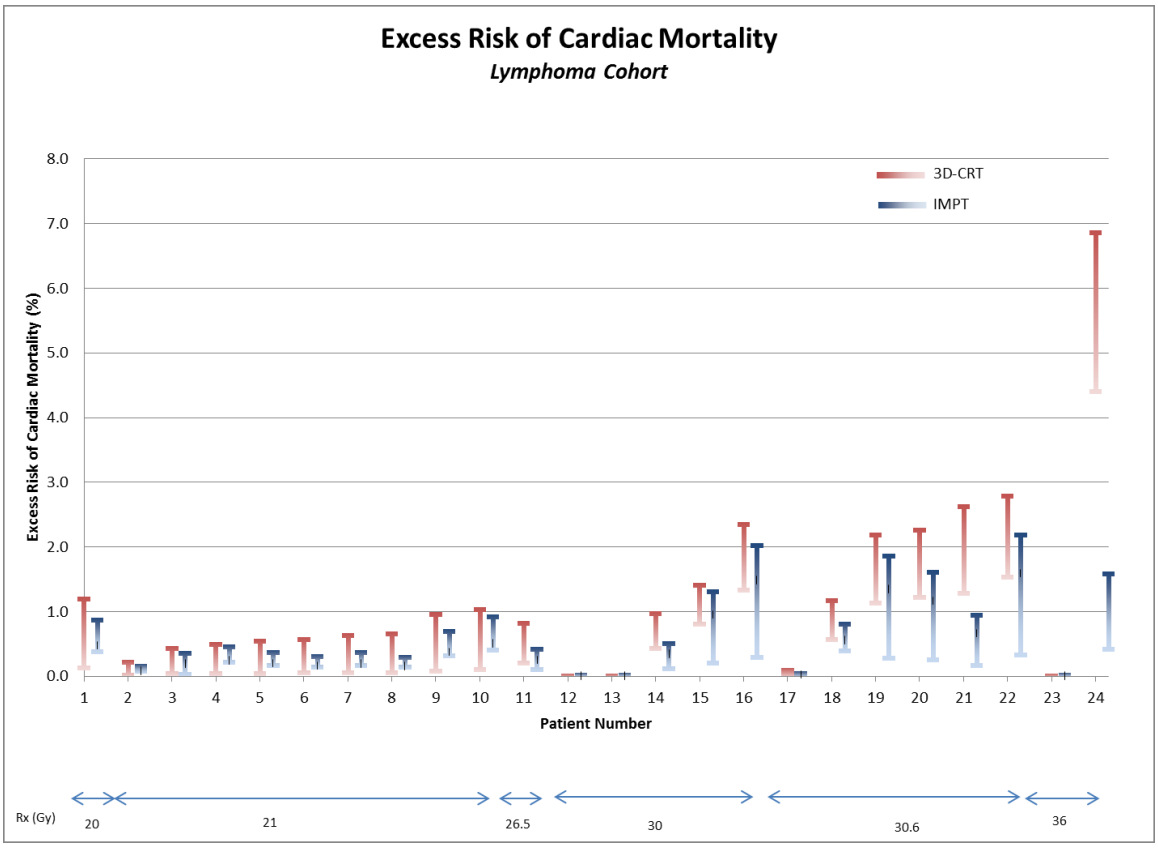

Figure 4-12: Excess risk of cardiac mortality at 15 years post irradiation for lymphoma patient cohort in order of ascending prescribed radiation dose. Dark red indicates maximum risk (of three parameter sets) for photon plan results (3D-CRT), pink indicates minimum risk for 3D-CRT plans. Dark blue indicates maximum risk for proton plan results (IMPT), light blue indicates minimum risk for IMPT plans.

4.2.2.2 Excess Absolute Risk for Lung Cancer at Thirty Years Post-Irradiation

The mean, range, and standard deviation of the results for excess absolute risk for lung cancer among the lymphoma cohort are shown in Table 4-10, and the individual patient results are shown in Figure 4-13. The maximum excess absolute risk of lung cancer among the lymphoma cohort at 30 years post irradiation was 37 cases per 10,000 persons

for 3D-CRT plans and 16 cases per 10,000 persons for IMPT. On average, the IMPT plans reduced the excess absolute risk for lung cancer by 9 cases per 10,000 persons.

Table 4-10: Risk modeling results for excess absolute risk for lung cancer at 30 years post-irradiation for lymphoma cohort. Individual patient results in Appendix C: Table C-8.

Lymphoma Cohort	*Statistic*	*3D-CRT*	*IMPT*
Excess Absolute Risk for Lung Cancer	mean	20.2	11.1
	range	7.7 - 37.0	2.8 – 16.5
	sd	7.1	3.8

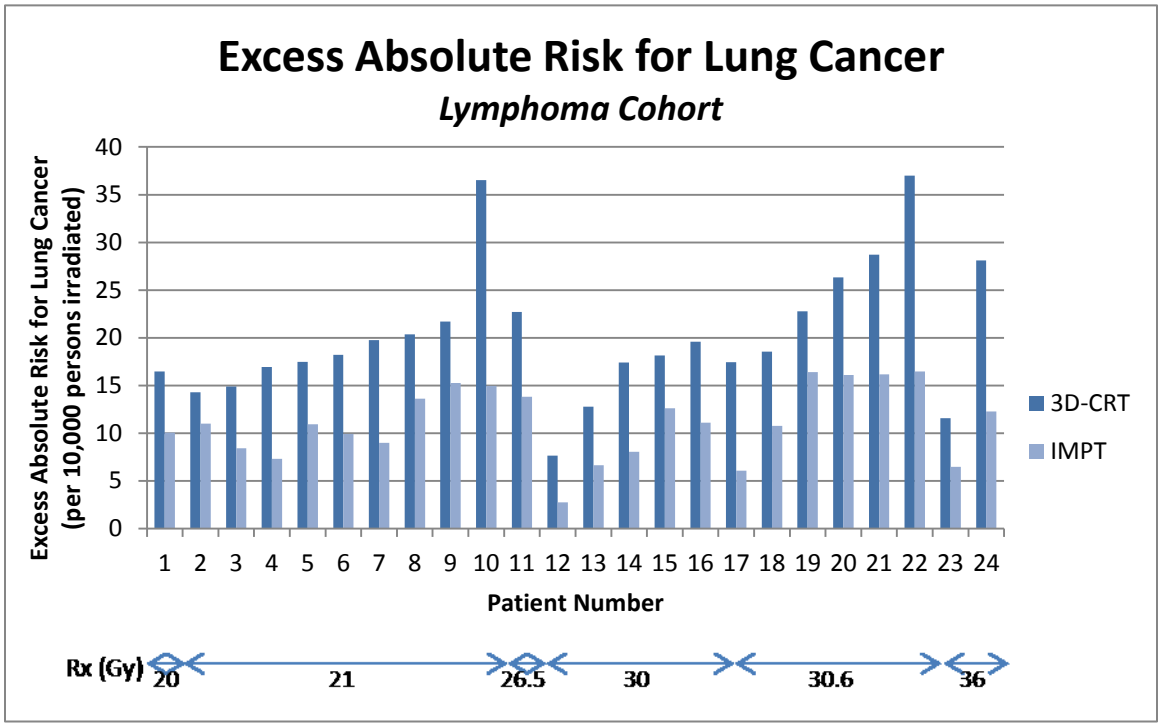

Figure 4-13: Excess absolute risk for lung cancer at 30 years post irradiation for each patient in the lymphoma cohort in order of prescribed dose. Darker bars are photon plan results (3D-CRT), lighter bars are proton plan results (IMPT).

4.2.2.3 Excess Absolute Risk for Breast Cancer at Thirty Years Post Irradiation

The mean, range, and standard deviation of the results for excess absolute risk for breast cancer among the female patients in the lymphoma cohort are shown in Table 4-11, and the individual patient results are shown in Figure 4-14. The maximum excess absolute risk of breast cancer among the female patients in the lymphoma cohort at 30 years post irradiation was 21 cases per 10,000 persons for 3D-CRT plans and 8 cases per 10,000 persons for IMPT. On average, the IMPT plans reduced the excess absolute risk for breast cancer by 8 cases per 10,000 persons.

Table 4-11: Risk modeling results for excess absolute risk for breast cancer at 30 years post-irradiation for lymphoma cohort. Individual patient results in Appendix C: Table C-10.

Lymphoma Cohort	*Statistic*	*3D-CRT*	*IMPT*
Excess Absolute Risk for Breast Cancer	mean	10.3	3.3
	range	2.0 – 21.1	0.1 – 7.5
	sd	6.1	2.6

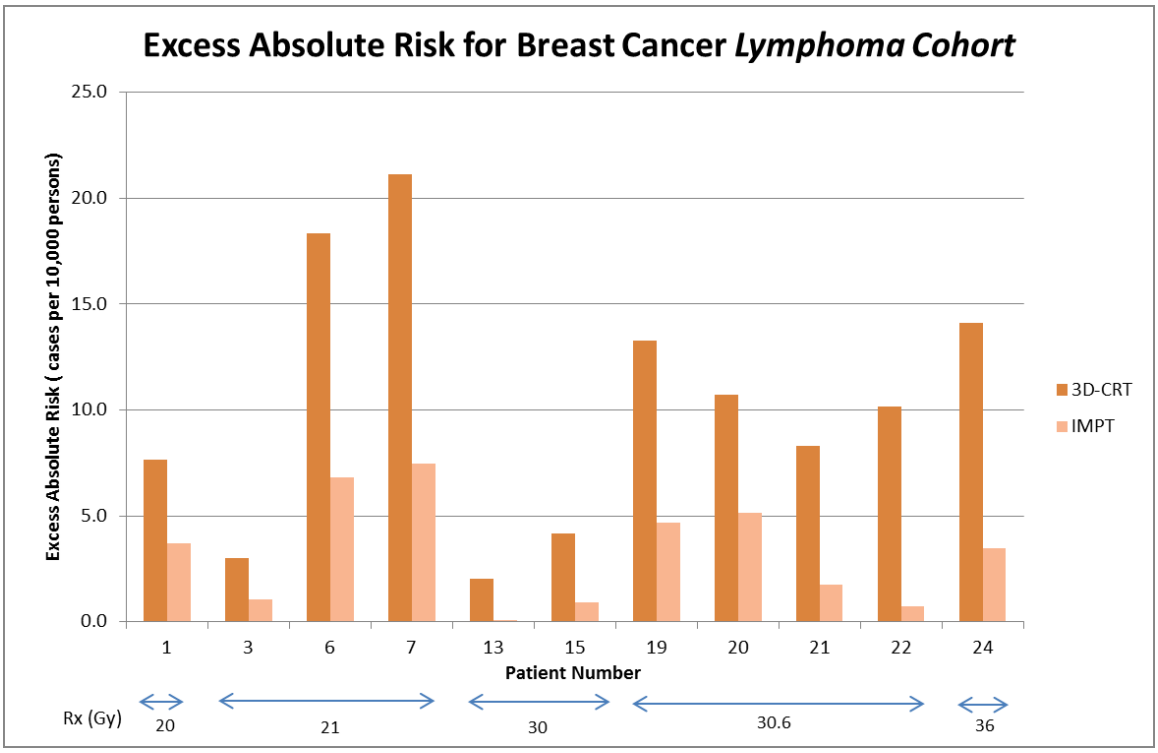

Figure 4-14: Excess absolute risk for breast cancer at 30 years post irradiation for female patients in lymphoma cohort in order of prescribed dose. Darker bars are photon plan results (3D-CRT), lighter bars are proton plan results (IMPT).

4.2.3 Breast Cancer Case

Risk modeling results for the same breast cancer case as presented in 4.1.3 are presented in this section. The excess risk of cardiac mortality was averaged over the three sets of parameters, and the average excess risk as well as the range over the three sets of parameters is shown in Table 4-12 for each treatment modality. The excess absolute risk for lung cancer for the breast cancer case is shown in Table 4-12. The percent reduction for risk from 3D-CRT to IMPT is also shown in Table 4-12.

Table 4-12: Risk modeling results for breast cancer case. Excess risk of cardiac mortality is evaluated at 15 years post irradiation, and excess absolute risks for lung and breast cancers are evaluated at 30 years post irradiation. Averaged excess risk of cardiac mortality over three parameter sets, and range expresses range of results over three parameter sets.

	Excess Risk of Cardiac Mortality (%)		*Excess Absolute Risk for Lung Cancer*
Treatment Modality	Average	Range	*(cases per 10,000 persons)*
3D-CRT	1.0	0.7-1.2	9.8
IMPT	0.2	0.1-0.2	6.6
% Reduction	85	71-92	33

4.2.4 Breast Cancer Cohort

4.2.4.1 Excess Risk of Cardiac Mortality at Fifteen Years Post Irradiation

The mean, range, and standard deviation of the results for excess risk for cardiac mortality for each set of parameters among the breast cancer cohort are shown in Table 4-13. The excess risk for cardiac mortality averaged over the three sets of parameters is shown for all patients in the breast cancer cohort in Figure 4-13. The maximum excess risk of cardiac mortality among all parameter sets among the breast cancer cohort was 1.2% for 3D-CRT plans and 0.2% for IMPT. The mean excess risk of cardiac mortality was reduced from 0.3% for 3D-CRT to 0.1% for IMPT.

Table 4-13: Excess risk of cardiac mortality at 15 years post irradiation results for lymphoma cohort. Individual patient results in Appendix C: Table C-7.

Parameter Set	*Statistic*	*3D-CRT*	*IMPT*
Gagliardi BC	mean	0.4	0.1
	range	0.0 – 1.2	0.0 – 0.2
	sd	2.6	0.1
Eriksson HL + BC	mean	0.3	0.1
	range	0.0 – 1.1	0.0 – 0.2
	sd	0.5	0.1
Eriksson HL	mean	0.2	0.1
	range	0.0 – 0.7	0.0 – 0.1
	sd	0.3	0.1
Over all parameter sets	mean	0.3	0.1
	range	0.0 – 1.2	0.0 – 0.2
	sd	1.5	0.7

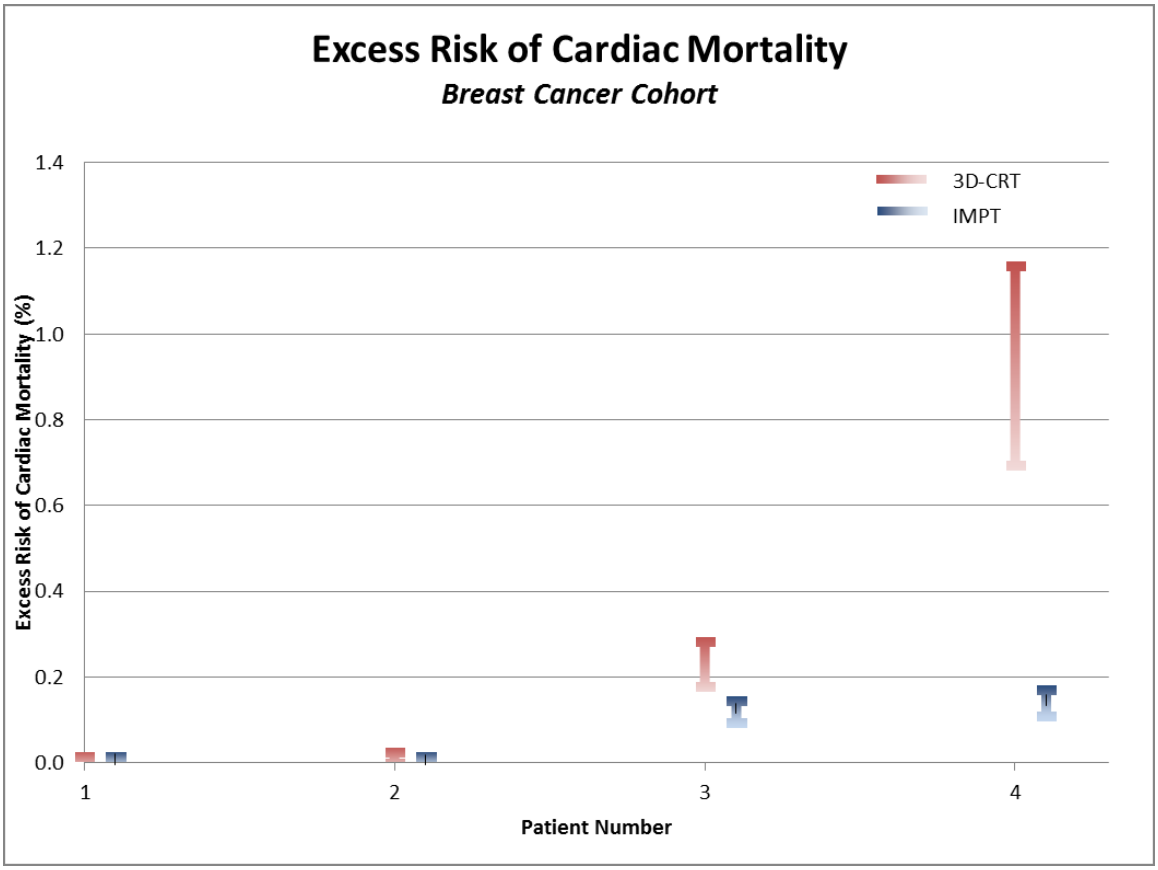

Figure 4-15: Excess risk of cardiac mortality at 15 years post irradiation for breast cancer patient cohort. Dark red indicates maximum risk (of three parameter sets) for photon plan results (3D-CRT); pink indicates minimum risk for 3D-CRT plans. Dark blue indicates maximum risk for proton plan results (IMPT); light blue indicates minimum risk for IMPT plans.

4.2.4.2 Excess Absolute Risk for Lung Cancer at Thirty Years Post-Irradiation

The mean, range, and standard deviation of the results for excess absolute risk for lung cancer among the lymphoma cohort are shown in Table 4-14, and the individual patient results are shown in Figure 4-16. The maximum excess absolute risk of lung cancer in the ipsilateral lung among the breast cohort at 30 years post irradiation was 13.6 cases per 10,000 persons for 3D-CRT plans and 10.9 cases per 10,000 persons for IMPT. On

average, the IMPT plans reduced the excess absolute risk for lung cancer by 1.7 cases per 10,000 persons.

Table 4-14: Risk modeling results for excess absolute risk for breast cancer at 30 years post-irradiation for breast cancer cohort. Individual patient results in Appendix C: Table C-9.

Breast Cancer Cohort	*Statistic*	*3D-CRT*	*IMPT*
Excess Absolute Risk for Lung Cancer	mean	8.4	6.7
	range	5.0 – 13.6	2.0 – 10.9
	sd	4.1	3.6

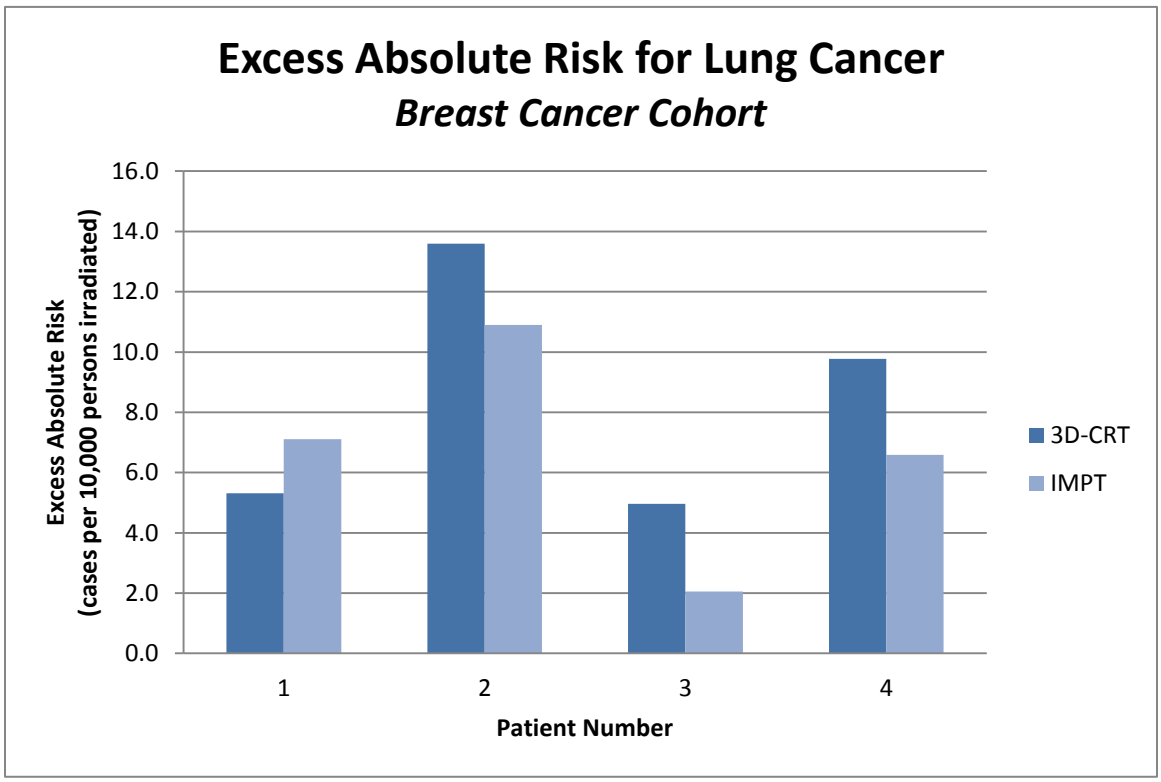

Figure 4-16: Excess absolute risk for lung cancer in the ipsilateral lung for breast cancer patient cohort. Darker bars are photon plan results (3D-CRT), lighter bars are proton plan results (IMPT).

Chapter 5

Discussion

5.1 Treatment Planning Discussion

5.1.1 Lymphoma Case and Cohort

IMPT was found to reduce the volume of heart receiving 2 Gy, the volume of lungs receiving 20 Gy, and the volume of breasts receiving 2 Gy for all patients in the lymphoma cohort as expected due to the advantages of intensity modulated proton therapy as discussed in section 2.1.2. The most significant sparing of the heart and lungs was observed for cases where there was significant mediastinal involvement of the PTV in the region anterior to the heart and lungs. This is attributable to the absence of exit dose characteristic to the proton beam at a gantry angle of 0 degrees. The most significant sparing of the breasts was observed for cases in which the $V_{2\ Gy}$ was greater than 15% for 3D-CRT (Figure 4-6). However, this trend is noted with caution due to the small cohort size and the breast volume variability combined with the small volume of breast in the field for the 3D-CRT plans.

A single Hodgkin's lymphoma case was selected for presentation in section 4.1.1. This case was found to be an exceptional case relative to the lymphoma cohort as a whole due to the proximity of the planning target volume to the heart, which was shown to have a significant impact on the planning and risk results (Figure 4-1). For this patient, the mediastinal involvement allowed for significant sparing of the heart for the IMPT plan as compared to the 3D-CRT plan (Figure 4-2). The dose volume histogram also confirms the significant sparing of the heart achievable with IMPT as compared to 3D-CRT (Figure 4-3). These results are consistent with a decrease in dosimetric parameters for

lungs and breasts when comparing 3D-CRT to proton therapy for a Hodgkin's lymphoma case in the study by and Chera[1] et al.

5.1.2 Breast Cancer Case and Cohort

IMPT was found to reduce the volume of heart receiving 2 Gy for three of the four breast cancer patients; the excepting patient's 3D-CRT plan was able to spare the heart entirely while the corresponding IMPT plan delivered 2 Gy to 1.5% of the heart. This exception may be due to the difficulty in assigning a clinical target volume for the breast cancer patients which would result in variability in the volume of heart considered to be in the field. This issue is further discussed in section 5.3.1. No trend was observed for the volume of lungs receiving 20 Gy for the IMPT plans relative to the 3D-CRT plans for the breast cancer cohort. This is again likely due to both the uncertainty in clinical target volume definition as well as the small patient cohort size.

A single breast cancer case was selected for presentation in section 4.1.3. This case was found to be an exceptional case relative to the breast cancer cohort as a whole due to the proximity of the planning target volume to the ipsilateral lung, which was shown to have a notable impact on the planning and risk results (Figure 4-7). For this patient, the significant reduction in the fractional volume of the heart receiving all doses was observed for the IMPT plan as compared to the 3D-CRT plan (Figure 4-9). The volumes of OARs receiving low doses were reduced, however the reduction in lung $V_{20\,Gy}$ (relative to the lymphoma cohort) is compromised by the range uncertainty characteristic of proton beam therapy (Figure 4-8). This issue is further discussed in section 5.3.1.

5.2 Risk modeling Discussion

5.2.1 Risk of Cardiac Mortality

5.2.1.1 Lymphoma Case and Cohort

Among the lymphoma cohort, the maximum volume of heart receiving the prescribed dose was 30%, and the average volume of heart receiving the prescribed dose was less than 10%. The average for excess risk of cardiac mortality was found to be 0.9% for 3D-CRT plans and 0.5% for IMPT plans. For volumes of less than 10% of the heart receiving the prescribed dose, the excess risk of cardiac mortality at fifteen years post-irradiation is expected to be less than 2% at a dose of 30 Gy and less than 1% at a dose of 20 Gy[2]. Thus the results from this study are in agreement with the results from Eriksson[3] et al. and Gagliardi[2] et al.

For perspective, the *maximum* risk of cardiac mortality at fifteen years post-irradiation was defined for this study to occur where the whole heart receives the prescribed target dose. The maximum risk of cardiac mortality at fifteen years post-irradiation at the prescription doses in the lymphoma cohort, corrected for the effects of fractionation, is expected to be less than 5% for a dose of 30 Gy and less than 1% for a dose 20 Gy[2]. Thus the results for excess risk of cardiac morality at fifteen years post-irradiation, which ranged from 0% to 3% for 3D-CRT for all but one in the lymphoma cohort, are within reason and in agreement with the results from Gagliardi[2] et al. The patient with the highest risk for cardiac mortality with 3D-CRT received a V_{Rx} to the heart of 20% at 36 Gy, the highest prescribed dose among the cohort. IMPT reduced the excess risk for cardiac mortality at fifteen years post-irradiation from 7% to 1% for this patient. A trend

for increasing risk with increasing prescribed radiation dose was observed for both modalities, and this is reflective of the dose-weighted relative seriality model for late cardiotoxicity, particularly where the heart is considered to be a purely serial structure.

The Hodgkin's lymphoma case selected is one of two cases among the lymphoma cohort for which the reduction of excess risk of cardiac mortality was found to be significant as defined by a lack of overlap in the range of estimated risks for 3D-CRT versus IMPT (Figure 4-12). The reduction of volume of heart receiving higher doses would correlate with larger reductions in excess risk of cardiac mortality at fifteen years post-irradiation using the relative seriality model. However, at the lower prescribed doses for lymphomas, the excess risk of cardiac mortality at fifteen years post-irradiation was not found to be significantly reduced for IMPT as compared to 3D-CRT for most patients in this study.

5.2.1.2 Breast Cancer Case and Cohort

For the breast cancer cohort, the maximum volume of heart receiving the prescribed dose was less than 2%, and the average volume of heart receiving the prescribed dose was less than 1%. The excess risk of cardiac mortality at fifteen years post-irradiation was found to be 0.3% for 3D-CRT plans and 0.1% for IMPT plans. For volumes of less than 1% of the heart receiving the prescribed dose, the excess risk of cardiac mortality at fifteen years post-irradiation is expected to less than 0.6% at a dose of 50 Gy^2. Thus the results from this study are in agreement with the results from Gagliardi[2] et al.

Excess risk of cardiac mortality at fifteen years post-irradiation was found to be significant for two of the four patients in the breast cancer cohort. The breast cancer case

selected for presentation in section 4.1.3 is one of the patients for whom the reduction was significant and is represented as patient 4 in Figure 4-15. For this patient the volume of heart receiving the prescribed dose of 50 Gy was 0% for both modalities, so the expected value for excess risk of cardiac mortality at fifteen years post-irradiation cannot be estimated from the Gagliardi[2] et al. study. However, the reduction in excess risk for cardiac mortality at fifteen years post-irradiation correlates with an 80% reduction of the $V_{2\,Gy}$ for IMPT as compared to 3D-CRT.

5.2.2 Excess Absolute Risk for Secondary Cancers

5.2.2.1 Lymphoma Case and Cohort

The excess absolute risk for lung cancer at thirty years post-irradiation was found to be reduced for IMPT as compared to 3D-CRT for all patients in the lymphoma cohort (Figure 4-13). Among the lymphoma cohort, the maximum mean lung dose was 15 Gy, and the average mean lung dose was 9 Gy. The average excess absolute risk for lung cancer at thirty years post-irradiation for the lymphoma cohort was 20 cases per 10,000 persons for 3D-CRT and 11 cases per 10,000 persons for IMPT. For a dose to lung of less than 15 Gy, the expected excess absolute risk for lung cancer at thirty years post-irradiation is less than 22 cases per 10,000 persons[4]. Thus the excess absolute risk results for lung cancer in the lymphoma cohort are comparable to the study by Schneider[4] et al.

The excess absolute risk for breast cancer at thirty years post-irradiation was found to be reduced for IMPT as compared to 3D-CRT for all patients in the lymphoma cohort (Figure 4-13). Among the lymphoma cohort, the average $V_{2\ Gy}$ for breast tissue was 14% for 3D-CRT and 6% for IMPT. The average excess absolute risk for breast cancer at thirty years post-irradiation for the lymphoma cohort was 10 cases per 10,000 persons for 3D-CRT and 3 cases per 10,000 persons for IMPT. For a dose to breast tissue of 2 Gy, the expected excess absolute risk for breast cancer at thirty years post-irradiation is less than 20 cases per 10,000 persons[5]. Thus the results for excess absolute risk for breast cancer at thirty years post-irradiation among female patients in the lymphoma cohort are comparable to the study by Schneider[5] et al.

5.2.2.2 Breast Cancer Case and Cohort

The excess absolute risk for lung cancer was found to be reduced for three of the four patients in the breast cancer cohort for IMPT as compared to 3D-CRT (Figure 4-13). Among the breast cancer cohort, the maximum mean lung dose was 14 Gy for 3D-CRT and 12 Gy for IMPT, and the average mean lung dose was 9 Gy for 3D-CRT and 8 Gy for IMPT. The average excess absolute risk for lung cancer at thirty years post-irradiation for the breast cancer cohort was 8 cases per 10,000 persons for 3D-CRT and 7 cases per 10,000 persons for IMPT. For a dose to lung of 9 Gy, the expected excess absolute risk for lung cancer at thirty years post-irradiation is less than 15 cases per 10,000 persons[4]. Thus the excess absolute risk results for lung cancer in the lymphoma cohort are comparable to the study by Schneider[4] et al. However because of the overlapping range of the risk results, likely due to the small size of this patient cohort, no conclusive

evidence has been acquired as to the potential for IMPT to reduce the excess absolute risk of lung cancer as compared to 3D-CRT.

5.3 Limitations of This Study

A number of assumptions were made in this work, which may affect the uncertainties in the results. Acknowledgement of these limitations and a discussion on their impact follows.

5.3.1 Target Volume Considerations

The planning target volume (PTV) concept was introduced in ICRU Report 50 as it pertains to photon therapy, and its intention is to expand the clinical target volume (CTV) in order to ensure that the volume irradiated includes the CTV with allowances for variation and uncertainty. The internal margin provides compensation for variation of position, size, and shape of the CTV at the time of treatment. The uncertainty in patient positioning and alignment is translated into a set-up margin. The final PTV combines both internal and set-up margins to form an overall margin[6].

This technique is well established for the conventional radiation modalities such as 3D-CRT, IMRT, and electron and orthovoltage radiation. However, there are scruples about applying this technique equally to proton therapy due to differences in uncertainties which are specific to proton therapy. Proton beam dose distribution is subject to uncertainty in beam range due to uncertainty in conversion of CT number to proton stopping power range. This implies that the lateral margins to the CTV are generally

different from the margins required in the axial direction. This results in the need for a separate PTV for each beam unless the range margins are accounted for in the treatment planning software dose calculation[6].

A beam-specific PTV which differs from the general PTV concept outlined in ICRU 78 complicates treatment planning comparison as well as dose reporting. Coverage to the CTV, not the PTV, would be the more appropriate variable for comparing treatment plans from differing modalities. Park et al. at MD Anderson Cancer Center in Houston, TX proposed a method for designing a beam-specific planning target volume (bsPTV) for spot scanned as well as passive scattering proton therapy. The bsPTV accounts for three types of uncertainties to produce a planning target volume that is specifically tailored to the uncertainties and variation in proton therapy: a lateral margin for lateral setup error and internal motion, a distal and proximal margin to address the systematic range error resultant from uncertainty in conversion of CT number to proton stopping power, and additional distal and proximal margins to account for the range error resulting from variation due to misaligned heterogeneities from patient setup error and organ motion. The beam specific target volume concept was found to be the more appropriate planning volume to plan and provide adequate coverage to the target volume for proton therapy[7].

5.3.2 Treatment Planning

A number of inconsistencies were observed in this work as a result of the nature of a multi-institutional, retrospective study. Procedures for planning varied from one hospital of data collection to another. The CT simulation acquisition parameters were not uniform.

The slice thickness, peak kilovoltage, tube current and bore size were sometimes inconsistent. The use of heterogeneity corrections for 3D-CRT was also applied in some centers but not in others. The plan normalization was also inconsistent. For the purpose of this work, these differences were overlooked (in the case of CT acquisition parameters and heterogeneity corrections) or corrected for (in the case of plan normalization). This was rationalized as the aim of this study was to predict the risk of late effects of differing modalities of radiotherapy based on a given treatment plan.

The patient positioning and use of bolus for treatment was suited to the application of photon radiotherapy, so the IMPT treatment plans may have fallen short of the most-advantageous application of proton therapy.

The dose calculation algorithm for proton therapy relies on a CT Hounsfield Unit to Proton Stopping Power calibration curve. The data set used for this study did not correspond to any of the CT simulators on which the patients were imaged. The accuracy of this calibration curve directly affects the accuracy of the dose calculation. Ideally, a separate calibration curve for each CT simulator would be used for the dose calculation.

Together, these treatment planning parameters and their variation likely cause uncertainty in the absolute values of the results found in this work. The comparison of the two treatment modalities by the relative reduction in risks provides a more reliable method for evaluation, though still subject to uncertainty.

5.3.3 Secondary Neutron Contamination

Secondary neutrons are of concern for several reasons. Neutrons can travel long distances from the site of their primary production and also have a high relative biological effect. Thus, secondary neutrons deposit dose to healthy tissue both in the primary treatment field and outside it. In the comparison of proton therapy to IMRT or 3D-CRT, the advantageous dose distribution exhibited by proton beams is somewhat compromised by the secondary neutron contamination.

The treatment planning system used for this study does not consider the dose from secondary neutrons in its calculations of dose distributions of proton beams. A more complete analysis of the dose distribution for a proton treatment plan would include the contribution of secondary neutron dose. The modeling of the secondary neutron dose is highly dependent upon the specifics of the beam delivery system and is both beyond the scope of this study as well as inapplicable at this time as this is a theoretical planning study. The presence of each beam delivery component must be modeled and accounted for in order to simulate the neutron dose, and the simulations would then require verification through experiment. As the facility at which this study has been undertaken is not currently equipped with a proton facility, the modeling of such is not possible at this time.

Secondary neutron dose during spot scanned delivery of a proton beam was modeled using Monte Carlo techniques and measured using a Bonner sphere at the Paul Scherrer Institute in Zurich, Switzerland by Schneider[8] et al. The experimental results were found

to agree well with the simulations, and it was determined that, for the spot scanning technique, secondary neutrons during proton radiotherapy were estimated to deposit an effective dose to the nontarget volume of 0.9-3.6 mSv per 1-Gy treatment dose. The effective dose from the primary beam to the nontarget volume as a result of scattered protons was determined to be 28 mSv. In the context of this work, this would result in an increase in the dose estimated by the treatment planning system of 0.1%.

A review of the current literature, such as the study cited above, provides justification for neglecting the secondary neutron dose for the purposes of this study although its inclusion, for completeness, is cause for future work.

5.3.4 Modeling Inaccuracies

A number of assumptions and procedures are cause for uncertainty in the modeling results. The relative seriality model parameters were derived from a retrospective study where patients were planned and treated without CT images. The dose distributions were originally calculated in only one cross-section of each patient, so the application of the relative seriality model by Gagliardi et al. relied on previous dose to the heart reconstructions of the same patient population. The model also assumes a homogeneous radiation sensitivity of the heart, though it is currently unclear whether this assumption is valid for the prediction of late cardiac complications[9]. There was inconsistency in the noted endpoint in the patient population studies used for the parameter fitting of the relative seriality model. Additionally, the treatment techniques in these trials were outdated in terms of higher prescribed doses and extended fields, and consequently the

application of the long term follow up to current practice is questionable. The use of risk prediction is therefore emphasized as a tool in the evaluation of a treatment plan.

The Schneider model also employs several assumptions in order to describe the complex process of cancer induction. Currently the dose-response relationships for radiation induced cancer due to doses in the therapeutic range are not well understood, and this model is described as an "attempt to acquire more information in this area" [10].

5.3.5 Confounding Factors

There are known confounding factors in the development of cardiac mortality and secondary malignancy that were not accounted for in this work. High incidence of cardiac mortality in the general population has demonstrated significance of smoking, family history, obesity, etc. in the expression of heart disease. Chemotherapy affects both cardiotoxicity and development of secondary malignancy. Genetic susceptibility is also a hypothesized factor affecting the development of secondary malignancy[11]. This work addressed the risks associated with external beam radiotherapy techniques, and as confounding factors were not included, these predictions may be conservative estimates.

5.4 Significance of This Study

In spite of the limitations of this study, the results and implications of this work were still found to have significance with regard to a number of issues. The models used were previously validated in other studies, and the risk modeling results reported in this study

were found to be in agreement with values in the literature modeling the same effects for similar patient populations.

Though intensity modulated photon therapy (IMRT) may offer more conformal dose distributions than the methods of 3D-CRT as applied in this study, this plan comparison study reflects the treatment methods in current practice as of 2010, in the province of Quebec. As the purpose of the study was to compare the actual treatment plans to those generated using IMPT, no investigation into the risk reduction possible with IMRT was undertaken and thus no conclusions as to the ability of IMRT to reduce the risks of late effects as compared to 3D-CRT were drawn.

While it is true that applying heterogeneity corrections to all photon treatment plans would result in more accurate dose calculation for the 3D-CRT plans, we have chosen to use the original dose matrix submitted by the institutions of treatment for the purposes of the planning comparison study. We feel that this is appropriate given the majority of patients were treated with a simple beam geometry, and the effect of a heterogeneity correction would have a very small effect on the dose distribution and thus an even smaller effect on the risk results, particularly at the prescribed doses in this study.

Accounting for all the limitations detailed in sections 5.3.1-5.3.5 would have been outside the scope of this study, but they are valid considerations which are cause for future work as discussed in section 6.2.

5.5 References

1. Chera BS, Rodriguez C, Morris CG, et al. Dosimetric comparison of three different involved nodal irradiation techniques for stage II Hodgkin's lymphoma patients: conventional radiotherapy, intensity-modulated radiotherapy, and three-dimensional proton radiotherapy. International journal of radiation oncology, biology, physics 2009;75:1173-80.

2. Gagliardi G, I. Lax, A. Ottolenghi, L.E. Rutqvist. Long-term cardiac mortality after radiotherapy of breast cancer-application of the relative seriality model. The British Journal of Radiology 1996;69:839-46.

3. Eriksson F, G. Gagliardi, A. Liedberg, I. Lax, C. Lee, S. Levitt, B. Lind, L.E. Rutqvist. Long term cardiac mortality following radiation therapy for Hodgkin's disease: analysis with the relative seriality model. Radiotherapy and Oncology 2000;55:153-62.

4. Schneider U, Stipper A, Besserer J. Dose-response relationship for lung cancer induction at radiotherapy dose. Zeitschrift fur medizinische Physik 2010;20:206-14.

5. Schneider U, Sumila M, Robotka J, Gruber G, Mack A, Besserer J. Dose-response relationship for breast cancer induction at radiotherapy dose. Radiation Oncology 2011;6:67.

6. ICRU Report 78: Prescribing, Recording and Reporting Proton-Beam Therapy. Oxford: Oxford University Press; 2007.

7. Park PC, Zhu XR, Lee AK, et al. A Beam-specific Planning Target Volume (PTV) Design for Proton Therapy to Account for Setup and Range Uncertainties. International journal of radiation oncology, biology, physics 2011.

8. Schneider U. Secondary Neutron Dose During Proton Therapy Using Spot Scanning. International journal of radiation oncology, biology, physics 2002;53:7.

9. Gagliardi G, I. Lax, S. Söderström, G. Gyenes, L. E. Rutqvist. Prediction of excess risk of long-term cardiac mortality after radiotherapy of stage I breast cancer. Radiotherapy and Oncology 1998;46:63-71.

10. Schneider U. Mechanistic model of radiation-induced cancer after fractionated radiotherapy using the linear-quadratic formula. Medical Physics 2009;36:1138.

11. Aleman BM, van den Belt-Dusebout AW, Klokman WJ, Van't Veer MB, Bartelink H, van Leeuwen FE. Long-term cause-specific mortality of patients treated for Hodgkin's disease. Journal of Clinical Oncology 2003;21:3431-9.

Chapter 6

Conclusion

6.1 Summary

Radiotherapy is a successful treatment modality for certain malignant diseases to the extent that patients can be cured from their primary disease. Hodgkin's lymphoma, a disease that primarily affects adolescents and young adults, is one such ailment that is treated with radiotherapy with favorable long-term prognosis[1]. The late radiation-induced toxicity to normal tissues is of great concern for this patient population due to the likelihood of long-term survival. Studies have shown that survivors of Hodgkin's lymphoma are at an increased risk of death due to cardiotoxicity and secondary malignancy as a result of the therapy for their primary disease[2]. Radiobiological models, which incorporate data from retrospective studies of incidence of these serious effects, predict the risks of these effects for a given radiotherapy treatment plan. The models provide a method for treatment plan evaluation and comparison in order to assess the potential reduction of risks for different radiotherapy modalities.

This work focused on the most-severe late radiation-induced effects that compromise the efficacy of radiotherapy in a particular patient population; risks for cardiac mortality and induction of secondary malignancy were predicted for adolescent and young adult patients treated with thoracic radiotherapy for malignant disease. Research has shown that reducing the radiation dose and/or fields is associated with lower risks of developing secondary cancer and inducing cardiotoxicity. The use of proton therapy for Hodgkin's lymphoma has been hypothesized to reduce these risks due to the increased normal tissue sparing achievable with this modality. [3] The patients in this study were treated using 3D-CRT, and radiobiological models were selected to predict the risks of late effects using the dose-volume data from the actual treatment plans and CT scans. New treatment plans using IMPT were then generated for each patient on the original CT scan images, and the modeled risks for the two radiotherapeutic modalities were compared.

The radiobiological models selected for this analysis were the relative seriality model for predicting risk of cardiac mortality and the Schneider modified linear quadratic model for predicting the induction of lung and breast cancers. Both models determine risks of these effects by relating a heterogeneous dose distribution within an organ of interest, calculated by treatment planning software and using the CT scans of the patient, to a corresponding toxicity based on a homogenous dose distribution within the organ. The values for the parameters in these models were determined through retrospective fitting studies in the literature for observed toxicity in an irradiated patient population.

It was hypothesized that the proton therapy plans would exhibit a reduction in the risks of the specified effects[3]. This hypothesis was confirmed for certain patient cases with

regards to risk of cardiac mortality. Risk of cardiac mortality was significantly reduced using IMPT for patients receiving radiotherapy to the lymph nodes anterior to the heart. Risk of induction of lung cancer was reduced for all patients in the study using IMPT. Risk of induction of breast cancer was proven to be reduced for all female patients in the study using IMPT. The results for risk of cardiac mortality were found to agree with similar studies by Gagliardi et al. and Eriksson et al. The results for risk of lung and breast cancer induction were found to agree with similar studies by Schneider et al. Thus through this work IMPT, as compared to 3D-CRT, was shown to reduce the risks of radiation induced cardiac mortality and secondary lung and breast cancers for young patients receiving thoracic radiotherapy for malignant diseases.

6.2 Future Work

In this work the patient population was narrowly confined to recipients of thoracic radiotherapy for malignant disease with curative intent who were under thirty years of age at the time of first treatment, which occurred between April and October of 2010, in the province of Quebec. Expansion of this patient cohort to include a larger time window of first treatment would provide more patients for this study. None of the lymphoma patients in this work were treated with intensity modulated radiotherapy (IMRT). Analysis and comparison of risks of cardiotoxicity and induction of secondary malignancy for this modern and debated modality would certainly be of value. A validation of the IMPT dose distributions calculated by the treatment planning system and the inclusion of secondary neutron dose would increase the accuracy of the dose-volume data used for the plan comparisons and risk calculations. A cardiotoxicity model

predicting the risk of cardiac events, including but not limited to cardiac mortality, would also provide an important point of comparison for radiotherapy modalities. Implementing a model for predicting risk of death due to secondary malignancy, as opposed to induction of such as in this work, would also prove meaningful. Risk of secondary malignancy can also be modeled using an integral dose model where the organ of secondary malignancy is not specified, as in the work of N. Shin[4]. Methods to address the other limitations discussed in 5.3 such as more rigorous target volume definition and accounting for confounding factors would also narrow the number of uncertainties and correct for some assumptions made in this work.

6.3 References

1. Canadian Cancer Statistics Special Topic: Cancer in Adolescents and Young Adults (15-29 Years). Toronto: Canadian Cancer Society; 2009.

2. Armitage JO. Early-Stage Hodgkin's Lymphoma. The New England Journal of Medicine 2010;363:653-62.

3. Hoppe B, Slopsema R, Specht L. Proton Therapy for Hodgkin Lymphoma. 2011:197-203.

4. Shin N. Modeling secondary cancer risk following paediatric radiotherapy: a comparison of intensity modulated proton therapy and photon therapy. Montreal: McGill University; 2011.

Appendix A

Derivation of Relative Seriality Model[1]

Beginning with the Poisson statistical model for cell kill (Eq. A.1)

$$P(D) = 2^{-e^{e\gamma\left(1-\frac{D}{D_{50}}\right)}} \quad [A.1]$$

P(D) probability for a given effect for a subvolume irradiated to dose D

D_{50} dose for 50% probability of response

γ maximum value of the normalized dose-response gradient

Probability of response of organ with serial-parallel structure (concept illustrated in Figure 2-6)

$$P = \prod_{j=1}^{n}\left[1 - \prod_{i=1}^{m}\left(1 - P_{ij}\right)\right] \quad [A.2]$$

P probability of the response of the organ

P_{ij} probability of response of subvolume ij

Probability of response of organ for a homogeneous dose distribution among all subvolumes within the organ

$$P = [1 - (1 - P_{\Delta})^{m}]^{n} \quad [A.3]$$

P probability of the response of the organ

$P_{\Delta} = P_{ij}$ probability of response of subvolume *ij*

m number of serial subunits

n number of parallel subunits

Probability of response of a single subvolume

$$P_{\Delta} = 1 - \left(1 - P^{\frac{1}{n}}\right)^{\frac{1}{m}} \quad [A.4]$$

P_{Δ} probability of response of subvolume

P probability of the response of the organ

m number of serial subunits

n number of parallel subunits

Probability of response of a fraction of the organ after volume $a \cdot b$ has been irradiated as illustrated in Figure 2-6 (c)

$$P_{ab} = [1 - (1 - P_{\Delta})^{a \cdot m}]^{b \cdot n} \quad [A.5]$$

P_{ab} probability of the response of fraction of the organ

P_{Δ} probability of response of subvolume

m number of serial subunits

n number of parallel subunits

$a \cdot b$ volume of organ irradiated

Probability of response for fraction of organ as a function of probability of response of whole organ

$$P_{ab} = \left[1 - \left(1 - P^{\frac{1}{n}}\right)^{a}\right]^{b \cdot n} \quad [A.6]$$

P_{ab} probability of the response of fraction of the organ

P probability of response of organ

n number of parallel subunits

$a \cdot b$ volume of organ irradiated

Parameter $b = 1$ to remove sensitivity of subvolume to geometrical alignment. Seriality parameter s introduced

$$s = \frac{m}{n \cdot m} = \frac{1}{n} \quad [A.7]$$

s seriality term

m number of serial subunits

n number of parallel subunits

Probability of response of subvolume in Eq. A.6 is expressed as function of seriality

$$P_v = [1 - (1 - P^s)^v]^{\frac{1}{s}} \quad [A.8]$$

P_v probability of the response of subvolume of the organ

P probability of response of organ

s seriality term

v volume of subvolume of organ

Probability of response of organ as a function of probability of response of subvolume

$$P = \left[1 - (1 - P_v^s)^{\frac{1}{v}}\right]^{\frac{1}{s}} \quad [A.9]$$

P probability of response of organ

P_v probability of the response of subvolume of the organ

s seriality term

v volume of subvolume of organ

Probability of response of whole organ to heterogeneous dose distribution by substituting Eq. A.9 into Eq. A2

$$P = \left[1 - \prod_{i=1}^{M}[1 - P_{\Delta v}(D_i)]\right]^{\frac{1}{s}} \quad [A.10]$$

P probability of response of organ

$P_{\Delta v}(D)$ probability of the response of subvolume of the organ irradiated to dose *D*

s seriality term

Δv fractional volume of subvolume relative to whole organ volume

i individual subvolume (voxel)

M total number of subvolumes

Probability of response of whole organ as a function of dose to voxel D_i by substituting Eq. A.4 into Eq. A.10.

$$P = \left[1 - \prod_{i=1}^{M}[1 - [P(D_i)]^s]^{\Delta v}\right]^{\frac{1}{s}} \quad [A.11]$$

P probability of response of organ

$P(D)$ probability of the response of the organ for subvolume irradiated to dose D_i

s seriality term

Δv fractional volume of subvolume relative to whole organ volume

i individual subvolume (voxel)

M total number of subvolumes

Probability of response for whole organ in heterogeneous dose distribution by substituting Eq. A.1 into Eq. A.11.

$$\boldsymbol{P = \left[1 - \prod_{i=1}^{M}\left[1 - \left(2^{-e^{\left[\gamma\left(1-\frac{D_i}{D_{50}}\right)\right]}}\right)^{s}\right]^{\Delta v}\right]^{\frac{1}{s}}} \qquad \textbf{[A.12]}$$

P probability of response of organ

D_i dose to subvolume i

D_{50} dose for 50% probability of response

γ maximum value of the normalized dose-response gradient

s seriality term

Δv fractional volume of subvolume relative to whole organ volume

i individual subvolume (voxel)

M total number of subvolumes

Reference

1. P. Källman, A.Å., A. Brahme, *Tumour and normal tissue responses to fractionated non-uniform dose delivery.* International Journal of Radiation Biology, 1992. **62**(2): p. 249-262.

Appendix B

Derivation of Schneider Modified Linear Quadratic Model[1]

Beginning with the set of differential equations describing the number of cells *N(D)* after one dose fraction *D*.

$$\frac{dN(D)}{dD} = -\alpha' \cdot N(D) \quad [B.1]$$

$$\frac{dR(D)}{dD} = -\alpha' \cdot R(D) + \xi[N_0 - N(D) - R(D)] \quad [B.2]$$

$$\frac{dM_c(D)}{dD} = -\alpha' \cdot M_c(D) + \mu[N(D) + R(D)] \quad [B.3]$$

N(D) number of cells surviving one fraction of dose *D*

R(D) number of cells repaired and repopulated cells after one fraction of dose *D*

$M_c(D)$ number of mutated cells (resulting in carcinogenesis) after one fraction of dose *D*

μ mutation parameter

ξ repopulation parameter

$$\alpha' = \alpha + \beta d \quad [B.4]$$

α/β dose at which linear cell kill is equivalent to quadratic cell kill (in this work for late responding normal tissue)

d dose per fraction

Initial conditions and fixed parameter values.

$$\alpha/\beta = 3 \text{ Gy} \quad [B.5]$$

$$N(0) = N_0 \quad [B.6]$$

$$R(0) = M_c(0) = 0 \qquad \text{[B.7]}$$

The solution for the number of original cells surviving one fraction of dose *D* (Eq. B.1) in its generic form is arrived upon as follows.

$$\int \frac{dN(D)}{N(D)} = -\alpha' \int dD$$

$$\ln(N(D)) = -\alpha' \cdot D + c_1$$

$$N(D) = c_1 \cdot e^{-\alpha' \cdot D} \qquad \text{[B.8]}$$

The constant c_1 can be solved for by implementing initial condition Eq. B.6.

$$N(0) = c_1 \cdot e^{-\alpha' \cdot 0} = N_0$$

$$c_1 = N_0$$

The solution for *N(D)* is thus

$$\boldsymbol{N(D) = N_0 \cdot e^{-\alpha' \cdot D}} \qquad \textbf{[B.9]}$$

The solution for the number of cells repaired and repopulated after one fraction of dose *D* (Eq. B.2) in its generic form is arrived upon as follows.

$$\frac{dR(D)}{dD} = -\alpha' \cdot R(D) + \xi\left[N_0 - N_0 e^{-\alpha' \cdot D} - R(D)\right]$$

$$\frac{dR(D)}{dD} + R(D)(\alpha' + \xi) = -\xi N_0\left(e^{-\alpha' \cdot D} - 1\right)$$

The variable y is introduced and both sides of the equation are multiplied by y.

$$y = e^{\int(\alpha' + \xi)dD} = e^{(\alpha' + \xi)D}$$

$$\frac{dR(D)}{dD}y + R(D)(\alpha' + \xi) \cdot y = -\xi N_0\left(e^{-\alpha' \cdot D} - 1\right) \cdot y$$

The solution for $\frac{dy}{dD}$ is then substituted into the differential equation.

$$\frac{dy}{dD} = \frac{d}{dD}\, e^{(\alpha' + \xi)D}$$

$$\frac{dy}{dD} = (\alpha' + \xi)e^{(\alpha' + \xi)D} = (\alpha' + \xi) \cdot y$$

$$\frac{dy}{dD} = (\alpha' + \xi) \cdot y$$

$$\frac{dR(D)}{dD}y + R(D)\frac{dy}{dD} = -\xi N_0\left(e^{-\alpha' \cdot D} - 1\right) \cdot y$$

The inverse product rule is used to rewrite the left-hand side of the differential equation and the variably *y* is replaced by its solution. Both sides are integrated to form the generic solution for *R(D)*.

$$\frac{d}{dD}\left(R(D) \cdot e^{(\alpha' + \xi)D}\right) = -\xi N_0\left(e^{-\alpha' \cdot D} - 1\right) \cdot e^{(\alpha' + \xi)D}$$

$$\int \frac{d}{dD}\left(R(D) \cdot e^{(\alpha' + \xi)D}\right)dD = -\xi N_0 \int \left(e^{-\alpha' \cdot D} - 1\right) \cdot e^{(\alpha' + \xi)D} dD$$

$$R(D) \cdot e^{(\alpha' + \xi)D} = \xi N_0 e^{\xi D}\left(-\frac{1}{\xi} + \frac{e^{\alpha' D}}{(\alpha' + \xi)}\right) + c_2 \qquad \text{[B.10]}$$

The constant c_2 is then solved for by implementing initial condition Eq. B.7.

$$R(0) = \xi N_0 \left(-\frac{1}{\xi} + \frac{1}{(\alpha' + \xi)}\right) + c_2 = 0$$

$$c_2 = N_0 \frac{\alpha'}{(\alpha' + \xi)}$$

The solution for *R(D)* is thus

$$\boldsymbol{R(D) = \frac{N_0}{(\alpha' + \xi)}\left[\xi - \alpha' \cdot e^{-\alpha' D} - \xi \cdot e^{-\alpha' D} + \alpha' \cdot e^{-(\alpha' + \xi) D}\right]} \qquad \textbf{[B. 11]}$$

The solution for the number of mutated cells after one fraction of dose *D* (Eq. B.3) in its generic form is arrived upon as follows. The variable *x* is introduced and both sides of Eq. B.3 are multiplied by *x*.

$$x = e^{\int \alpha' dD} = e^{\alpha' D}$$

$$\frac{dM_c(D)}{dD} x + \alpha' \cdot M_c(D) \cdot x = \mu[N(D) + R(D)] \cdot x$$

The solution for $\frac{dx}{dD}$ is then substituted into the differential equation.

$$\frac{dx}{dD} = \frac{d}{dD}\ e^{\alpha' D}$$

$$\frac{dx}{dD} = \alpha' e^{\alpha' D}$$

$$\frac{dx}{dD} = \alpha' \cdot x$$

$$\frac{dM_c(D)}{dD} x + \frac{dx}{dD} \cdot M_c(D) = \mu[N(D) + R(D)] \cdot x$$

The inverse product rule is used to rewrite the left-hand side of the differential equation and the variable *x* is replaced by its solution. The functions *N(D)* and *R(D)* are replaced by their solutions (Eq. B.9 and Eq. B.11). Both sides are integrated to form the generic solution for $M_c(D)$.

$$\frac{d}{dD}\left(M_c(D)\cdot e^{\alpha' D}\right) = \mu[N(D)+R(D)]\cdot e^{\alpha' D}$$

$$\frac{d}{dD}\left(M_c(D)\cdot e^{\alpha' D}\right) = \mu\frac{N_0}{(\alpha'+\xi)}\left[\xi\cdot e^{\alpha' D}+\alpha'\cdot e^{-\xi D}\right]$$

$$\int \frac{d}{dD}\left(M_c(D)\cdot e^{\alpha' D}\right)dD = \frac{\mu N_0}{(\alpha'+\xi)}\int\left[\xi\cdot e^{\alpha' D}+\alpha'\cdot e^{-\xi D}\right]dD$$

$$M_c(D)\cdot e^{\alpha' D} = \frac{\mu N_0}{(\alpha'+\xi)}\left[\frac{\xi\cdot e^{\alpha' D}}{\alpha'}-\frac{\alpha'\cdot e^{-\xi D}}{\xi}\right]+c_3 \qquad \text{[B.12]}$$

The constant c_3 is then solved for by implementing initial condition Eq. B.7.

$$M_c(0) = \frac{\mu N_0}{(\alpha'+\xi)}\left[\frac{\xi}{\alpha'}-\frac{\alpha'}{\xi}\right]+c_3 = 0$$

$$c_3 = \frac{\mu N_0}{(\alpha'+\xi)}\left[\frac{\alpha'}{\xi}-\frac{\xi}{\alpha'}\right]$$

In the limit of high dose, the repopulation fraction $R_f = R/N_0$ can be written as a function of ξ and α' [1].

$$R_f = \frac{R(D\to\infty)}{N_0} = \frac{\xi}{\alpha'+\xi}$$

The solution for the number of mutated cells resulting in carcinogenesis after one dose fraction $M_c(D)$ is thus

$$\boldsymbol{M_c(D) = \mu N_0 \cdot \frac{e^{-\alpha' \cdot D}}{\alpha' \cdot R_f}\left[1 - 2R_f + {R_f}^2 e^{\alpha' \cdot D} - (1 - R_f)^2 \cdot e^{-\frac{\alpha' \cdot R_f}{1 - R_f} \cdot D}\right]} \quad \textbf{[B.13]}$$

N_0 number of original cells

ξ repopulation parameter

R_f repopulation fraction

μ mutation parameter

α repairable damage component

$\alpha' = \alpha + \beta d$

α/β = 3 Gy

d dose per fraction

The excess absolute risk of carcinoma in an organ is the volume weighted sum of the number of mutated cells per the original number of cells over all subvolumes in the organ[1-3].

$$\boldsymbol{EAR_{organ} = \frac{M_c(D)}{N_0} = \frac{1}{V_{organ}} \sum_i V_i \cdot M_c(D_i)} \quad \textbf{[B.14]}$$

V_{organ} volume of the organ

V_i volume of subvolume

D_i dose to subvolume

$M_c(D)$ number of mutated cells resulting in carcinogenesis after one dose fraction D

N_0 number of original cells

References

1. Schneider, U., *Mechanistic model of radiation-induced cancer after fractionated radiotherapy using the linear-quadratic formula.* Medical Physics, 2009. **36**(4): p. 1138.

2. Schneider, U., A. Stipper, and J. Besserer, *Dose-response relationship for lung cancer induction at radiotherapy dose.* Zeitschrift fur medizinische Physik, 2010. **20**(3): p. 206-14.

3. Schneider, U., et al., *Dose-response relationship for breast cancer induction at radiotherapy dose.* Radiation oncology, 2011. **6**: p. 67.

Appendix C

Individual Patient Results

C.1 Treatment Planning Results

C.1.1 Dosimetric Indices for Heart

Table C-1: Individual patient dosimetric planning results for the heart for the lymphoma cohort.

Dosimetric Indices for the Heart								
	3D-CRT				*IMPT*			
Patient Number	*Mean dose (Gy)*	$V_{2\ Gy}$ *(%)*	$V_{5\ Gy}$ *(%)*	V_{Rx} *(%)*	*Mean dose (Gy)*	$V_{2\ Gy}$ *(%)*	$V_{5\ Gy}$ *(%)*	V_{Rx} *(%)*
1	13.72	78.83	74.32	13.60	9.70	58.20	53.55	14.60
2	3.76	24.70	20.48	0.47	2.45	16.89	14.37	1.61
3	6.24	35.96	30.61	11.69	5.15	31.84	28.25	12.27
4	7.72	46.02	39.70	7.22	6.66	40.97	36.33	7.43
5	8.09	48.14	42.23	7.28	5.14	30.25	27.26	4.26
6	8.86	56.02	48.73	9.38	5.28	38.55	33.93	2.98
7	9.59	67.28	46.42	15.47	5.31	33.70	29.28	8.47
8	8.29	49.45	42.86	0.50	1.85	16.91	12.47	1.05
9	13.61	77.14	69.37	8.34	9.46	54.41	49.53	18.12
10	13.82	74.44	69.53	30.95	11.05	57.30	53.82	40.45
11	8.01	47.60	40.37	7.10	3.95	23.40	20.17	3.55
12	0.58	0.00	0.00	0.00	0.00	0.00	0.00	0.00
13	0.64	3.05	1.00	0.00	0.02	0.20	0.00	0.00
14	6.54	40.77	27.06	0.20	3.49	21.69	17.60	1.17
15	7.42	36.17	28.30	9.69	6.44	29.17	25.96	8.08
16	12.22	62.72	46.72	7.66	9.46	39.19	36.12	8.57
17	1.62	13.92	6.34	0.00	0.40	3.44	2.42	0.00
18	7.71	47.87	35.02	9.82	5.05	26.36	22.50	2.80
19	12.62	61.72	49.70	4.97	9.20	38.00	34.70	5.16
20	12.58	66.57	45.83	8.48	8.36	37.06	33.20	9.79
21	15.95	83.34	65.65	8.18	5.32	25.99	22.38	4.95
22	15.08	76.44	55.50	11.54	10.94	45.19	41.30	13.70
23	0.48	0.00	0.00	0.00	0.00	0.00	0.00	0.00
24	25.20	94.50	82.74	19.70	12.04	67.30	63.00	1.10

Table C-2: Individual patient dosimetric planning results for the heart for the breast cancer cohort.

Dosimetric Indices for the Heart								
	3D-CRT				*IMPT*			
Patient Number	*Mean dose (Gy)*	$V_{2\ Gy}$ *(%)*	$V_{5\ Gy}$ *(%)*	V_{Rx} *(%)*	*Mean dose (Gy)*	$V_{2\ Gy}$ *(%)*	$V_{5\ Gy}$ *(%)*	V_{Rx} *(%)*
1	0.38	0.00	0.00	0.00	0.10	1.46	0.50	0.00
2	1.87	41.64	0.00	0.00	0.06	0.74	0.30	0.00
3	2.29	7.56	5.75	1.94	0.58	4.60	2.63	0.00
4	4.10	23.36	10.57	0.00	0.73	4.79	3.47	0.00

C.1.2 Dosimetric Indices for Lungs

Table C-3: Individual patient dosimetric planning results for the lungs for the lymphoma cohort.

Dosimetric Indices for the Lungs								
	3D-CRT				*IMPT*			
Patient Number	*Mean dose (Gy)*	$V_{20\ Gy}$ *(%)*	$V_{5\ Gy}$ *(%)*	V_{Rx} *(%)*	*Mean dose (Gy)*	$V_{20\ Gy}$ *(%)*	$V_{5\ Gy}$ *(%)*	V_{Rx} *(%)*
1	6.38	2.47	35.43	2.47	3.98	2.61	25.30	2.61
2	5.77	15.30	30.03	1.14	3.25	4.41	20.56	2.19
3	5.58	15.09	28.92	10.20	4.44	8.52	26.16	4.34
4	8.03	25.56	41.23	6.67	5.24	10.43	31.39	5.04
5	7.11	18.44	37.29	5.31	3.31	5.11	20.63	2.48
6	8.76	26.03	46.26	9.20	6.26	13.57	36.11	4.50
7	8.44	25.48	41.54	11.81	2.95	3.39	20.98	1.38
8	6.50	20.30	33.72	2.31	2.99	4.04	19.12	1.61
9	7.10	17.56	38.00	5.38	3.91	6.29	24.01	5.18
10	6.77	19.85	35.04	10.78	4.01	6.39	24.78	3.61
11	9.95	30.19	44.17	17.60	6.01	16.13	31.20	4.60
12	3.12	7.88	11.20	0.46	1.14	2.43	6.04	0.35
13	5.75	13.62	26.20	2.34	3.23	7.95	15.77	1.80
14	7.99	20.08	33.93	3.04	3.69	8.71	18.08	1.78
15	9.90	28.97	38.11	9.24	7.09	20.45	29.80	6.23
16	9.54	26.26	37.02	2.82	5.72	15.50	26.20	2.70
17	7.67	18.28	40.06	6.38	2.93	7.46	13.78	1.17
18	10.88	27.09	45.80	12.13	7.38	16.84	38.46	1.80
19	13.62	37.74	55.70	2.92	7.90	19.97	37.84	3.15
20	9.77	27.37	36.36	5.14	5.52	14.64	24.83	3.80
21	15.12	41.90	59.12	9.22	8.15	21.83	37.14	4.50
22	12.70	33.64	49.50	3.72	5.04	10.94	26.08	1.68
23	6.42	16.68	19.40	1.94	3.43	9.07	13.00	1.57
24	14.59	35.11	58.50	2.50	5.36	11.00	27.30	0.31

Table C-4: Individual patient dosimetric planning results for the ipsilateral lung for the breast cancer cohort.

Dosimetric Indices for the Ipsilateral Lung								
	3D-CRT				*IMPT*			
Patient Number	*Mean dose (Gy)*	$V_{20\ Gy}$ *(%)*	$V_{5\ Gy}$ *(%)*	V_{Rx} *(%)*	*Mean dose (Gy)*	$V_{20\ Gy}$ *(%)*	$V_{5\ Gy}$ *(%)*	V_{Rx} *(%)*
1	4.82	8.61	16.91	0.00	7.69	16.74	30.25	0.31
2	14.55	26.68	53.01	0.00	11.88	26.50	47.84	0.81
3	3.89	7.40	11.42	0.60	3.71	8.07	16.19	0.40
4	12.55	26.70	32.60	1.85	6.76	14.69	27.90	0.00

C.1.2 Dosimetric Indices for Breasts

Table C-5: Individual patient dosimetric planning results for the breasts for the lymphoma cohort.

Dosimetric Indices for the Breasts								
	3D-CRT				*IMPT*			
Patient Number	*Mean dose (Gy)*	$V_{2\ Gy}$ *(%)*	$V_{5\ Gy}$ *(%)*	V_{Rx} *(%)*	*Mean dose (Gy)*	$V_{2\ Gy}$ *(%)*	$V_{5\ Gy}$ *(%)*	V_{Rx} *(%)*
1	1.55	10.04	7.51	0.88	0.93	8.11	6.48	0.00
3	0.50	3.06	2.02	0.17	0.23	2.27	1.61	0.00
6	4.03	32.80	33.94	5.10	1.31	14.53	12.08	0.00
7	3.00	19.92	14.59	5.84	1.13	9.92	8.28	0.00
13	0.31	1.67	1.05	0.00	0.01	0.12	0.00	0.00
15	0.77	5.24	3.77	0.00	0.28	1.87	1.51	0.00
19	1.65	10.49	5.25	0.75	0.62	3.39	2.87	0.13
20	0.84	5.27	2.77	0.00	0.08	1.10	0.48	0.00
21	3.33	15.58	12.30	4.01	1.86	9.95	8.90	0.00
22	3.72	19.12	14.54	3.30	1.61	9.05	7.72	0.00
24	24.26	25.90	18.46	2.82	0.83	6.80	5.78	0.00

C.2 Risk Modeling Results

C.2.1 Excess Risk for Cardiac Mortality Results

Table C-6: Individual patient results for excess risk for cardiac mortality at 15 years post-irradiation for lymphoma cohort. Parameter sets I. Gagliardi[1] BC, II. Eriksson[2] BC and HL, III. Eriksson[2] HL.

Excess Absolute Risk for Cardiac Mortality (%)						
	3D-CRT			*IMPT*		
Patient Number	*I*	*II*	*III*	*I*	*II*	*III*
1	0.1	1.2	0.7	0.1	0.9	0.5
2	0.0	0.2	0.1	0.0	0.2	0.1
3	0.0	0.4	0.2	0.0	0.4	0.2
4	0.0	0.5	0.3	0.0	0.5	0.2
5	0.0	0.5	0.3	0.0	0.4	0.2
6	0.0	0.6	0.3	0.0	0.3	0.2
7	0.1	0.6	0.3	0.0	0.4	0.2
8	0.1	0.7	0.4	0.0	0.3	0.2
9	0.1	0.9	0.5	0.1	0.7	0.4
10	0.1	1.0	0.6	0.1	0.9	0.5
11	0.2	0.8	0.5	0.1	0.4	0.2
12	0.0	0.0	0.0	0.0	0.0	0.0
13	0.0	0.0	0.0	0.0	0.0	0.0
14	0.4	1.0	0.6	0.2	0.5	0.3
15	0.8	1.4	0.9	0.8	1.3	0.8
16	1.3	2.3	1.4	1.2	2.0	1.2
17	0.0	0.1	0.0	0.0	0.0	0.0
18	0.6	1.2	0.7	0.4	0.8	0.5
19	1.1	2.2	1.3	1.1	1.9	1.1
20	1.2	2.3	1.4	0.9	1.6	1.0
21	1.3	2.6	1.6	0.5	0.9	0.6
22	1.5	2.8	1.7	1.3	2.2	1.3
23	0.0	0.0	0.0	0.0	0.0	0.0
24	6.0	6.9	4.4	0.9	1.6	1.0

Table C-7: Individual patient results for excess risk for cardiac mortality at 15 years post-irradiation for breast cancer cohort. Parameter sets I. Gagliardi[1] BC, II. Eriksson[2] BC and HL, III. Eriksson[2] HL.

	Excess Absolute Risk for Cardiac Mortality (%)					
	3D-CRT			*IMPT*		
Patient Number	*I*	*II*	*III*	*I*	*II*	*III*
1	0.00	0.02	0.01	0.00	0.02	0.01
2	0.00	0.03	0.02	0.00	0.01	0.01
3	0.28	0.27	0.18	0.14	0.15	0.10
4	1.16	1.05	0.69	0.16	0.17	0.11

C.2.2 Excess Absolute Risk for Lung Cancer Results

Table C-8: Individual patient results for excess absolute risk for lung cancer at 30 years post-irradiation for lymphoma cohort.

Patient Number	Excess Absolute Risk for Lung Cancer (cases per 10,000 persons)		*Absolute Reduction*
	3D-CRT	*IMPT*	
1	16.5	10.1	6.4
2	14.9	8.4	6.5
3	14.3	11.0	3.3
4	20.4	13.6	6.8
5	19.7	9.0	10.8
6	21.7	15.2	6.5
7	36.5	14.9	21.6
8	16.9	7.3	9.6
9	18.2	9.9	8.3
10	17.5	10.9	6.5
11	22.7	13.8	8.9
12	7.7	2.8	4.9
13	12.8	6.6	6.1
14	17.4	8.0	9.4
15	18.1	12.6	5.5
16	19.6	11.1	8.5
17	17.4	6.1	11.4
18	22.8	16.4	6.4
19	26.3	16.1	10.2
20	18.5	10.8	7.8
21	28.7	16.2	12.6
22	37.0	16.5	20.5
23	11.6	6.5	5.1
24	28.1	12.3	15.8

Table C-9: Individual patient results for excess absolute risk for lung cancer at 30 years post-irradiation for breast cancer cohort.

Patient Number	Excess Absolute Risk for Lung Cancer (cases per 10,000 persons)		*Absolute Reduction*
	3D-CRT	*IMPT*	
1	5.3	7.1	-1.8
2	13.6	10.9	2.7
3	5.0	2.0	2.9
4	9.8	6.6	3.2

C.2.3 Excess Absolute Risk for Breast Cancer Results

Table C-10: Individual patient results for excess absolute risk for breast cancer at 30 years post-irradiation for lymphoma cancer cohort.

Patient Number	Excess Absolute Risk for Breast Cancer (cases per 10,000 persons)		*Absolute Reduction*
	3D-CRT	*IMPT*	
1	7.7	3.7	3.9
3	3.0	1.0	1.9
6	18.3	6.8	11.5
7	21.1	7.5	13.6
13	2.0	0.1	2.0
15	4.2	0.9	3.3
19	8.3	1.7	6.6
20	10.2	0.7	9.4
21	10.7	5.1	5.6
22	13.3	4.7	8.6
24	14.1	3.5	10.6

References

1. Gagliardi G, I. Lax, S. Söderström, G. Gyenes, L. E. Rutqvist. Prediction of excess risk of long-term cardiac mortality after radiotherapy of stage I breast cancer. Radiotherapy and Oncology 1998;46:63-71.

2. Eriksson F, G. Gagliardi, A. Liedberg, I. Lax, C. Lee, S. Levitt, B. Lind, L.E. Rutqvist. Long term cardiac mortality following radiation therapy for Hodgkin's disease: analysis with the relative seriality model. Radiotherapy and Oncology 2000;55:153-62.

Bibliography

Aleman BM, van den Belt-Dusebout AW, Klokman WJ, Van't Veer MB, Bartelink H, van Leeuwen FE. Long-term cause-specific mortality of patients treated for Hodgkin's disease. Journal of Clinical Oncology 2003;21:3431-9.

Andratschke N, Maurer J, Molls M, Trott KR. Late radiation-induced heart disease after radiotherapy. Clinical importance, radiobiological mechanisms and strategies of prevention. Radiother Oncol 2011;100:160-6.

Armitage JO. Early-Stage Hodgkin's Lymphoma. The New England Journal of Medicine 2010;363:653-62

Behringer K, Josting A, Schiller P, et al. Solid tumors in patients treated for Hodgkin's disease: a report from the German Hodgkin Lymphoma Study Group. Ann Oncol 2004;15:1079-85.

Bentzen SM, Constine LS, Deasy JO, et al. Quantitative Analyses of Normal Tissue Effects in the Clinic (QUANTEC): an introduction to the scientific issues. Int J Radiat Oncol Biol Phys 2010;76:S3-9.

Bhatia S, Sklar C. Second cancers in survivors of childhood cancer. Nat Rev Cancer 2002;2:124-32.

Burman C, Kutcher, G.J., Emami, B., and Goitein, M. Fitting of Normal Tissue Tolerance Data to an Analytic Function. International Journal of Radiation Oncology Biology Physics 1991;21:123-35.

Canadian Cancer Statistics 2011. Toronto: Canadian Cancer Society, Statistics Canada, Provincial/Territorial Cancer Registries, Public Health Agency of Canada; 2011.

Canadian Cancer Statistics Special Topic: Breast Cancer. Toronto: Canadian Cancer Society; 2007.

Canadian Cancer Statistics Special Topic: Cancer in Adolescents and Young Adults (15-29 Years). Toronto: Canadian Cancer Society; 2009.

Cancer Facts & Figures 2012. Atlanta: American Cancer Society; 2012.

Chera BS, Rodriguez C, Morris CG, et al. Dosimetric comparison of three different involved nodal irradiation techniques for stage II Hodgkin's lymphoma patients: conventional radiotherapy, intensity-modulated radiotherapy, and three-dimensional proton radiotherapy. International journal of radiation oncology, biology, physics 2009;75:1173-80.

Delaney T, Kooy, H., ed. Proton and Charged Particle Radiotherapy. Philadelphia: Lippincott Williams & Wilkins; 2008.

Emami B, Lyman, J., et al. Tolerance of Normal Tissue to Therapeutic Irradiation. International Journal of Radiation Oncology Biology Physics 1991;21:109-22.

Eriksson F, G. Gagliardi, A. Liedberg, I. Lax, C. Lee, S. Levitt, B. Lind, L.E. Rutqvist. Long term cardiac mortality following radiation therapy for Hodgkin's disease: analysis with the relative seriality model. Radiotherapy and Oncology 2000;55:153-62.

Feng M, Moran JM, Koelling T, et al. Development and validation of a heart atlas to study cardiac exposure to radiation following treatment for breast cancer. International Journal of Radiation Oncology Biology Physics 2011;79:10-8.

Fowler J. Brief Summary of Radiobiological Principles in Fractionated Radiotherapy. Seminars in Oncology 1992;2:16-21.

Gagliardi G, Constine LS, Moiseenko V, et al. Radiation dose-volume effects in the heart. Int J Radiat Oncol Biol Phys 2010;76:S77-85.

Gagliardi G, I. Lax, A. Ottolenghi, L.E. Rutqvist. Long-term cardiac mortality after radiotherapy of breast cancer-application of the relative seriality model. The British Journal of Radiology 1996;69:839-46.

Gagliardi G, I. Lax, S. Söderström, G. Gyenes, L. E. Rutqvist. Prediction of excess risk of long-term cardiac mortality after radiotherapy of stage I breast cancer. Radiotherapy and Oncology 1998;46:63-71.

Heron M. Deaths: Leading Causes for 2008: U.S. Department of Health and Human Services, Centers for Disease Control and Prevention, National Center for Health Statistics, National Vital Statistics System; 2012.

Hoppe B, Slopsema R, Specht L. Proton Therapy for Hodgkin Lymphoma. 2011:197-203.

Horning SJ. Hodgkin's Lymphoma. In: Abeloff, ed. Abeloff's Clinical Oncology. 4th ed. Philadelphia: Churchill Livingstone Elsevier; 2008.

ICRU Report 62: Prescribing, Recording, and Reporting Photon Beam Therapy (Supplement ot ICRU Report 50). Bethesda, Md.: International Commission on Radiation Units and Measurements; 1999.

ICRU Report 78: Prescribing, Recording and Reporting Proton-Beam Therapy. Oxford: Oxford University Press; 2007.

Källman P, A. Ågren, A. Brahme. Tumour and normal tissue responses to fractionated non-uniform dose delivery. International Journal of Radiation Biology 1992;62:249-62.

Kong FM, Pan C, Eisbruch A, Ten Haken RK. Physical models and simpler dosimetric descriptors of radiation late toxicity. Semin Radiat Oncol 2007;17:108-20.

Kutcher GJ, Burman, C. et al. Histogram Reduction Method for Calculating Complication Probabiliities for Three-Dimensional Treatment Planning Evaluations. International Journal of Radiation Oncology Biology Physics 1991;21:137-46.

Lee CKK, D. Aeppli, M. E. Nierengarten. The Need for Long-Term Surveillance for Patients Treated with Curative Radiotherapy for Hodgkin's Disease: University of Minnesota Experience. International Journal of Radiation Oncology Biology Physics 2000;48:169-79.

Lyman J. Complicaqtion Probability as Assessed from Dose-Volume Histograms. Radiat Res 1985;Supplement 8:S-13 - S-9.

Oeffinger K, Mertens, A., Sklar, C., Kawashima, T. et al. Chronic Health Conditions in Adult Survivors of Childhood Cancer. New England Journal of Medicine 2006;355:1572-82.

Park PC, Zhu XR, Lee AK, et al. A Beam-specific Planning Target Volume (PTV) Design for Proton Therapy to Account for Setup and Range Uncertainties. International journal of radiation oncology, biology, physics 2011.

Preston DL, Ron E, Tokuoka S, et al. Solid cancer incidence in atomic bomb survivors: 1958-1998. Radiat Res 2007;168:1-64.

Proton Algorithm Reference Guide. In: Varian Medical Systems; 2009.

Roberge D. FRSQ-MSSS Recherches Sur le Cancer. In. Centre Universitaire de Santé McGill, Hôpital Général de Montréal: Fonds de la recherche en santé Québec; 2009.

Radiation Oncology Physics: A Handbook for Teachers and Students. Vienna: International Atomic Energy Agency; 2005.

Schneider U. Mechanistic model of radiation-induced cancer after fractionated radiotherapy using the linear-quadratic formula. Medical Physics 2009;36:1138.

Schneider U. Secondary Neutron Dose During Proton Therapy Using Spot Scanning. International journal of radiation oncology, biology, physics 2002;53:7.

Schneider U, Lomax A, Pemler P, et al. The impact of IMRT and proton radiotherapy on secondary cancer incidence. Strahlenther Onkol 2006;182:647-52.

Schneider U, Lomax A, Timmermann B. Second cancers in children treated with modern radiotherapy techniques. Radiother Oncol 2008;89:135-40.

Schneider U, Stipper A, Besserer J. Dose-response relationship for lung cancer induction at radiotherapy dose. Z Med Phys 2010;20:206-14.

Schneider U, Sumila M, Robotka J, Gruber G, Mack A, Besserer J. Dose-response relationship for breast cancer induction at radiotherapy dose. Radiat Oncol 2011;6:67.

Schneider U, Zwahlen D, Ross D, Kaser-Hotz B. Estimation of radiation-induced cancer from three-dimensional dose distributions: Concept of organ equivalent dose. International journal of radiation oncology, biology, physics 2005;61:1510-5.

Simmons PS, Jayasinghe YL, Wold LE, Melton LJ, 3rd. Breast carcinoma in young women. Obstet Gynecol 2011;118:529-36.

Shin N. Modeling secondary cancer risk following paediatric radiotherapy: a comparison of intensity modulated proton therapy and photon therapy. Montreal: McGill University; 2011.

Travis LB, D. Hill, G. Dores, M. Gospodarowicz, F. van Leeuwen, E. Holowaty, M. Andersson, et al. Breast Cancer Rollowing Radiotherapy and Chemotherapy Among Young Women with Hodgkin Disease. Journal of the American Medical Association 2003;290:465-75.

Travis LB, M. Gospodarowicz, R. Curtis, E.A. Clarke, M. Andersson, B. Glimelius, et al. Lung Cancer Following Chemotherapy and Radiotherapy for Hodgkin's Disease. Journal of the National Cancer Institute 2002;94:182-92.

Van Dyk J. The modern technology of radiation oncology : a compendium for medical physicists and radiation oncologists. Madison, Wis.: Medical Physics Pub.; 1999.

White J, A. Tai, D. Arthur, T. Buchholz, et al. Breast Cancer Atlas for Radiation Therapy Planning: Consensus Definitions.

Yan X, Titt U, Koehler AM, Newhauser WD. Measurement of neutron dose equivalent to proton therapy patients outside of the proton radiation field. Nucl Instrum Meth A 2002;476:429-34.